UCLouvain

epl

École polytechnique de Louvain

Sensitivity analysis of a Maisotsenko sub-atmospheric inverted Brayton cycle and comparison with relevant technologies

Authors: **Zakarie Bruyr, Nicolas Dewaersegger**
Supervisor: **Francesco Contino**
Readers: **Francesco Contino, Ward De Paepe, Aggelos Gaitanis**
Academic year 2021–2022
Master [120] in Mechanical Engineering

Acknowledgements

First of all, we would like to thank our supervisor Professor Francesco Contino for his availability, his advice and his feedback all along the year.

We would also like to thank Aggelos Gaitanis for the continuous monitoring of our work, his critical view on the encountered problems and his availability for a quick response to our many questions.

Furthermore, our acknowledgements go to our reader Professor Ward De Paepe for his interest in our work, his valuable advice during the two meetings we had and the time he spent reading our manuscript.

Finally, we would like to thank our friends and families for their support during the year and especially Caroline, Ines, Vincent, Marc and Gregory for their precious proofreading recommendations.

Abstract

Decentralised cogeneration appears as a versatile alternative towards a greater flexibility of our energy production system. Developing small-scale Combined Heat and Power (CHP) units is therefore required. The current market is mainly composed of Internal Combustion Engines (ICE). Still, micro Gas Turbine (mGT) cycles constitute another promising technology. Their current low market penetration is explained by their limited electrical efficiency (around 30% for a 100 kW_e unit), which induces that heat supply is currently their main work field (with a considerable overall efficiency of 85%). This heat-driven aspect reduces their profitability when the consumer's heat demand decreases. Indeed, the thermal power output of the unit is lost which makes the overall efficiency drop to the limited electrical efficiency. Increasing the commercial availability of mGT units requires thus to find a solution to decouple the heat and electricity production.

Humidifying a mGT cycle is a potential way to use the available heat in order to improve the electrical performance. More than that, the Maisotsenko Cycle (M-Cycle) is a promising thermodynamic conception aiming at increasing the heat recovery by exchanging heat while taking advantage of the psychrometric energy available when evaporating water in the air. This best-performing humidified heat recuperator might allow to boost the electrical efficiency of mGT cycles thanks to its dew point cooling capacity.

Unlike the typical Brayton cycle configuration used in most mGT systems, the Inverted Brayton Cycle (IBC) layout gives the possibility to reduce the power outputs of the cycle while keeping a modest efficiency. This downsizing asset is particularly interesting in the quest of small-scale power units.

In this Thesis, the M-power component is numerically implemented and then introduced into a previously validated IBC model. The resulting cycle is called the Maisotsenko sub-atmospheric inverted Brayton cycle (M-SAB cycle). This model is thereafter used to assess the cycle performance and to understand how the M-saturator is influencing it. By drawing the related Sankey diagrams, the variation of the energy fluxes between each component is investigated. More than that, a sensitivity analysis is conducted to evaluate the impact of the M-Cycle performance parameters, the initial conditions of the working fluid and the design and control parameters. In order to adequately compare the electrical power output to the thermal one, an exergetic analysis is done using Grassmann diagrams.

The results show that the M-SAB cycle offers the best electrical efficiency when the M-Cycle heat recovery is the highest (43.5% with an associated load of 30 kW_e). Such efficiency exceeds that of current commercial small-scale CHP units. This latter is reached when fixing a wet-bulb effectiveness of 98% and injecting as much water as possible (48 g/s in that case, corresponding to a proportion of roughly one third with respect to the total mass flow through the cycle). These two parameters might constitute technological challenges in order to reach the performance achieved by our

numerical model. Indeed, arriving at such effectiveness will probably require methods increasing the pressure drops, the size and the cost of the recuperator. At the same time, the high proportion of water injected might be restricted by the surge limit of the compressor. Another consideration associated with the discussed performance corresponding to the effectiveness of 98% is the low exergy content of the recovered heat which removes its cogenerative character. This latter is present with a lower effectiveness of 90%. But the electrical performance of the M-SAB cycle in that case (21.3% of electrical efficiency with an electrical power output of 20.1 kW_e) is too low to justify the investment in such unit.

Contents

1 Context **1**

2 Research question & Methodology **5**

3 Literature review **9**
3.1 micro Gas Turbine . . . 9
3.2 Inverted Brayton cycle . . . 12
3.3 Humidified mGT cycles . . . 16
3.4 Maisotsenko saturator . . . 22
3.5 M-SAB Cycle . . . 28

4 Inverted Brayton Cycle **31**
4.1 Air and flue gases modelling . . . 31
4.2 IBC modelling . . . 31
4.2.1 Heat exchanger . . . 32
4.2.2 Combustion chamber . . . 32
4.2.3 Turbine . . . 35
4.2.4 Economizer . . . 35
4.2.5 Compressor . . . 35
4.2.6 Pressure drops . . . 36
4.2.7 Miscellaneous losses . . . 36
4.2.8 Heat losses . . . 37
4.3 IBC Validation . . . 37
4.3.1 Effect of the heat losses . . . 40
4.3.2 Effect of the turbine expansion ratio . . . 42
4.3.3 Effect of the TIT . . . 44

5 Maisotsenko Cycle **47**
5.1 Humid air properties . . . 47
5.1.1 Enthalpy . . . 47
5.1.2 Entropy . . . 48
5.2 M-cycle modelling . . . 48
5.3 Results & Comparison . . . 53
5.3.1 Classical model . . . 54
5.3.2 Model with boosted T_4 . . . 55

6 M-SAB cycle **58**
6.1 IBC : addition of a preheater . . . 58
6.2 IBC : Conversion from the MTT to the T100 . . . 60
6.2.1 Specifications of the T100 mGT . . . 60
6.2.2 Pressure drops & heat losses . . . 61
6.2.3 T100 maps . . . 62

6.2.4 IBC performance with the T100 mGT 65
6.3 Merging of the two models 66

7 Sensitivity analysis **72**
7.1 Preliminary considerations 72
7.2 Impact of the injected water mass flow 74
7.3 M-Cycle performance parameters 79
7.4 Initial conditions of the flow 84
7.5 Design parameters 88
7.6 Control parameter 95

8 Exergetic analysis **99**
8.1 Exergy definition & dead state 99
8.2 Exergy analysis 100

9 Comparison with other technologies **106**
9.1 M-SAB performance 106
9.2 Comparison 107
9.3 Design requirements for a high ϵ_{WB} 109

10 Conclusion **112**

List of Figures

1.1 Global fuel supply prediction 2
1.2 Centralised vs decentralised systems 3
1.3 World global share of electricity generation in 2019 4

2.1 IBC scheme 5
2.2 M-Cycle scheme 6
2.3 M-SAB scheme 7

3.1 BC mGT scheme 10
3.2 IBC scheme 13
3.3 Humidified mGT cycle layouts 18
3.4 MBC and M-ABC schemes 23
3.5 DEC and IEC: configuration and psychrometric chart 24
3.6 M-Cycle principle and psychrometric chart 26
3.7 M-Cycle principle and psychrometric chart with 2 different inlet flows 27
3.8 M-Cycle configuration 27
3.9 M-SAB cycle scheme 28

4.1 IBC scheme 32
4.2 Energy balance of the combustion chamber 34
4.3 IBC : validation of the temperature evolution 39
4.4 IBC : impact of the expansion ratio on the compressor ratio and the cycle efficiencies 43
4.5 IBC : impact of the expansion ratio on the power outputs 44
4.6 IBC : impact of the TIT on the compressor ratio and the heat losses . 45
4.7 IBC : impact of the TIT on the power outputs 45
4.8 IBC : impact of the TIT on the cycle efficiencies 46

5.1 MBC scheme 49
5.2 M-Cycle scheme and states numeration 49
5.3 Heat fluxes in M-Cycle (classical model, $\epsilon_{\mathrm{WB}} = 0.9$) 55
5.4 Heat fluxes in M-Cycle (classical model, $\Delta T = 50°\mathrm{C}$) 55
5.5 Heat fluxes in M-Cycle (boosted T_4, $\epsilon_{\mathrm{WB}} = 0.9$) 57

6.1 M-Cycle : influence of its cold inlet temperature on the cold pinch . . 59
6.2 IBC scheme with a preheater 59
6.3 T100 compressor iso-speed line 63
6.4 M-SAB cycle final scheme 66
6.5 Sankey diagram of the M-SAB cycle ($\epsilon_{\mathrm{WB}} = 0.9$ and $\dot{m}_{\mathrm{H2O}} = 30$ g/s) 70
6.6 Sankey diagram of the M-SAB cycle ($\Delta T = 50°\mathrm{C}$ and $\dot{m}_{\mathrm{H2O}} = 30$ g/s) 71

7.1 Impact of the injected water mass flow on the electrical performance . 75
7.2 Impact of the injected water mass flow on the thermal performance . 77

7.3 Variation of ϵ_{WB} with the injected water mass flow at $\Delta T = 50°\mathrm{C}$ . . 79
7.4 Impact of ϵ_{WB} on the electrical performance 80
7.5 Impact of ϵ_{WB} on the thermal performance 82
7.6 Impact of ϵ_{dew} on the electrical performance 83
7.7 Impact of ϵ_{dew} on the thermal performance 84
7.8 Impact of T_{in} on the electrical performance 85
7.9 Impact of T_{in} on the thermal performance 86
7.10 Impact of ϕ_{in} on the electrical performance 87
7.11 Impact of ϕ_{in} on the thermal performance 88
7.12 Impact of the heat losses on the electrical performance 89
7.13 Impact of the heat losses on the thermal performance 90
7.14 Impact of the pressure drops on the electrical performance 91
7.15 Impact of the pressure drops on the thermal performance 92
7.16 Impact of the TIT on the electrical performance 93
7.17 Impact of the TIT on the thermal performance 95
7.18 Impact of the expansion ratio on the electrical performance 96
7.19 Impact of the expansion ratio on the thermal performance 97

8.1 Grassmann diagram of the M-SAB cycle with $\epsilon_{\mathrm{WB}} = 0.9$ and $\dot{m}_{\mathrm{H_2O}} =$ 20 g/s 102
8.2 Grassmann diagram of the M-SAB cycle with $\epsilon_{\mathrm{WB}} = 0.9$ and $\dot{m}_{\mathrm{H_2O}} =$ 50 g/s 103
8.3 Grassmann diagram of the M-SAB cycle with $\epsilon_{\mathrm{WB}} = 0.98$ and $\dot{m}_{\mathrm{H_2O}} =$ 20 g/s 104
8.4 Grassmann diagram of the M-SAB cycle with $\epsilon_{\mathrm{WB}} = 0.98$ and $\dot{m}_{\mathrm{H_2O}} =$ 48 g/s 105

List of Tables

3.1 Current commercial mGT . . . 9
3.2 Main investigations on M-Cycle coupled GT and mGT systems. . . . 30

4.1 Fuel molar composition . . . 33
4.2 Fuel properties . . . 33
4.3 IBC pressure drop coefficients (MTT mGT) . . . 36
4.4 IBC : initial heat loss coefficients (MTT mGT) . . . 37
4.5 IBC : inputs for the validation . . . 38
4.6 IBC validation of performances . . . 40
4.7 IBC : adapted heat loss coefficients (MTT mGT) . . . 41
4.8 IBC : modified heat loss coefficients . . . 41

5.1 M-Cycle inputs . . . 53
5.2 M-Cycle results comparison (classical cases) . . . 54
5.3 M-Cycle results comparison (boosted T_4 cases) . . . 57

6.1 Turbec T100 mGT specifications . . . 61
6.2 T100 : pressure drop and heat loss coefficients . . . 61
6.3 Input values of the IBC adapted to the T100 . . . 65
6.4 Performance of the IBC with the T100 mGT. . . . 65
6.5 Boundary conditions of the M-SAB cycle. . . . 67
6.6 M-SAB cycle performance ($\dot{m}_{\mathrm{H2O}} = 30$ g/s and either $\epsilon_{\mathrm{WB}} = 0.9$ or $\Delta T = 50$°C) . . . 68

8.1 Exergetic analysis : efficiencies of each study case . . . 100

9.1 M-SAB cycle performance . . . 106
9.2 Performance comparison of different CHP units . . . 108

Chapter 1

Context

Nowadays, the significance of energy is continuously growing in the needs of our everyday life. Ensuring a clean and sustainable energy production is therefore one of the biggest challenges our society has to deal with. There is no need to go into the details of the multiple negative effects and consequences arising from this growing production. But to put it briefly, the massive use of fossil fuels (coal, natural gas, oil) contributes considerably to the increasing pollution due to the huge quantity of carbon dioxide and other greenhouse gases released in the atmosphere. To face global warming and its different consequences, scientists and engineers are intensively working on developing a cleaner energy production. This includes the introduction of renewable technologies (solar and photovoltaic panels, wind turbines, hydro-energy, etc) as well as the enhancement of the current production systems. Finally, the main goal is to reach the objectives adopted and signed in 2015 as part of COP21 [1], which urge to reach the peak of global emissions as soon as possible as well as limiting the global temperature increase.

The exponentially growing use of renewable technologies is definitely a huge step towards a clean power production. However, the intermittent facet of the renewable sources of energy implies a more unstable grid. Therefore, back-up power production systems must be used in order to provide energy when the demand exceeds the renewable production. For this purpose, conventional thermal production units could be an alternative. Such systems as gas turbine cycles offer a high electrical efficiency and specific power output. These gas turbine cycles related to electricity production, like the Brayton cycle, usually use fuel in a gaseous state which is burned in a combustion chamber. Nowadays and for the coming years, one of the most common fuel is natural gas. According to the International Energy Agency (IEA) [2], even though the natural gas demand decreased due to the COVID pandemic and its related lower global energy demand, it started to increase again after the lockdown and is reported to keep on rising in the coming years with a predicted consumption increase of around 1000 Mtoe for 2040 (see Figure 1.1). Therefore, part of our future energetic mix will consist of gas turbine cycles.

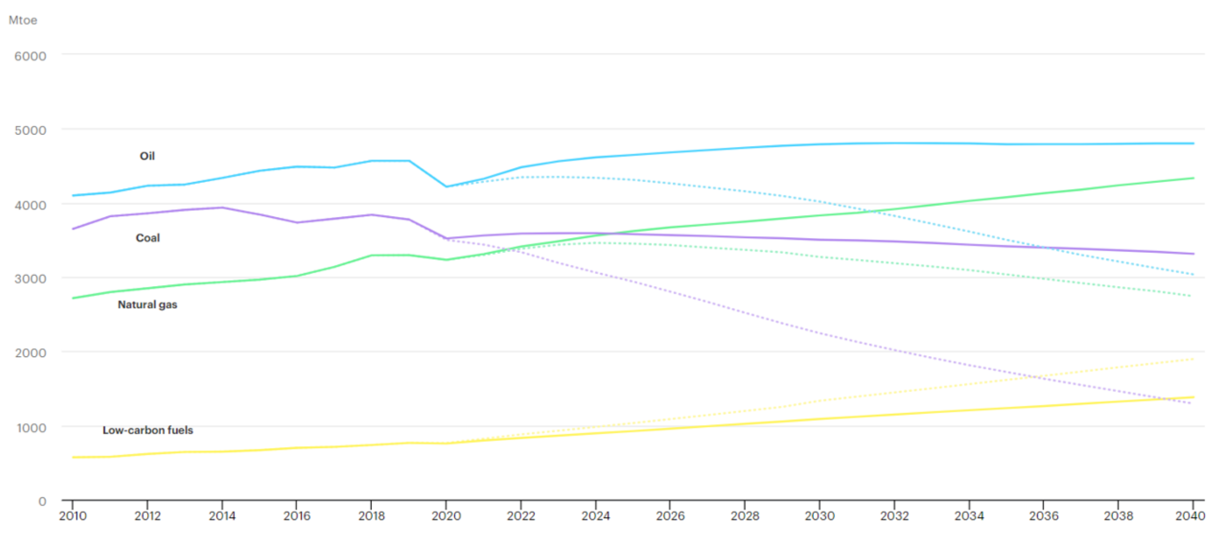

Figure 1.1: Evolution and prediction of the global fuel supply from 2010 to 2040 [2]. Natural gas features the most increasing trend.

Up to now, electricity has been produced in large power plants with an average and maximal load capacity of respectively around 250 MW_e and 1000 MW_e for pulverized coal boilers [3] and a maximal plant capacity around 700 MW_e for a conventional gas turbine combined cycle plant [4]. From that central production point, electricity is then delivered to every consumer by a single network. This kind of system is called 'centralised system' (see Figure 1.2(a)). However, it is unable to respond to the unexpected peaks of demand and is also not resilient in case of a breakdown of a critical transmission line [5]. Adding these drawbacks to the stochastic nature of renewable energy sources shows the need of a versatile alternative.

In contrast, a recent trend has been to focus on 'decentralised systems' (see Figure 1.2(b)) which consist of local and smaller power units (from few to several hundreds kW_e) located close to the point of consumption. It does not only eliminate the transmission and distribution losses but more importantly it increases the flexibility of the system by removing the dependency to the grid. Over recent years, decentralised units mostly include on-site renewable energy systems and Combined Heat and Power (CHP) units. The second type of system has the advantage of providing both electricity and heat (also possibly under the form of hot water) to local consumers. The idea is then to move from conventional boilers, used for example in residential buildings (whose demand is expecting to increase towards nearly 6000 TWh in 2040, which is two times more than in 2018 [6]), towards small-scale CHP units.

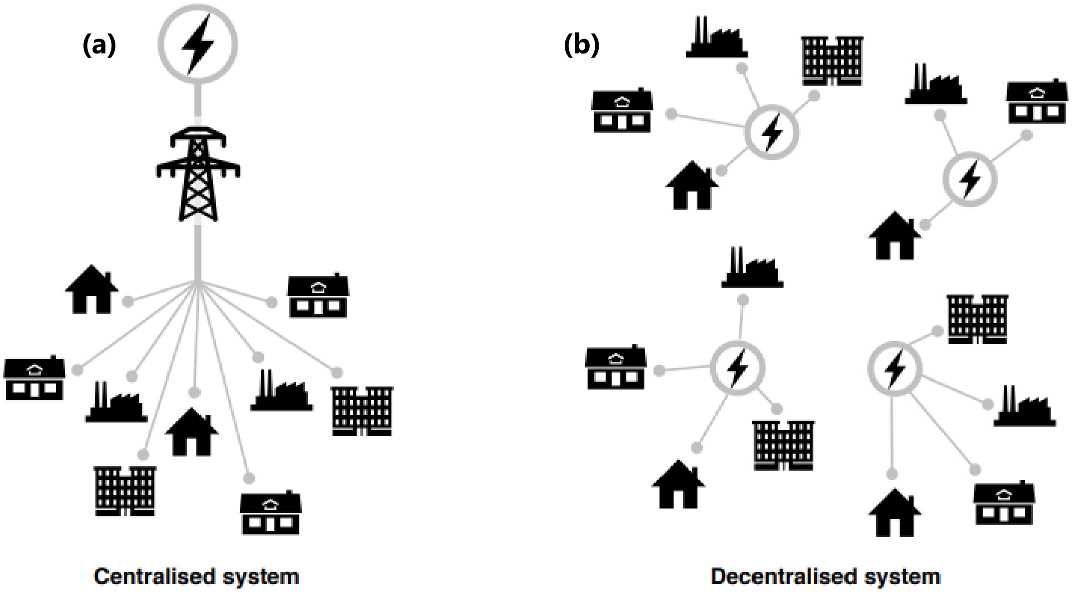

Figure 1.2: A centralised system consists of a single large power plant producing electricity which is transmitted to the consumers using a distribution network. On the contrary, a decentralised system is composed of several small-scale production units close to the consumption point. Figures come from [5].

With the purpose of helping the transition from a conventional centralised energy production to a cleaner and smaller decentralised production, micro Gas Turbine (mGT) cycles might be helpful. Their main advantage is their high overall efficiency while keeping the ability to fit the varying energy needs of a single or several housings [7]. Such cycles have several other benefits such as a high fuel flexibility, low pollutant emissions and low maintenance costs [8]. Nevertheless, downsizing the turbomachinery components can lead to a decrease of the electrical efficiency due to several losses like seal and tip leakages [9]. As it is the case for traditional fossil-fuel power plants, mGT are usually based on a Brayton cycle configuration where the unused heat is recovered as an useful thermal product of the cycle. This heat recovery allows conventional GT cycles (large power plants generating hundreds of MW_e) to go from an electrical efficiency slightly higher than 40% to an overall efficiency of more than 85% [4]. Although the potential overall efficiency reachable by a mGT cycle is pretty good (similar to that of a typical GT), heat supply is currently the main work field of current mGT units due to their limited electrical efficiency (around 30% for a 100 kW_e unit) [10]. This is due to the high temperature of their exhaust gases. When the heat demand is lower than the potential recovered heat (in summer for example), the overall efficiency of the mGT cycle significantly drops to the electrical efficiency (case of a zero heat demand scenario). From an economic point of view, this may lead to a non-profitable situation forcing the shut down of the unit [11]. As a consequence, running a mGT cycle is only profitable when heat demand is large enough. Increasing the electrical efficiency of that kind of system could considerably help its introduction into the energy market.

Carrero et al. [11] proved that introducing humidification into a mGT cycle is beneficial in terms of energetic efficiency. On the other hand, the exergetic efficiency is lower when injecting water. Nevertheless, despite the small increase in energy efficiency, this shows there is a potential for decoupling heat and electricity production in a humidified mGT cycle. Indeed in case of a low heat demand, the unused heat from the exhaust gases is used to evaporate water into the flow and increase the electricity production. Some work must still be fulfilled in order to find new humidification systems that could significantly increase mGT cycle electrical performance.

To conclude this introductory chapter, let us take a helicopter view. Burning natural gas in gas turbine cycles constitutes a large share of the world's electricity production. According to the IEA [12], 23.6% of the world's total electricity generation in 2019 was produced by natural gas (see Figure 1.3). This is the second highest proportion behind coal (with 36.7%), which is expected to decrease in the coming years in order to limit its associated significant greenhouse gases emissions. To sump up, natural gas and gas turbine cycles will keep playing a major role in the future energy production. Therefore, it is now essential to find new solutions and improvements in order to optimize this technology and make it cleaner and more efficient. Every small increment of efficiency goes in pair with fuel saving and is a little step towards a cleaner energy production.

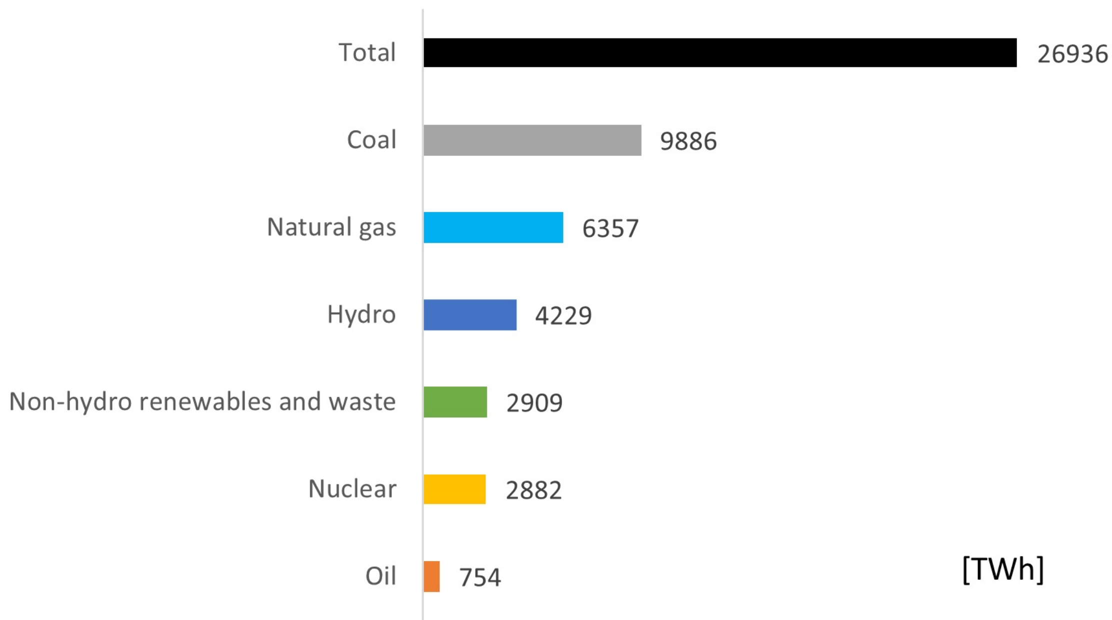

Figure 1.3: World global share of electricity generation in 2019 (data from the IEA [12]). Natural gas has the second highest contribution (23.6%) behind coal (36.7%).

Chapter 2

Research question & Methodology

The current Master Thesis treats the development of a numerical model of a humidified mGT cycle: the Maisotsenko sub-atmospheric inverted Brayton cycle (M-SAB cycle). Starting from scratch, every component has been implemented using Python. Using such a modular manner allows us to be flexible to add, remove or relocate any component. In order to deeply understand how the M-SAB cycle works, a sensitivity analysis is thereafter conducted using the final model as well as an exergetic analysis. Taking away from that investigation the best cycle performance, the results are compared to those achieved by other small-scale CHP commercial applications.

Numerical modelling

As a first step, a classical Inverted Brayton Cycle (IBC) has been modelled (see Figure 2.1). In chapter 4, the way each component has been implemented is meticulously presented and the validation of our model is demonstrated. As our work has been based on the numerical and experimental investigation from Agelidou et al. [8, 9], the validation is consequently established using their work as a reference. This latter is based on a modified EnerTwin which is a recuperated mGT, developed by MTT (Micro Turbine Technology) [13], intended to meet the energy needs of a single family household (with an installed capacity of around 1 kW_e).

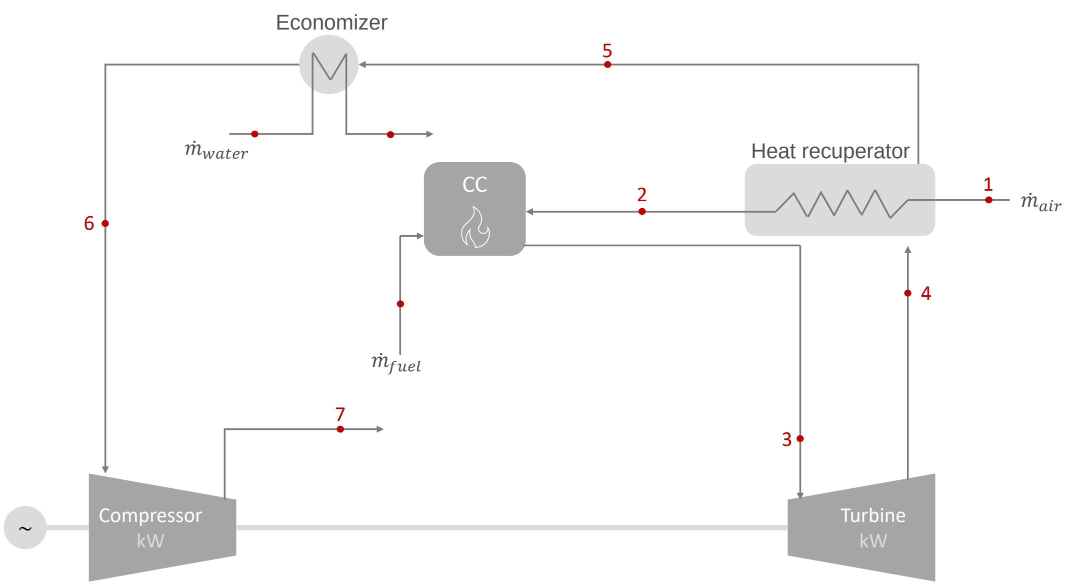

Figure 2.1: Scheme of the IBC.

The second model separately developed from the first one treats the Maisotsenko heat recuperator (see Figure 2.2). Our numerical adaptation, largely detailed in chapter 5, has been based on the numerical work carried out by De Paepe et al. [10]. The same paper is used as a comparison to the results achieved by our model.

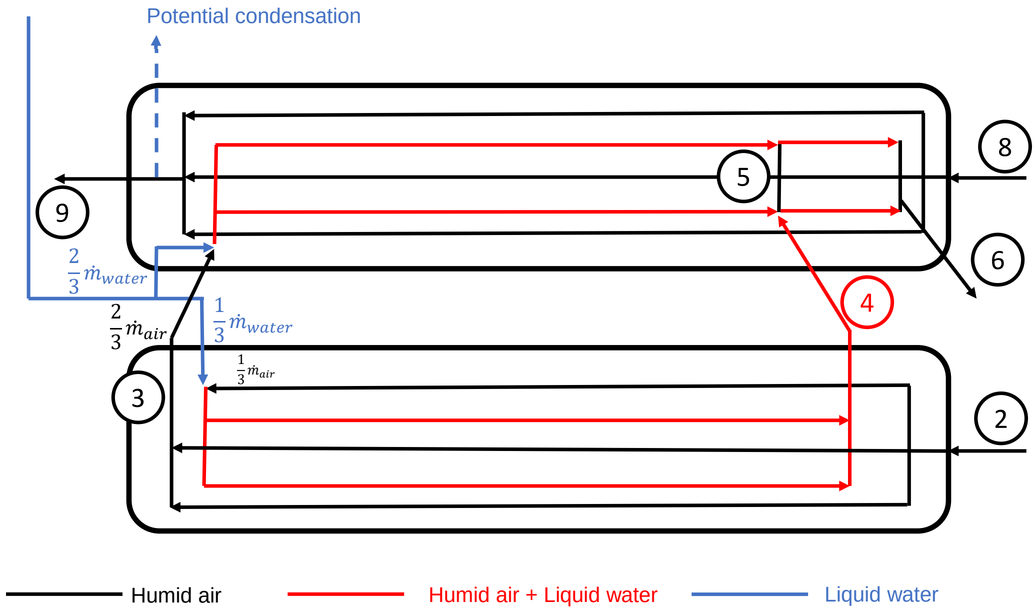

Figure 2.2: Scheme of the M-Cycle.

The final step of the numerical modelling is to merge the two models into a single cycle. More precisely, the conventional heat exchanger present in the initial IBC model is replaced by the M-power component. As specified in chapter 6, the merging implies the introduction of a preheater. The resulting and final cycle is shown on Figure 2.3. As the main goal of the introduction of the M-Cycle is to promote electricity production, our final model is adapted to another mGT. Indeed, the EnerTwin MTT mGT used in the IBC model is focused on heat production. This is demonstrated by its low electricity production which does not even account for one quarter of its heat production (1 kW_e compared to 4.1 kW_{th} [8]). Another consideration is that introducing humidity into cycles which feature very low power outputs is not economically profitable. Therefore, the final numerical model is adapted to another mGT: the Turbec T100 mGT. This unit is present at the VUB (Vrije Universiteit Brussel) laboratories and the introduction of a humidification system has already been studied by Marina Montero Carrero during her PhD thesis [5]. The unit nominal power output is 100 kW_e of electricity and 165 kW_{th} of heat. This is associated with an electrical efficiency of 30% and a thermal efficiency of 50%, which means an overall efficiency of 80%. Compared to the MTT mGT used in the IBC model, the Turbec T100 mGT has clearly better specifications for an application aiming at favoring the electricity production. It is important to note that even if our model is adapted to a particular mGT, the purpose of our work is to assess the thermodynamic potential of the M-SAB cycle in general. Potential technological issues related to the particular engine considered in our model might be ignored.

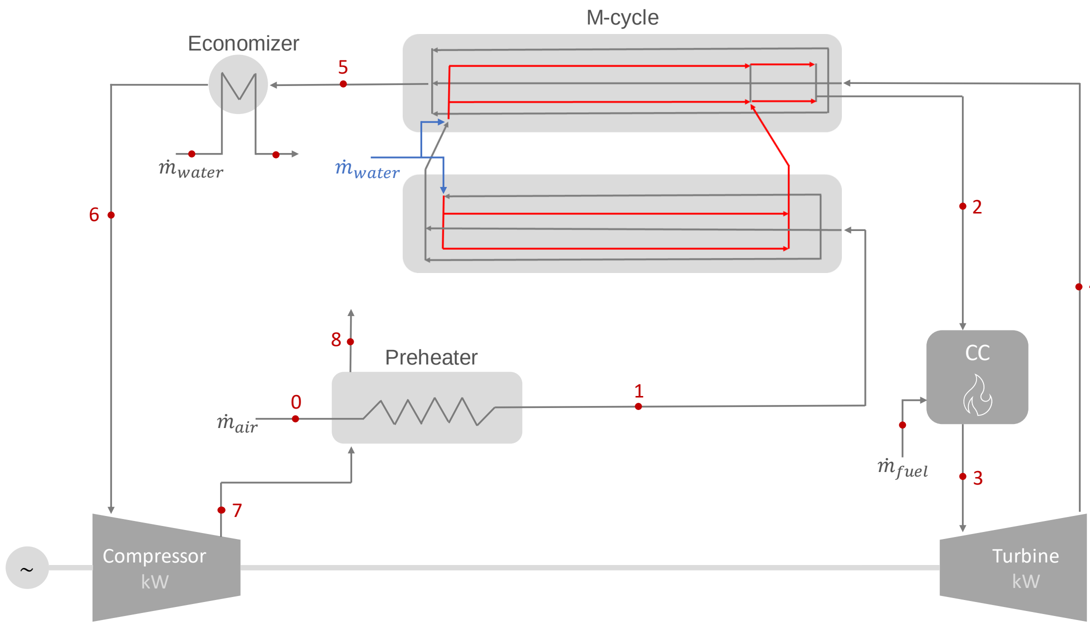

Figure 2.3: Scheme of the M-SAB cycle.

To our knowledge, only two numerical studies [14, 15] have been conducted on a reverse Brayton Cycle containing the M-power unit. On top of that, as covered in chapter 3, the first one ([14]) includes a solar preheater which is not part of our work and which changes considerably the cycle efficiencies. Indeed, more than complicating the cycle, introducing such a system in a mGT could increase substantially the overall cost of the installation. Additionally, a major advantage of mGT cycles is their flexibility. Therefore, adding solar energy into such a cycle would make it lose its interest compared to intermittent renewable technologies. As already mentioned, another solution to preheat the flow is considered in our model, taking advantage of the available heat in a preheater. The other study ([15]) analyses the M-SAB cycle as a low heat recovery system following a topping cycle, which is not the aim of our work. Our numerical analysis will consequently be the first of its kind.

Sensitivity and exergetic analysis

As soon as the merging process is completed, the next part consists in using the final version of our model to perform a sensitivity analysis (see chapter 7). By investigating how the M-SAB cycle reacts to different changes, an in-depth understanding of its behaviour is gained. The studied parameters are the performance parameters of the M-Cycle, the control parameters of the turbomachinery components, the initial conditions of the working fluid and the general design parameters of several components. Particular attention is placed on the evolution of the electrical and overall efficiency. This study is followed by an exergetic analysis (see chapter 8) to establish the thermodynamic limit of this machine.

Comparison to other technologies

As a last part, the performance of our model is compared to that of other commercial systems. The technologies of comparison must be relevant regarding the size and load capacity of our application. Indeed, it would not make sense to compare a mGT cycle with a powerful steam power plant. Therefore, the comparison is conducted with three different types of CHP units: internal combustion engines (ICE), other mGT CHP units or Stirling engines. In chapter 9, the comparison is followed by an examination of the design requirements needed to reach the best performance achieved by our model.

Research question

Let us finally wrap up this chapter by formulating our research question:

'***In which operating conditions can the combination of a mGT IBC with a Maisotsenko Cycle be competitive in terms of electrical and overall efficiency with other similar energy production technologies ?***'

Chapter 3

Literature review

The coming review starts by defining in detail the characteristics of mGT cycles and their associated pros and cons. Then a particular attention is paid to the IBC and more specifically to its advantages compared to a classical Brayton Cycle. The third part summarises the different ways of introducing humidity in a mGT cycle and the associated benefits. Thereafter, the concept of the Maisotsenko cycle is explained and its promising potential towards an optimal waste heat recovery is emphasized. Finally, the combination of the IBC with the M-power unit leading to the final M-SAB cycle is justified.

3.1 micro Gas Turbine

The term 'micro Gas Turbine' is usually used for an application ranging between 30 and 200 kW [16]. To this range must be added the single family units of a few kW. Several current mGT available on the market are listed in Table 3.1.

Table 3.1: Main specifications of different mGT present on the market. The electrical efficiency lies around 30%.

Manufacturer	Model	Nominal Power [kW_e]	Electrical efficiency [%]
Capstone Turbine	C30	30	26 [17]
Corporation	C65	65	28 [18]
	C200	200	33 [19]
Ansaldo Energia	AE-T100	100	30 [20]

Most of the mGT cycles follow a Brayton Cycle (BC) layout and constitute usually a cogenerative system. Thus, they produce both heat and electricity. The general layout of such a system can be observed on Figure 3.1. The air is firstly compressed in a compressor. The compression ratio depends on the nominal power output but is often between 3 and 5. mGT manufacturers generally use such low compression ratios to avoid multiple turbomachinery stages and/or specialised cooling that would induce higher costs [21]. Furthermore in most of the mGT, radial flow compressors are used since they allow to achieve a good turbomachinery efficiency even with small volumetric flows [22]. The compressed air is thereafter heated thanks to a heat recuperator (cooling at the same time the hot gases flowing out of the turbine) followed by the combustion chamber. The introduction of a heat recuperator enables to achieve higher electrical efficiencies by saving fuel thanks to a higher inlet temperature at the combustion chamber. The temperature achieved after the combustion corresponds to the inlet temperature of the turbine and is usually referred as the Turbine Inlet

Temperature (TIT). This is the highest temperature reached in the cycle. As presented further in this section, the maximum reachable TIT is limited by the resistance of the materials. After the combustion chamber, the fluid is expanded in a turbine which drives the compressor and produces electricity in the generator which is connected to the shaft. As explained before, the flow then heats the compressed air in the recuperator. Finally, the flue gases are cooled down in an economizer in order to get some heat back. This recovered heat allows the cycle to be considered as a CHP unit and comes usually in the form of hot liquid water (around 90°C to 100°C in order to be used for domestic or district heating [23]). The overall efficiency of such a cycle could reach more than 80% [16].

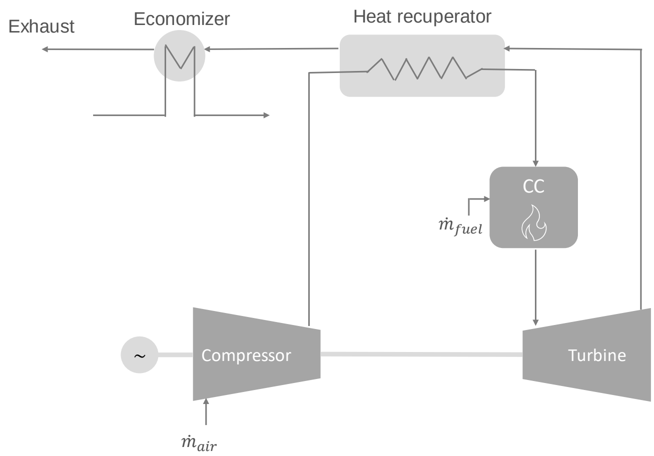

Figure 3.1: Schematic of a typical BC mGT.

As mentioned before, the TIT and the Turbine Outlet Temperature (TOT) are critical for the materials selection of the turbine and the heat recuperator. According to the U.S. Department of Energy in its study about Advanced Microturbine Systems [21], current ceramic turbines for mGT could sustain a TIT between 1038°C and 1093°C. This temperature range induces a temperature from 621°C to 677°C at the inlet of the recuperator, which could be sustained by stainless steel. If the TIT can be increased up to a temperature between 1093°C and 1260°C with advanced ceramic technologies, the resulting TOT would lie between 732°C and 788°C. A commonly chosen material for the recuperator in this case is the Haynes 230 alloys, which is 5.5 times more costly than stainless steel [21]. According to McDonald et al. [24], very advanced ceramic recuperators and turbines for mGT might sustain temperatures up to respectively 989°C and 1371°C. Still, the higher the TIT is (and consequently the TOT), the higher the price of the cooling technologies and materials to sustain these temperatures are. Thus, a satisfactory increase in efficiency must go hand in hand with the increase in temperatures to justify the associated increased investment costs. According to different mGT papers, the TIT usually lies around 900°C to 950°C [8, 10, 11].

According to Boukhanouf [16], conventional gas turbines have electrical efficiencies ranging between 30% and 40% while mGT electrical efficiencies range between 20% and 30% (but as shown in Table 3.1, the electrical efficiency may reach 33% for the C200 application [19]). There are several reasons for the reduced mGT electrical efficiency. Firstly, the main drivers of efficiency are the TIT and the compression ratio. In fact, high values of those parameters influence the efficiency positively. For the time being, gas turbines TIT are well above the mGT ones if both of them are made with typical gas turbine alloys. As a matter of fact, gas turbines use internal cooling whereas mGT blades are too small to allow manufacturers to use this technology at a reasonable price [22]. A lot of research is conducted on ceramic blades for mGT in order to increase their TIT. Concerning the compression ratio, mGT applications feature lower ones as explained above because of the cost of multistage turbomachinery. Finally, the tip leakage losses are relatively more important due to the downsizing of the turbomachinery components, which also have an impact on the electrical efficiency [9].

As mentioned earlier, the main goal of mGT systems is to achieve a distributed energy generation. According to C. Soares [22], mGT is, in competition with ICE (a detailed comparison of the two is made later in this section), the best suited technology for distributed power. Indeed, their modular electricity production, also called distributed electricity, does not rely on large transmission lines. In this case, the production units are located near or at the consumer's location. The main advantages she has listed are the following. Firstly, it provides a higher power reliability because it reduces or avoids outages for consumers using a distributed power unit. Not only for them but also for the consumers still served by the main grid, the power reliability is improved because there is less stress on the grid. Then, there is no need for new transmission lines that are costly and difficult to install, for instance due to the local resistance of people living close to the installation point. Furthermore, it decreases the reserve margins because of the lowered power level of the main grid. This latter should finally experience less peak demand. However, distributed generation also has disadvantages. To begin with, the costs for the equipment and maintenance are higher by unit power output. Indeed in centralised power generation, there are some economies of scale. The lifetime of mGT is also shorter (estimated to 10 years) [21]. Therefore to be economically viable, the electrical efficiency of the mGT should be greater than the grid efficiency (i.e. the mean electrical efficiency of the power units of the centralised power generation minus the losses due to transportation and transmission, which could be up to 30% in less industrialised countries [22]).

For the time being, the mostly used technology in those ranges of power is the reciprocating internal combustion engine. Its main advantage is its electrical efficiency that could reach 40% [16], compared to 30% for mGT, depending on the level of electrical power output. But mGT has several advantages compared to ICE. Because of its relatively low TIT and its relatively high air excess, it has lower NOx emissions [22]. The combustion chamber of a mGT cycle is sometimes even named as a low-NOx burner. As an example, the NOx content in the exhaust of an AE-T100 is below 15 ppm [20] and that of a Capstone C30 is below 9 ppm [17].

It also allows multi-fuel applications: it can operate with natural gas, sour gases (high sulfur, low BTU content), landfill gas, digester gas, and liquid fuels (e.g. gasoline, kerosene, and diesel fuel/heating oil) [22]. Furthermore, a mGT makes less noise, has lower vibration levels [25] and offers a compact size and a low weight per unit power [16]. It also features less balancing problems and requires less lubricant oil than ICE thanks to the absence of reciprocating and friction components [5]. Finally, as a cogeneration unit, the recoverable heat is high-grade and concentrated in the exhaust gases, while in an ICE it is distributed in different parts: cooling system, exhaust gases and lubricating system [5].

According to Boukhanouf, the latest introduction of packaged mGT provides similar capital costs as reciprocating ICE but with lower maintenance costs and higher availability [16]. Those advantages could offset for the lower electrical efficiency, so the interest for mGT is growing. Another benefit of mGT cycles is their high rotational speed thanks to their small size. This leads to a high conversion efficiency of the electrical power to the grid voltage [25]. Also by running the unit at partial load, the rotational speed can be decreased instead of changing the TIT and compressor air flow rate. This provides a higher partial load efficiency [25].

However, mGT cycles present a major drawback: their heat-driven use. As it was detailed in chapter 1, the reduced electrical efficiency limits their profitability when the heat demand is low. Indeed, mGT cycles are really good at producing heat while producing electricity. It can be observed from their high overall efficiency that can range between between 75% and 85% according to Boukhanouf [16]. In case of low heat demand, in order to keep the engine at high load, some of the heat has to be discarded which makes the mGT less attractive compared to ICE. In this situation, it is presently advisable to simply shut down the mGT units, which decreases their economic performance by not making any return on their still high specific capital cost [26].

3.2 Inverted Brayton cycle

Up to now, the majority of mGT cycle studies was focused on the Brayton Cycle. Different analysis have been conducted to assess its pros and cons and several alternatives aimed at improving its performance. Our work does not treat this particular layout but rather another one: the Inverted Brayton configuration. In our quest towards efficient small-scale CHP units, this layout appears indeed, as justified below, as a good opportunity to decrease the power outputs while keeping a noble efficiency.

The components are relatively identical to those used in a BC. As an example, Agelidou et al. conducted an experimental investigation to show the feasibility of running a conventional mGT, the EnerTwin developed by MTT [13], in the inverted mode using the same components [9]. Still, the order in which the flow faces each element is different. Instead of firstly being compressed to a higher pressure than the ambient one, the flow goes directly through the combustion chamber. Then follows the expansion in the turbine. So the working pressure of this cycle is below the atmospheric pressure, which explains why the IBC is also called as a sub-atmospheric cycle. Then finally comes the compressor which puts the flow back to atmospheric pressure. In order to take advantage of the available heat which would be wasted otherwise, a heat recuperator is usually present to heat up the initial cold flow going to the combustion chamber with the hot flow leaving the turbine. This heat recovery is mandatory to achieve a decent electrical efficiency. The described cycle is sketched on Figure 3.2. Naturally, other components can be introduced to optimize the cycle and maximize its performance.

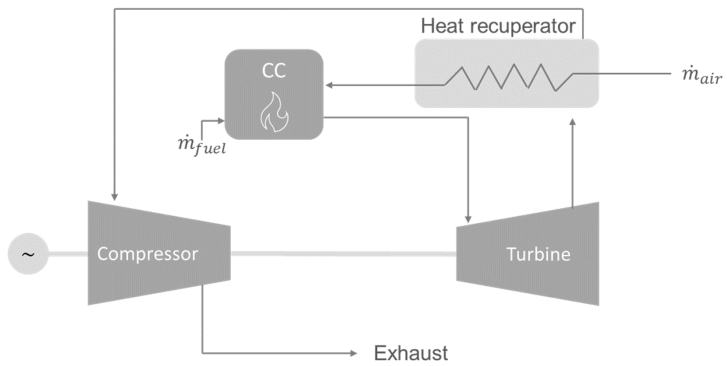

Figure 3.2: Schematic of a typical IBC.

In addition to the cited experimental investigation, Agelidou and its research team studied numerically the advantages of running a small-scale CHP unit in the inverted mode [8]. The term 'small-scale' means here a system able to meet the needs of a single family house with an electrical demand generally around 1 kW_e. Such systems with a small electrical power output undergo a reduced electrical efficiency due to higher losses in the small turbocharger components. The turbomachinery losses are for instance seal and tip leakages, Reynolds effects, surface roughness and tolerances [8]. But according to Agelidou et al., the inverted configuration allows to avoid this typical problem encountered when downsizing a conventional mGT. Indeed, these losses depend mainly on the volumetric flows. But the low pressure level of the IBC results in high volumetric gas flows. In this direction, the volumetric flows stay constant when downsizing from a BC to an IBC while the mass flow and thermodynamic works vary depending on the pressure level. Therefore, the same components can be used without deteriorating the turbomachinery performance. This allows finally to run a cycle with lower power outputs but with the same efficiencies. They achieved an electrical efficiency of 16% with an electrical power output of 1.05 kW_e and at the same time their overall efficiency reaches 78.5% corresponding to a thermal power output of 4.14 kW_{th}. Nevertheless, running a conventional mGT cycle in the inverted mode practically involves several challenges due to the sub-atmospheric pressure such as leakage and structural failure [9]. For instance, the sealing of the different components must be tested to pressures down to 0.2 bar. Another drawback of switching from the BC to the IBC configuration highlighted by the experimental investigation on the MTT [9] is the increased kinematic viscosity of the working fluid due to the lower compressor inlet pressure. This can have a negative impact on the turbomachinery efficiencies. In general, the different pressure level in the cycle might also change the operating point of the turbomachines influencing their efficiencies as well. Nevertheless as explained above, these efficiencies remain at a level comparable to that of a BC (between 75% and 85%).

Matsui et al. [15] described the IBC as a good solution to enhance the energetic and exergetic overall efficiency. The importance of maximising the waste heat recovery in such a configuration was then highlighted. However, this cycle layout is often associated with a reduced electrical efficiency compared to the BC configuration. The interest of the IBC as a low temperature cogenerative application was also proved by Bianchi et al. [27]. They have conducted a thermodynamic analysis on an IBC working with the gas exhausted from a topper power plant like a classical BC. The results show that the net specific work produced by the cycle is satisfactory (above 20 kJ/kg) when the TIT is higher than 500°C and the turbine outlet pressure below 0.7 bar. In order to increase even more this specific work, it was encouraged by the authors to decrease the Compressor Inlet Temperature (CIT). This is achieved in practice by recovering as best as possible the available heat in the flow between the turbine and the compressor thanks to a heat exchanger. But this is not the only location where useful heat can be retrieved. Indeed since the last component is a compressor (which increases the temperature as a side effect of the pressure increase), adding a second heat exchanger after it allows a thermal power output increase. The last two considerations show the convenience of the IBC as a cogenerative application for low temperature thermal load (around 90°C to be used in district or residential heating [23]). Several other papers also cover the use of a bottoming IBC as a waste heat recovery technique. We decided not to summarise them here as the purpose of our thesis is to work with an independent and unique cycle. Still, an interesting paper produced by Kennedy et al. studied the potential water condensation from the flue gases of a bottoming IBC located after an internal combustion engine [28]. Such phenomenon is interesting for us, since it is highly possible to appear and it improves the performance of our model. This condensation might occur between the turbine and the compressor thanks to the post-turbine cooling of the flow in the heat recuperator. Its main advantage is that it decreases the mass flow through the compressor and concurrently its power consumption. The parameters that most influence the start of condensation are the CIT, the outlet air humidity ratio and the fuel H-C ratio. The two latter affect the water content of the flow. The higher it is, the faster starts the condensation. 'Faster' in this case means that condensation starts at a higher temperature (less cooling is needed). Varying these last two parameters has almost no effect if condensation does not take place. But as far as it starts, a change of air humidity ratio from 10 to 20 g_{H2O}/kg_{air} gives an increase of 0.17% in cycle efficiency while increasing the fuel H-C ratio from 2 to 2.5 increases the cycle efficiency by 0.33%. Concerning the CIT, the lower it is the higher are the cycle specific work and efficiency. This effect is even more pronounced as far as condensation starts because it increases the amount of condensed water. Decreasing the CIT is therefore one of the key parameters towards higher performance. Another parameter influencing the start of the condensation is the turbine expansion ratio. Indeed when the pressure is reduced, a lower temperature must be reached to start the condensation of water out of the air. Then, condensation starts later when the turbine expansion ratio increases. But it must not be forgotten that this effect is small and increasing the turbine expansion ratio increases the cycle efficiency due to a higher turbine work (the compressor work also increases but a bit less). This effect is even more pronounced in the condensing region as the mass flow through the compressor is reduced.

The same paper [28] highlights two important parameters largely influencing the IBC performance: the heat exchanger pressure drop and the TIT. Decreasing the heat exchanger pressure drop of the gas side by 1 kPa increases the cycle efficiency of 0.37%. This effect does not depend on whether condensation occurs or not as it only influences the compressor pressure ratio. If the pressure drop is high, the compressor has to compress more the flow and its required power then increases. Concerning the TIT, increasing it from 700°C to 800°C goes in pair with a 0.89% increase in cycle efficiency. Let us recall that this temperature is limited by the resistance of the materials of the components as presented in the previous section.

Henke et al. performed a numerical study of an IBC which includes exhaust gas recirculation (EGR) as well as two heat recuperators and two economizers [29]. Their results demonstrate that using EGR gives a total efficiency increase of 10% to 15% in absolute points. But on the other side, it decreases the electrical efficiency by 0.5% to 1% absolute point due to a higher compressor inlet temperature. This latter comes from a higher inlet temperature of the cycle leading to a reduced heat exchange in the first heat recuperator between the turbine and the compressor. As mentioned in the work from Kennedy et al. [28], the increase in overall efficiency is even more pronounced when condensation takes place in the exhaust gases. Their paper also highlights once again the importance of the CIT on the electrical efficiency. To increase it, the mentioned temperature should be as low as possible. This is done in their work by including an additional heat recuperator. One must still pay attention to the fact that the induced pressure drops inside this additional component has not a bigger detrimental impact that the gain of decreasing the CIT. In a BC, the CIT directly depends on the ambient temperature. Therefore, the impact of this parameter on the electrical efficiency is quite important in that configuration. Running a BC in hot external conditions is consequently less interesting. This dependency is removed when using an IBC as the CIT mainly depends in this case on the amount of heat recovered after the turbine. This shows one more interest of maximizing this waste heat recovery.

Based on the work from Henke et al. on the introduction of EGR inside an IBC [29], Agelidou et al. confirmed what has been proved by showing an equivalent positive impact on the overall efficiency (from 78.5% to 88% with respectively an EGR rate[1] of 0% and 79%) [8]. But at the same time, the electrical efficiency, which is already

[1]Mass fraction of the exhaust flow which is deviated towards the inlet of the cycle.

quite low, decreases by 0.5% absolute points.

Another important asset of the IBC is that the combustion occurs at atmospheric pressure. This leads to a simpler design and the use of cheaper materials for the combustion chamber [30]. For instance, no fuel gas compressor is needed, saving its previously required compression power consumption [9]. In addition, the exhaust gas temperature of an IBC is colder than for a BC [29]. These two last observations explain why the overall efficiency of an IBC is higher than that of a BC, assuming here the same power output for both cycles [29].

Alongside these advantages, the reduced gas pressure difference in the heat recuperator induces a lower mechanical stress on its materials [29]. More generally, the mass flow in an IBC is lower than in a BC which, with the low pressure level, leads to reduced stress on the components of the cycle.

3.3 Humidified mGT cycles

Despite a variety of assets, the low electrical efficiency of mGT cycles, which is also the case for the IBC configuration, is still a barrier to their commercial success. In order to boost their market penetration, they first need to become more economically attractive compared to other applications as ICE. Indeed, both technologies feature the same investment cost (between 1500 and 2500€/kW according to [25]), but the electrical efficiency is higher for an ICE as specified above. To tackle this issue, research has been conducted on improvements of the efficiency and effectiveness of respectively turbomachines and heat exchangers, higher combustion temperature with more robust materials for the combustion chamber and alternative cycle layouts. In this last research area, one potential solution is the introduction of water in the cycle. The resulting cycle is called *humidified mGT cycle*. The idea there is to use the wasted heat from the exhaust gases to vaporize water steam into the working flow. More than potentially increasing their electrical efficiency, it could also boost their flexibility by decoupling electricity and heat production. Water injection could therefore be a good possibility to improve the electrical performance of the IBC using the available heat of the flue gases. Even though the positive impacts of humidification have already been theoretically highlighted in several papers, experimental validation is still missing as well as commercial applications [25]. One must take notice that below a value of 20 kW_e, water introduction is not very attractive as it unnecessarily increases the complexity and costs of the cycle [5].

The current section reviews several humidification techniques with their pros and cons. A specific focus is then taken in the next section on the Maisotsenko saturator and its potential applications.

Looking initially at the classical recuperated Brayton Cycle (as depicted on Figure 3.1), the main idea behind humidifying it is to inject water after the compressor. In this way, the mass flow rate through the compressor does not change while the one through the turbine increases. Therefore when keeping the same rotational speed, the turbine power is higher while the compressor work is the same. Taking into account that compressing a liquid (because the water must be injected at a same pressure range than the compressed air) is less energy consuming than a gas, the final result is a gain in electricity production.

Introducing water in the cycle also increases the heat capacity of the working fluid. Benefit can be gained by injecting the water before the heat recuperator. More than the cited increased heat capacity, humidification lowers the recuperator cold inlet temperature. Both effects lead to a higher heat recovery in that component [25].

Another positive side effect of humidification is the low NOx content in the exhaust gases. Indeed, the effects of water steam on NOx production depend on two mechanisms: chemical and physical. The first effect is related to the change in concentration of hydroxyl radicals involved in the formation of NOx [31]. The second effect has to do with the dilution of the combustible mixture. This goes in pair with a lower flame temperature and a subsequent lower NOx production. Nevertheless as mGT cycles are usually already using a low-NOx burner, the effect of NOx reduction thanks to humidification is not considerable.

Diving a bit deeper into the particular types of humidified mGT cycle, the review article from De Paepe et al. [25] presents three classical layouts. Depending on the state at which water is introduced as well as on the technology used for it, the different options are:

1. To inject liquid water that will fully evaporate by mixing.
2. To directly inject steam.
3. To inject liquid water in a saturation tower with a water recovery loop.

Based on the mentioned article [25], these three main configurations (see Figure 3.3) are firstly reviewed before presenting the particular application of the Maisotsenko saturator in the next section.

Liquid water that will fully evaporate can be injected at different locations in the cycle, offering then different benefits. As already explained before, the classical way is to introduce it between the compressor and the recuperator. This allows an increase in the turbine power and a colder temperature at the entry of the recuperator leading to a better heat recovery. If the water is introduced before the compressor, the advantage of having a lower turbine mass flow rate is lost. The purpose in that case is then to reduce the compressor work by decreasing the temperature at its inlet thanks to evaporative cooling. This can be done either using inlet air cooling (IAC) or wet compression. The difference between the two is the presence of water droplets inside the compressor for the second method. On one side, this reduces even more the compressor work. On the other side, water droplets can damage more easily the compressor blades. Both techniques increase the specific power output but do not enhance the waste heat recovery. As demonstrated by Comodi et al. [32] in their work on a Turbec T100 HP mGT, hot ambient conditions lead to a loss of electrical power output. But under the same conditions, IAC appears to be particularly effective in increasing the net electrical power by up to 8.5% and the electrical efficiency by up to 1.6%. Finally, water could be injected directly in the combustion chamber. The main effects are a lower combustion temperature going in pair with a lower NOx production and a higher power output. As for the typical humidified cycles, introduction of water increases the specific heat capacity of the working flux. Then, burning this air-vapor mixture gives a more uniform temperature distribution inside the combustion chamber. It consequently leads to a lower probability of NOx production that is associated with the presence of hot spots [33]. However, these effects must be nuanced as firstly the NOx production is already low in dry mGT applications. Secondly, this requires a higher fuel consumption leading to a lower electrical efficiency even if the power output increases.

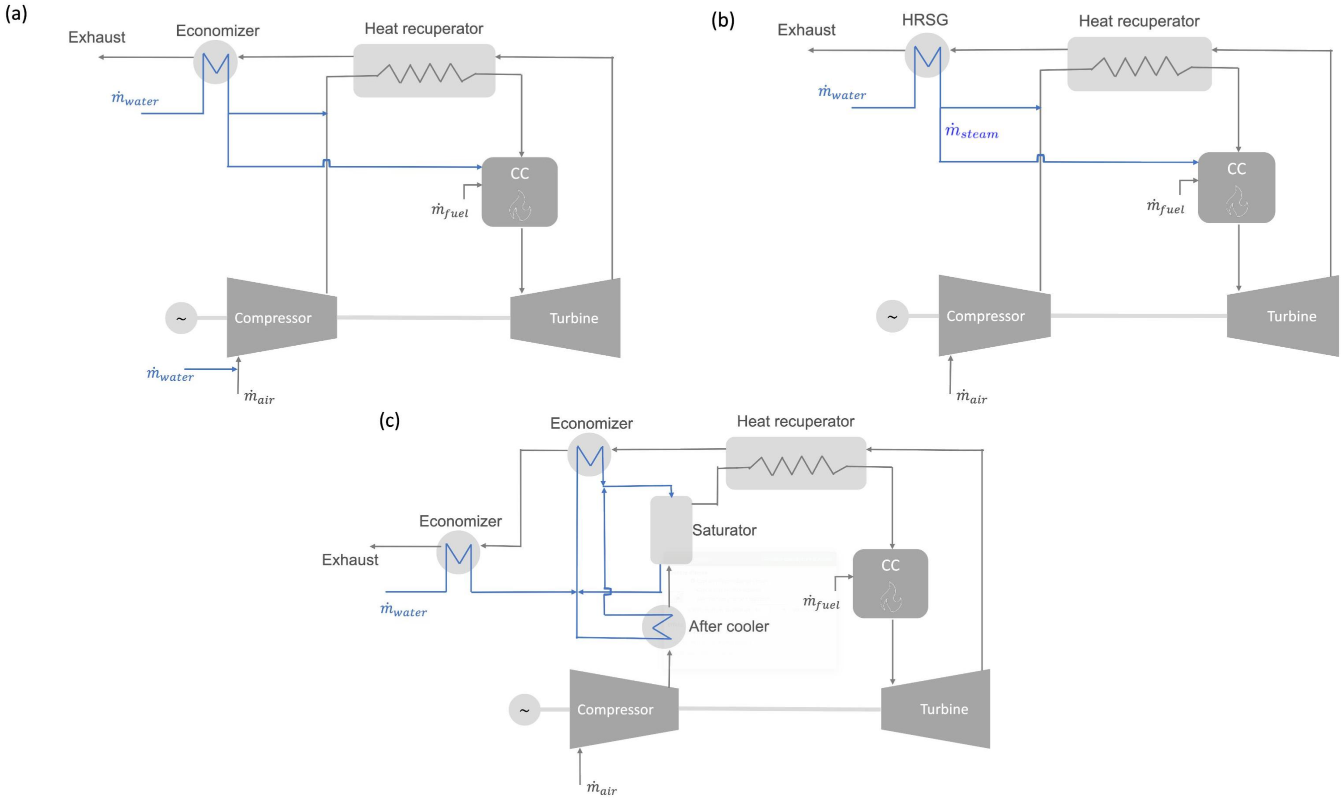

Figure 3.3: Overview of the 3 different types of layout for a humidified mGT cycle. (a) Cycles with injected water that fully evaporate by mixing (b) Cycles with steam injection (c) Cycles with injected water in a saturation tower with water recovery loop.

Water can also be directly introduced in the form of steam using the remaining heat in a Heat Recovery Steam Generator (HRSG). The steam is then injected either in the compressor outlet or in the combustion chamber. It has been proved numerically by Lee et al. [34] (working with a 30 kW_e commercial mGT), by the research group at VUB [35] (which also performed experimental validation on a Turbec T100 mGT) and other researchers that it has a positive effect on the electrical efficiency. The increase is higher if it is injected at the recuperator inlet. Injecting steam there instead of water offers a gain in electrical efficiency. Meanwhile, water injection still allows to provide some heat as a thermal power output. This is not the case with steam injection as this heat is used in the HRSG. As explained by Lee et al. [34], injecting water or steam in the combustion chamber reduces the electrical efficiency while giving more useful heat.

Lastly, the third possible configuration is the introduction of a saturation tower between the compressor outlet and the recuperator inlet. The resulting cycle is called micro Humid Air Turbine (mHAT). If additionally an aftercooler is included (as shown on Figure 3.3(c)), the cycle is called mHAT-plus. The saturation tower aims at saturating the air by evaporating water using the required energy from the excess liquid water. The remaining water leaving the tower has then been cooled and will be heated again in the heat recovery loop. The main interest of using a saturation tower is the associated low exergy destruction. Indeed, the evaporation of water gradually takes place following the variation of temperature. This consequently narrows the temperature difference and so the destroyed exergy. This is for example not the case in a classical HRSG where steam is created at constant temperature leading to a higher temperature difference with the exhaust gases. Therefore, converting a dry mGT cycle into a mHAT features a good potential in increasing the cycle efficiency. A very complete experimental analysis has been conducted by the VUB research group which transformed a Turbec T100 dry mGT into a mHAT [5, 11, 36]. This shows that the electrical efficiency can be risen up to 4.2% absolute points. This technique of introducing a saturation tower with water recovery loop was highlighted by De Paepe et al. as the best option for humidified mGT cycles [25]. Even though studying the economic potential of our cycle is out of the scope of our work, it is worth noting that Montero Carrero et al. showed that a potential investment into a mHAT could be interesting but still depends on electricity and gas prices as well as the demand profile of the customer [37].

Another more advanced humidified cycle configuration has been investigated by Wan et al. the BAHAT cycle [38]. Their purpose is to enhance the plant electrical efficiency by adding an IBC as the bottoming cycle of a mHAT, therefore expanding to a pressure lower than atmospheric pressure. Their simulation of the BAHAT cycle shows an improvement of the electrical efficiency of around 2% compared to a classical mHAT cycle. This comes mainly from a reduced compression work thanks to a lower inlet temperature of the exhaust compressor. Another point of interest to reduce the work of this second compressor is the introduction of a condenser just before it. Indeed as the compressor is positioned after the humidification system, it faces a higher mass flow leading to a higher compressor power consumption. Consequently, water condensation appears as a good solution to limit it. Nevertheless, even if this cycle theoretically improves the electrical efficiency, it is recorded as too complex and expensive for a humidified mGT application by De Paepe et al. [25].

One must take care that when speaking about efficiencies, (almost) only energy efficiencies were mentioned until now. But it is also essential to investigate the effect of humidifying a mGT cycle on the second law efficiencies, also termed exergy efficiencies. The latter take into account the quality of the energy. For example, a huge quantity of heat at low temperature could constitute a big quantity of energy while its exergy content is poor. To this extent, Montero Carrero et al. conducted a thermodynamic assessment of a mHAT cycle based on the Turbec T100 mGT [11]. For this purpose, using Sankey and Grassmann diagrams respectively for enthalpy and exergy flows allows to analyse how energy is distributed between the components and where exergy is destroyed in the cycle. The dry BC working as a CHP unit features a cogeneration efficiency of 79.5% of which 30% comes from the electricity production and 49.5% from the recovered heat. However, its exergy efficiency accounts only for 35.7% (with a contribution of 29.3% and 6.4% respectively from the electricity and heat power output). The introduction of water which aims at increasing the electrical efficiency by using the available heat from the flue gases provides a 1.4% absolute increase for this latter efficiency. On the other hand, the second law efficiency drops to 30.6% (fully coming from the electricity output). By taking a look to the Grassmann diagram, the component where the most exergy is destroyed can be identified. For example, because of the increased water temperature at the entry of the economizer due to the saturation loop, the remaining exergy content inside the flow going to the stack is bigger for the mHAT cycle (19 kW) than for the dry mGT cycle (3 kW). Some more examples are presented in the paper: the exergy destroyed in the saturation tower due to water evaporation, the increased destruction of exergy inside the recuperator as a consequence of the greater temperature difference between hot and cold sides, etc. Still by looking at the total exergy destroyed relatively to the exergy input, it is very close for both cycles. Thus when no heat is required, the mHAT cycle contributes to a higher flexibility while still using the same proportion of the exergy input. To sum up this short analysis, the discussed paper shows the importance of looking at both energetic and exergetic flows and efficiencies inside the cycle. It has also shown that running the T100 mGT in CHP mode leads to higher efficiencies (both energetic and exergetic). This should then be the case as often as possible. But in the case of a low heat demand, it has also been demonstrated that water injection allows to take advantage of the unused heat to increase the electrical efficiency of the system.

In parallel of pointing up the positive consequences of the introduction of humidification in a mGT cycle, it is also essential to display the negative ones. The review of these limitations is still based on the article from De Paepe et al. [25].

First of all, injecting water after the compressor aims at increasing the turbine mass flow rate compared to the compressor one. This asymmetry creates a mechanical stress on the shaft which can possibly lead to rotor instabilities. Nevertheless, this additional load has been tested experimentally, among others for the mHAT case [36], and does not lead to any problem. Another consequence of the two different mass flows is the shifting of the operating point. The turbine is usually choked which determines the maximum mass flow rate. But since some water is injected after the compressor, it means that this latter component faces a reduced mass flow rate. This goes in pair with a lower surge margin. This is even more critical when operating at constant rotational speed as the speed lines are quite flat.

A second limitation is related to the potential addition of new components (heat exchanger, saturation tower, etc). This might firstly produce additional pressure drops significantly impacting the performance of the mGT which features usually a rather low pressure ratio. In the case of an IBC, if several components with non-negligible pressure losses are introduced before the turbine, this might limit the mass flow rate and consequently the electrical power output of the cycle. Secondly, the additional volume occupied by the working flow must be considered. Indeed, if the volume is too high this can lead to compressor surge during transitory regime like a shutdown. The control system must then be adjusted which increases the complexity of the previously easily operated system. Additionally, the introduction of pressurised volumes apart from the mGT casing (like a saturation tower) implies stricter safety measures increasing the investment cost of such application.

The reduced NOx emissions from the combustion thanks to the presence of water has already been pointed out. Nonetheless, it can also affect the flame stability inducing an incomplete combustion and associated CO emissions. One must thereby be careful to remain below acceptable limits. A possible action is to take advantage of the flexibility of mGT systems by changing the fuel composition. Marina du Toit et al. studied the influence of burning H_2 - CH_4 fuel blends in a modified MTT EnerTwin mGT allowing for the enrichment of CH_4 with added H_2 [39]. They revealed that burning a mixture of 15% and 85% in volume respectively for H_2 and CH_4 reduces the CO emissions from 47 to 33ppm compared to pure methane combustion. This comes mainly from the combustion of the carbon-free fuel fraction. The energy efficiency also slightly decreased from 12.75% to 12.32%.

Concerning the effect of water on the materials, one could directly think of corrosion problems. These are critical in the hot side of the recuperator which is also the most expensive component. Adding water might then reduce its lifetime and that of the mGT in itself. Running the cycle with a lower temperature there could be a potential solution but it would also downgrade the cycle performance. Going back to the recuperator, adding water was presented as a way to increase the recuperated heat. However when switching from a dry to a wet configuration, the heat exchange surface is the same. This might prevent a complete heat recovery or it requires a redesign of the recuperator.

Eventually, the quality of the injected water depends on the specific cycle. Each type of humidification requires a dedicated water make-up plant and must bear the associated costs. Water of lower quality can be used in cycles using a saturation tower as not all the water will evaporate, keeping non-volatile contaminants in the liquid phase. For the two other types of cycle, fully demineralised water must be used. Still the water make-up cost is rather low compared to the investment required by a humidified mGT.

3.4 Maisotsenko saturator

Despite the different humidified cycle layouts covered in the literature, their commercial development is still limited [5]. The development of a best-performing heat recuperator might help to progress into improving mGT cycle efficiency, consequently increasing their profitability. Furthermore, it was highlighted that the performance of the IBC highly depends on its ability to recover the available heat between the turbine and the compressor. Improving it might reinforce the interest for this particular mGT cycle layout. To this end, the Maisotsenko Cycle is a promising thermodynamic conception aiming at increasing the waste heat recovery by exchanging heat while taking advantage of the psychrometric energy available when evaporating water in the air [40]. This energy is called the latent heat of evaporation (or vaporization). The M-Cycle is then a humidified heat recuperator. Combining heat exchange and evaporative cooling gives to this component the ability to cool the working gas to the dew point temperature instead of the wet-bulb temperature [40].

The idea of the M-Cycle dates back to 1976 and the work of Maisotsenko [30]. The same author is the first to introduce this particular component in a power cycle application, originally called the 'Maisotsenko Combustion Turbine Cycle (MCTC)' [40]. In the recent literature, the introduction of the M-Cycle into a conventional BC layout is also called the Maisotsenko Brayton Cycle (MBC). Its configuration is represented on Figure 3.4(a). Its overall efficiency reached around 60%. Compared to the previously developed Humid Air Turbine (HAT) cycles, the MBC has the advantage of decreasing the number of components used in the cycle. Indeed, a HAT Brayton cycle firstly includes a heat recuperator to preheat the compressed air before entering the combustor with the heat available from the turbine exhaust gases. But it also has a saturation tower to humidify the flow before entering the turbine and an economizer to further cool the turbine exhaust gases after the heat recuperator. All of these components are included into the single M-Cycle saturator. Reducing the number of components reduces considerably the complexity of the cycle, the capital cost of the technology as well as the pressure drop in the cycle. Consequently, the Maisotsenko Cycle features a cost-effective solution towards the development of humidified mGT cycles.

Based on the work from Maisotsenko, the introduction of the M-power component into conventional cycle layouts has been further studied. Reyzin [33] showed that replacing the conventional heat recuperator in a BC with the M-Cycle humidified heat recuperator allows to reach an overall efficiency of 80%. Zhu et al. [41] recently deepened the analysis of the MCTC including an inlet evaporative cooler by showing the interest of using it with biogas. The exergy efficiency of a biogas-fueled MCTC could be increased compared to conventional GT by 10% or 52% in relative terms respectively when the methane volume ratio in the biogas is 0.9 and 0.45. Saghafifar and Gadalla [42] studied the influence of several parameters on the MBC such as the air saturator degree of humidification. They proved that the introduction of an air saturator is more beneficial in terms of exergetic overall efficiency (with an increase of 7% in absolute points) compared to a conventional heat exchanger. Depending on the running parameters of the power plant, the efficiency of the MBC might also overcome the one of the HAT cycle. The same authors analysed the use of the MBC as a bottoming cycle to a topping classical BC compared to a case with a bottoming cycle containing a conventional air heat exchanger. One must pay attention to the fact that in the literature when using a Maisotsenko Cycle as the heat recuperator for the bottoming cycle, it is sometimes called 'Maisotsenko Bottoming Cycle' and has therefore the same acronym as the Maisotsenko Brayton Cycle. In order to distinguish the two cases, the complete combined cycle using a classical BC followed by a MBC is called Maisotsenko air bottoming cycle (M-ABC) [30]. This combined cycle layout is displayed on Figure 3.4(b). Saghafifar and Gadalla also have shown that using the MBC as the bottom cycle leads to an efficiency enhancement of 3.7% [43] and it constitutes the most cost effective combined cycle configuration with a levelized cost of electricity of 64.41 US$/MWh [44]. Other papers take in-depth look at the optimised conditions for this bottoming cycle. However, since our work is focused on mGT applications, we will not go further on that application of combined cycles. Back to the MBC, Chen et al. [45] optimised its power and efficiency and showed better performance compared to traditional regenerated Brayton Cycles. All the cited papers highlight the theoretical potential of the introduction of the M-Cycle in several GT cycle layouts. Still, experimental validation is required.

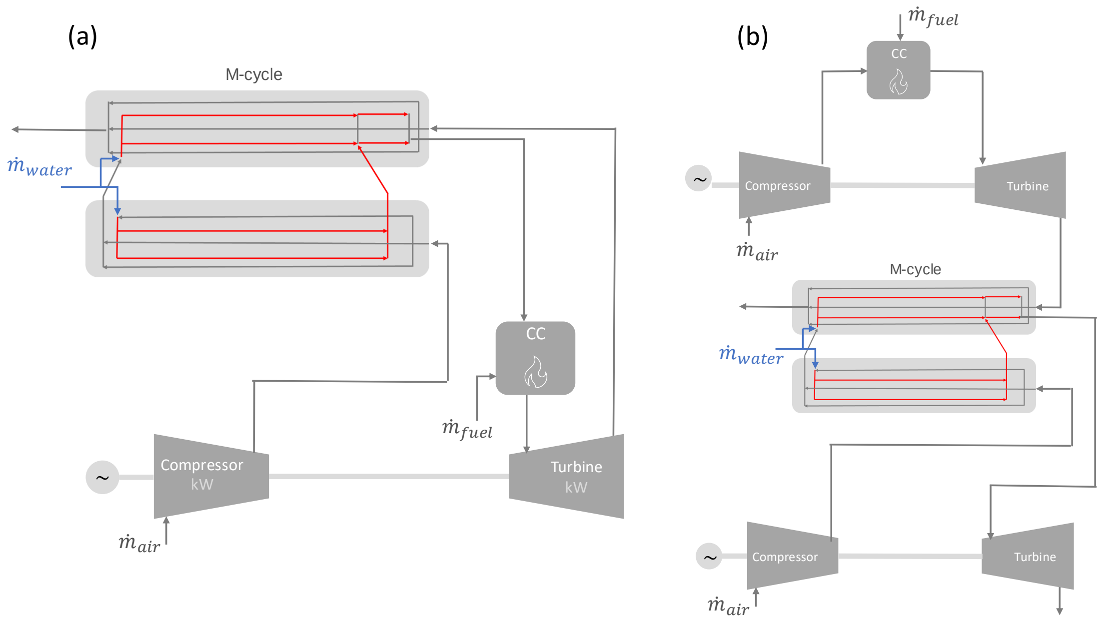

Figure 3.4: Investigated cycle layouts containing the M-power cycle: (a) Maisotsenko Brayton Cycle (MBC) or Maisotsenko Combustion Turbine Cycle (MCTC) and (b) Maisotsenko Air Bottoming Cycle (M-ABC).

Furthermore, De Paepe et al. [10] developed a numerical model of the MBC applied on a mGT scale with the Turbec T100 (a 100 kW$_e$ mGT). The results are promising and show that using the M-power cycle leads to the highest heat recovery with an electrical efficiency of 42.1%. Still, this latter efficiency is associated with a high wet-bulb effectiveness of 98%. This might constitute a technological challenge for the practical development of the cycle. In the same paper, a sensitivity analysis is presented about the impact of various inputs.

Even though our analysis is centered on gas turbine power cycles, the interest for the M-saturator and its dew-point evaporative cooling goes beyond that field. The two other fields are heating, ventilation and air-conditioning (HVAC) systems as well as cooling systems. The paper produced by Mahmood et al. [30] is a complete review of the different possible applications. We are not going to develop more here the other systems than the M-Cycle conception in gas turbines.

Now, the reader might wonder how the M-Cycle is composed and how it works. Its purpose is to cool a flow on one side while heating and humidifying/ saturating another flow on the other side. In gas turbine applications, the relevant flows are most likely a flow of air to be heated and saturated and the flow of flue gases to be cooled. As already mentioned, the specificity of the M-Cycle is the ability to cool the flue gases until the dew point temperature instead of the wet-bulb temperature which is usually reached [30]. On Figure 3.5 are illustrated two conventional ways of cooling: direct evaporative (or isenthalpic) cooling (DEC) and indirect evaporative (or sensible) cooling (IEC). Both of them feature a cooling limitation equal to the wet-bulb temperature of the initial flow.

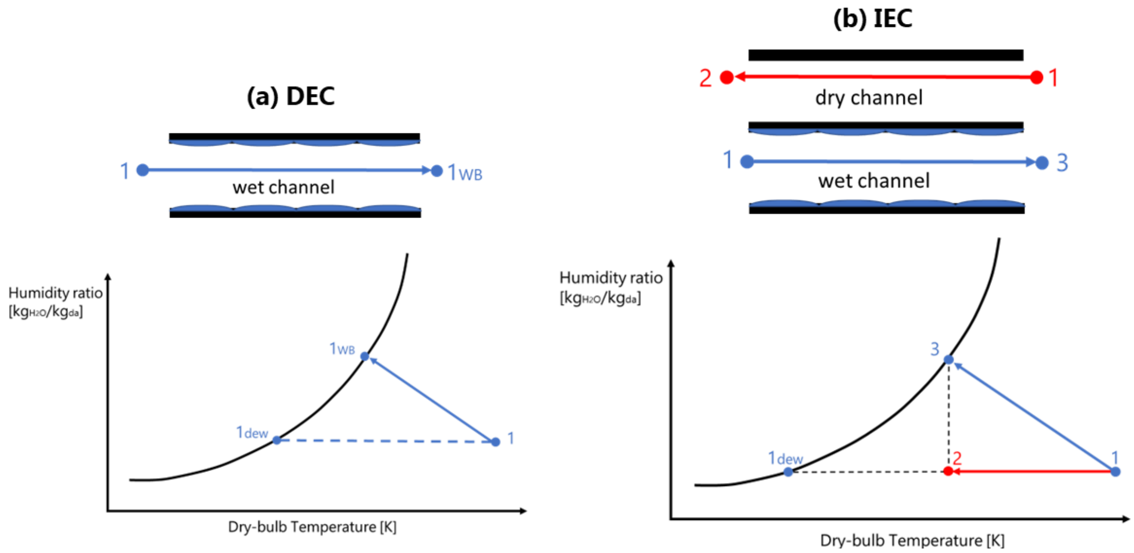

Figure 3.5: The conventional cooling techniques have a cooling limitation equal to the wet-bulb temperature of the initial flow as shown on their associated psychrometric chart.

Before immersing ourselves in the functioning of each cooling technique, it might be useful to recall the difference between wet-bulb and dew point temperature. The first one is expressed as the lowest temperature of adiabatic cooling of air. In other words, this is the saturation temperature reached when evaporating water into moist air. On the other hand, the dew point temperature is the temperature of moist air reached when saturating it while keeping the same pressure and water content.

The principle of the DEC is to decrease the temperature of the air by using its heat content to evaporate water in it. As no heat is added or removed, the process is adiabatic. The water is consequently evaporated at the wet-bulb temperature of the air [40]. This latter is also the temperature to which the flow is cooled from its initial temperature to saturation ($1 \rightarrow 1WB$ on Figure 3.5(a)). Concerning the IEC, the flow to be cooled is separated in a dry and a wet channel. The wet side absorbs heat from the dry side by evaporating water in the air ($1 \rightarrow 3$ on Figure 3.5(b)). This allows the flow on the dry side to be cooled, without increasing its water content, to the wet-bulb temperature of the initial flow from the wet side ($1 \rightarrow 2$ on Figure 3.5(b)). But as here the same initial flow is considered for both channels, the limitation is identical to the DEC [40]. To overcome this latter, the concept of the M-Cycle is to use the same principle of having a dry and wet side as the IEC but with a slightly different configuration.

In comparison, you can see on Figure 3.6 how the M-Cycle works. It is composed, like the conventional IEC design, of two channels: dry and wet. The main difference is that the cooled flow going out of the dry channel (state 2) constitutes the inlet flow of the wet channel. In other words, the stream in the dry channel is cooled by the same stream in the wet channel. This allows to cool the flow in the dry channel ($1 \rightarrow 2$) below its initial wet-bulb temperature, ideally to its dew point temperature. As for the IEC, the dry channel flow is cooled to the wet-bulb temperature of the initial wet channel flow. In this case, the latter is then the cooled dry channel flow itself. Consequently, the concept can be seen as an iterative sequence of states where the dry channel flow is cooled to the wet-bulb temperature of this same resulting flow. As mentioned already, the iterative sequence is supposed to converge towards the dew point temperature of the initial flow. Simultaneously, the dissipated heat is recovered in the wet channel where the air is heated and saturated ($2 \rightarrow 3$). The evolution of the temperature and water content in that channel is based on the fact that humid air can accumulate more water if its temperature increases. So the wet channel can also be seen as a succession of states following the saturation curve where the air is heated and then saturated.

The presented design allows to work only with one single input flow which then gives two output flows. But the heat recuperator in a mGT cycle is usually composed of two inputs flows, one to be heated while the other must be cooled. The design of the cooling system is then adapted by introducing a new dry channel as shown on Figure 3.7. This gives the possibility to cool down the incoming hot flow (state 4) in the upper dry channel, without adding any humidity inside, to the dew point temperature of the other incoming cold flow (state 1) in the lower dry channel. In a gas turbine application, the incoming flow to be cooled in the upper dry channel is constituted of the hot flue gases flow while cold air passes through the lower part in order to be heated and humidified. One can note that if the cooled flow contains water (which is the case in a humidified gas turbine cycle), water condensation might take place. If condensation actually occurs in the dry channel, a collecting device must be added to collect the condensate [14, 30, 33]. According to the work of De Paepe et al. [10], the highest heat recovery which goes in pair with the highest electrical efficiency is reached when condensation of the exhaust gases actually takes place.

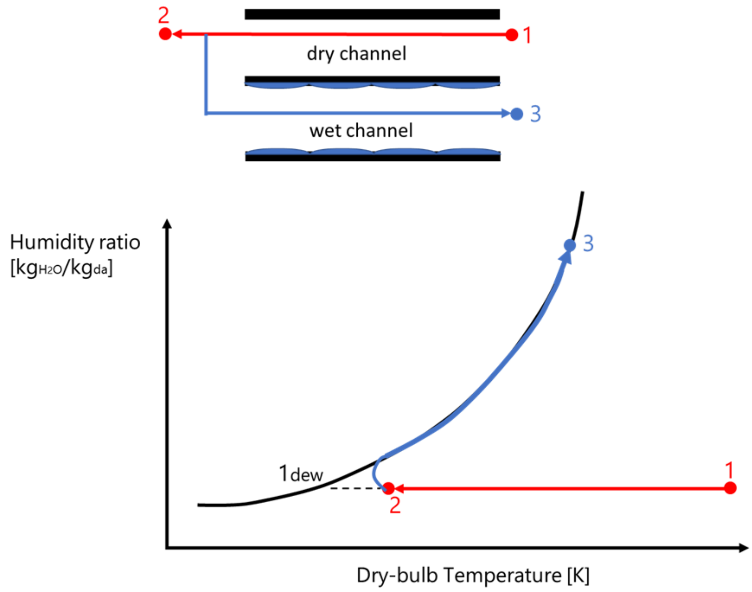

Figure 3.6: Using the outlet of the dry channel as the inlet of the wet channel allows to cool the initial flow up to ideally its dew point temperature.

Let us now explain in more detail what happens with the configuration from Figure 3.7. As mentioned above, state 1 is associated with a flow of air which must be heated and saturated while state 4 corresponds to a hot flow of flue gases that must be cooled. According to what was explained before, the initial cold flow is firstly cooled to almost its dew point temperature ($1 \rightarrow 2$). The remaining difference between the final cooled temperature and the dew point temperature is accounted by an effectiveness, called the dew point effectiveness (ϵ_{dew}) [10]. As the dew point temperature is not exactly reached (unless the previous effectiveness is equal to 1), when a portion of the cooled dry air is exposed to the injected water ($2 \rightarrow 2\text{WB}$) it is humidified and cooled to its wet-bulb temperature, as it was the case for a DEC when putting water and air directly in contact. Therefore, the lowest temperature that could be reached by the hot flow to be cooled ($4 \rightarrow 5$) is the wet-bulb temperature of the cold flow which has been cooled to almost its dew point temperature. In practice, a second effectiveness, called the wet-bulb effectiveness (ϵ_{WB}) [10], is introduced to account for the gap between this temperature (state 2WB) and the really reached one (state 5). Evolution of the flow in the wet channel ($2\text{WB} \rightarrow 3$) is similar to what has been presented before: as the flow is heated and saturated, it follows the saturation curve.

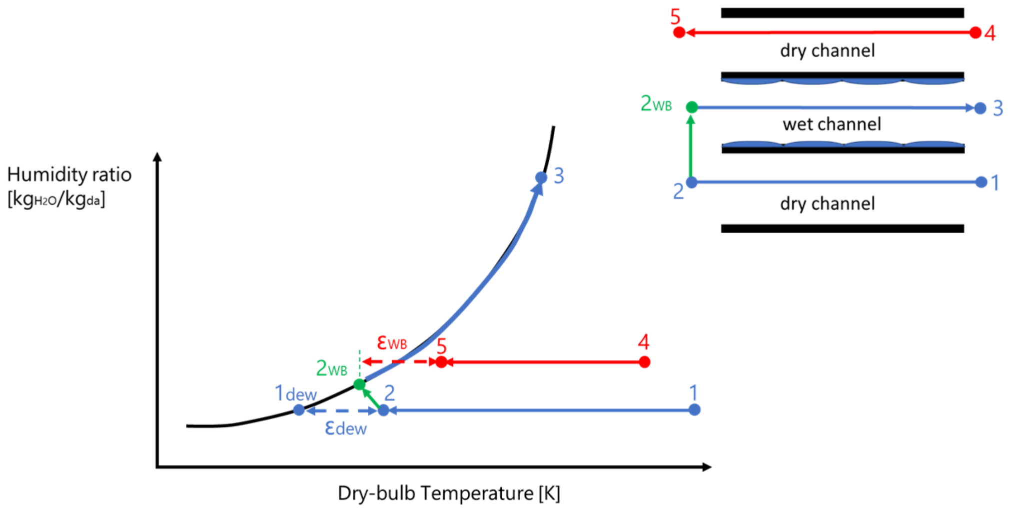

Figure 3.7: The introduction of a second dry channel allows to work with two different input flows. The hot flow might then ideally be cooled until the dew point temperature of the cold flow.

Following the previous explanation, the most common configuration of the M-Cycle in the literature is depicted on Figure 3.8.

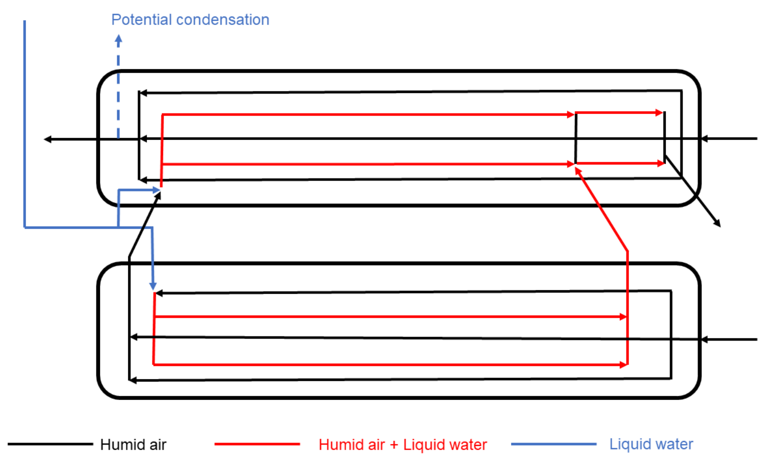

Figure 3.8: The M-Cycle is made up of two parts, each containing a dry and a wet channel.

3.5 M-SAB Cycle

Following the different considerations presented until now, combining water injection with the introduction of the Maisotsenko recuperator inside an IBC might constitute a favorable concept towards the development of more efficient decentralised cogeneration units. The resulting cycle is called the M-SAB cycle and its schematic is shown on Figure 3.9. This layout comes from the review paper of the different applications of the M-Cycle [30]. One can see that the flow cooled by flowing through the dry channel comes from the exit of the turbine. The air to be heated and saturated comes from the (solar) preheater before going to the combustion chamber.

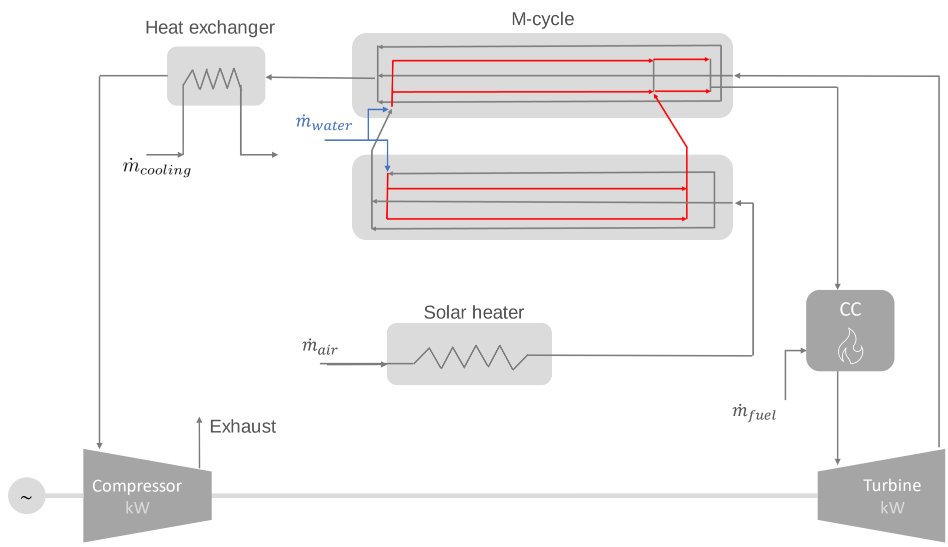

Figure 3.9: Schematic of the M-SAB cycle [30].

Regarding the outlined advantages of an IBC and the promising potential for waste heat recovery of the M-Cycle, combining them could constitute a performing application for mGT systems. Indeed by maximising the heat recovery from the exhaust gases of the turbine, the CIT decreases. Subsequently, this temperature decrease is associated with an increase in density. This finally results in a lower compressor power consumption at constant rotational speed and an increase in its isentropic efficiency [46]. Also if water condensation occurs in the M-Cycle, more than increasing the recovered heat, the work done by the compressor also decreases due to a lower mass flow passing through it. This might offset slightly the lost asset of a conventional humidified BC, when using an IBC configuration, which is the increased mass flow through the turbine compared to the compressor thanks to the injected water after this latter. Another good effect of the presence of the M-Cycle is that it provides with saturated hot air the combustion chamber leading to two interesting impacts. On one hand, the high moisture conditions of the combustion increases the combustion efficiency and decreases the emissions of NOx [30], even though they are already at a rather low level in mGT applications as mentioned already. Still, it is always good to decrease them. On the other hand as the air at the inlet of the turbine is very wet, it carries more enthalpy than typical combustion gases due to the sensible enthalpy of water. Therefore to reach a same level of enthalpy, wet air can, at a lower temperature, be compared to dry air [14]. This leads to a lower turbine inlet temperature and then a design with cheaper materials. Just like the absence of a fuel gas compressor thanks to the atmospheric pressure level at the combustion chamber, the injected water in the M-Cycle must not be compressed as it was the case when introducing it in a typical BC. This also results in saving the compression water power consumption. Moreover, combining the saturation tower, economizer and recuperator into a single component is an efficient way to decrease the complexity of the cycle and its associated investment costs. This constitutes a particularly interesting asset for mGT cycles.

Yet, combining the M-Cycle with an IBC instead of a conventional BC adds the constraint to preheat the initial flow entering the M-saturator as the cold source. Even if this flow is said to be 'cold', it is firstly used to heat and saturate the counter-current flow in the wet channel as explained by De Paepe et al. [10]. In consequence, keeping that flow at atmospheric conditions is not adequate. In addition, an acceptable pinch of temperature between the inlet of the 'cold' dry channel and the outlet of the associated 'cold' wet channel must be guaranteed. It is actually not a problem when dealing with a conventional BC as the mentioned cold flow has already been compressed. The compression increases the temperature of the flow from a bit more than 100°C up to around 200°C depending on the compression ratio and the compressor isentropic efficiency. A possibility to preheat the initial flow from atmospheric conditions is to use a solar preheater [14, 30]. Although this theoretically seems to be a good solution, heating a flux of air from ambient temperature to around 100°C to 200°C requires a complex system of humidifiers, dehumidifiers, fan and piping systems [47].

So far, Khalatov et al. [14] produce the first numerical study of the presented M-SAB cycle using the same layout as displayed on Figure 3.9. But their results seem rather optimistic with an electrical efficiency of 79% with a TIT of 340°C. This might come from the use of a solar preheater and its potential associated fuel-saving ability. Also, they have used a different definition for their electrical efficiency, subtracting the amount of heat recuperated in the M-Cycle to the injected primary energy (therefore increasing significantly the efficiency). Both considerations could explain their surprising result. Another numerical study of the M-SAB cycle has been conducted by Matsui et al. [15] on low-temperature waste heat recovery. The combustion chamber is there theoretically replaced by a low heat source which provides a TIT from 50°C to 150°C. Their application reaches an electrical efficiency of 10.53%. However, it is more intended to be implemented as a way to improve the combined efficiency when using the available heat from a topping cycle than to work as an independent cycle. Regarding the few number of articles about the M-SAB cycle and its application without the solar preheater, our work might be the first of its kind. It would therefore be interesting to see how the M-SAB cycle performs compared to the other cycles presented until now and summarised in Table 3.2.

Table 3.2: Main investigations on M-Cycle coupled GT and mGT systems.

Authors	Maisotsenko et al.[40]	Reyzin[33]	Saghafifar & Gadalla[42]	Saghafifar & Gadalla[43]	Matsui et al.[15]	De Paepe et al.[10]
Year	2003	2011	2015	2015	2020	2020
Cycle type	MBC	MBC	MBC	M-ABC	M-SAB	MBC
Maximum energetic						
Overall efficiency	60%	80%	-	-	-	-
Electrical efficiency	-	-	-	44.9%	10.53%	42.1%
Maximum exergetic						
Overall efficiency	-	-	47.4%	-	-	-
Electrical efficiency	-	-	-	-	-	36%

Chapter 4

Inverted Brayton Cycle

As a first step towards the modelling of the M-SAB cycle, a typical inverted Brayton cycle containing a conventional gas-gas heat recuperator should be modelled. Once the model of the Maisotsenko saturator is completed (which constitutes the second step of our work, explained in the next chapter), it will replace the heat exchanger. We chose to model the cycle in a modular manner with the aim of increasing its flexibility. It is therefore possible to add or remove any component as well as to change the order in which the flow is facing them. This chapter provides a description of the way each component has been implemented. Unless specified in the next chapters, the implementation does not change if the same component has to be reused.

4.1 Air and flue gases modelling

Before plunging into the description of every component, let us take a brief look at how the thermodynamic properties of the working flow have been computed. This latter is only composed of pure air or flue gases in this first model. An ideal gas library of Python (Pyromat) could then be used. The enthalpy of the flow is therefore computed as a mass weighted sum of the enthalpy of each component at a given temperature. The same applies for the entropy, adding the influence of the partial pressure of each species. One can note that the reference point for this model is taken at 15°C and at a sub-atmospheric pressure. This consideration will be covered rigorously when addressing the exergy computation of every state in this sub-atmospheric cycle (see chapter 8).

4.2 IBC modelling

In the following, the different assumptions taken are presented component by component in the order in which the flow faces them. As a reminder, the scheme of an IBC and its associated state numeration is displayed on Figure 4.1. The modelling has been based on the work of Agelidou et al. who developed a numerical model and conducted an experimental validation of this model [8, 9]. They have used as mGT a modified EnerTwin, developed by MTT [13], with an electrical load of 1 kW_e (and a thermal power output of around 4 kW_{th}). The same mGT is considered in our model and the two papers from Agelidou and his research team [8, 9] constitute our reference. To fully understand the coming explanation, the reader must know that the input parameters of our model are the TIT, the turbine expansion ratio and the air mass flow. This choice is justified in section 4.3.

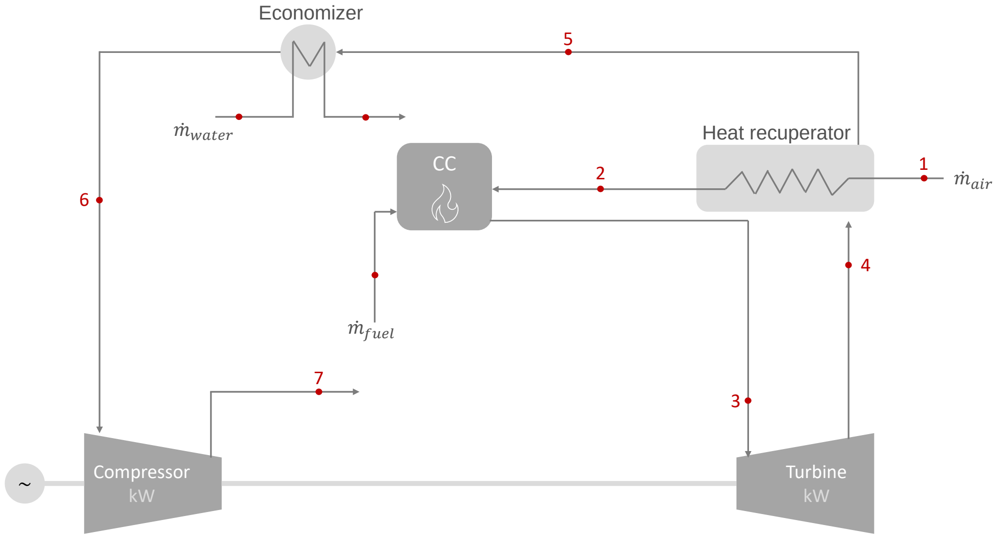

Figure 4.1: IBC scheme and state numeration.

4.2.1 Heat exchanger

The first component faced by the initial working fluid, which is pure air at atmospheric conditions (15°C and 1.01 bar), is the heat exchanger (also called 'heat recuperator'). Its purpose is to recover as much heat as possible from the hot flue gases in order to increase the temperature of the air before entering the combustion chamber. As this allows to decrease the amount of fuel needed, it significantly increases the electrical efficiency of the cycle. The heat exchanger effectiveness is defined accordingly to the reference paper [8]:

$$\eta_{\text{rec}} = \max\left(\frac{\int_{T_{\text{air,out}}}^{T_{\text{air,in}}} c_{\text{p,air}}(T)dT}{\int_{T_{\text{exh,in}}}^{T_{\text{air,in}}} c_{\text{p,air}}(T)dT}, \frac{\int_{T_{\text{exh,out}}}^{T_{\text{exh,in}}} c_{\text{p,exh}}(T)dT}{\int_{T_{\text{air,in}}}^{T_{\text{exh,in}}} c_{\text{p,exh}}(T)dT}\right) \tag{4.1}$$

This effectiveness either fixes the air outlet temperature (state 2) or the flue gases outlet temperature (state 5). It depends on what is the maximum value between the two expressions from Equation 4.1. Whatever the case, knowing one outlet temperature by fixing the effectiveness allows to compute the other one and the total heat exchanged using an energy balance on the entire component.

4.2.2 Combustion chamber

After being heated in the heat recuperator, the air flow goes through the combustion chamber in order to be heated until the TIT. Let us firstly describe the fuel burned in that component. Like most of the mGT applications, we have decided to use natural gas as the operational fuel in all our simulations. The considered molar composition, which is the one used at UCLouvain [48], is shown in Table 4.1.

Table 4.1: Natural gas composition considered for the fuel.

Species	Molar fraction [%]
CH_4	82.7
C_2H_6	3.9
C_3H_8	1.2
CO_2	1.4
N_2	10.8

One can notice the presence of inert species (CO_2 and N_2), which do not react. Therefore, they are also present in the combustion products. Knowing the molar composition allows to compute the lower heating value of the fuel (LHV) as a mass weighted sum of the LHV of each species. The contribution of the inert species is evidently nil. The same reasoning is used to compute the exergy content of the fuel. As indicated in Table 4.2, this latter is slightly higher than the energy content (with a ratio of 1.044).

The general formulation of the fuel is written as C_zH_y, with z = 1.07 and y = 4.14. The reaction of combustion thereafter reads:

$$\begin{aligned} C_{1.07}H_{4.14} \ + \ 2.11\lambda(O_2 + 3.76N_2) \ + \ 0.016CO_2 \ + \ 0.123N_2 \rightarrow \\ 1.088CO_2 \ + \ 2.072H_2O \ + \ 2.11(\lambda - 1)O_2 \ + \ (3.76 \cdot 2.11\lambda + 0.123)N_2 \end{aligned} \tag{4.2}$$

where λ is the air excess coefficient. It is defined as the actual air mass flow injected divided by the mass flow required to be in stoichiometric conditions. It is also important to compute the specific combustive index of the fuel (m_{a1}). This parameter represents the mass of air that must be injected in the combustion chamber per mass of fuel in order to have a stoichiometric combustion. Based on the equation of combustion, it can be found with the following relation:

$$m_{a1} = (M_{O_2} + 3.76M_{N_2})\frac{z + y/4}{zM_C + yM_H + 0.016M_{CO_2} + 0.123M_{N_2}} \tag{4.3}$$

The resulting specific combustive index and the energy and exergy content of the fuel are summarised in Table 4.2.

Table 4.2: Characteristics of the considered natural gas.

Characteristics	Symbol	Value
Lower Heating Value [kJ/kg_{fuel}]	LHV	39949
Exergy content [kJ/kg_{fuel}]	e_c	41742
Exergy-to-Energy ratio [-]	e_c/LHV	1.044
Specific combustive index [$kg_{air,stoich}$/kg_{fuel}]	m_{a1}	13.68

Now that the fuel is correctly characterised, the purpose is to find the rate at which it must be injected. To do so, an energy balance is formulated based on the different inlet and outlet fluxes (see Figure 4.2). This latter reads:

$$\dot{m}_{\mathrm{a}} * h_{\mathrm{a}} + \dot{m}_{\mathrm{f}} * (h_{\mathrm{f}} + \eta_{\mathrm{comb}} * LHV) = \dot{m}_{\mathrm{g}} * h_{\mathrm{g}} + \dot{Q}_{\mathrm{loss}} \tag{4.4}$$

where the subscripts 'a', 'f' and 'g' correspond respectively to the air, fuel and flue gases quantities. The combustion efficiency (η_{comb}) expresses that not all the energy coming from the fuel is captured by the air (mainly due to incomplete localised combustion). The heat losses ($\dot{Q}_{\mathrm{loss}}$) are computed as explained in subsection 4.2.8.

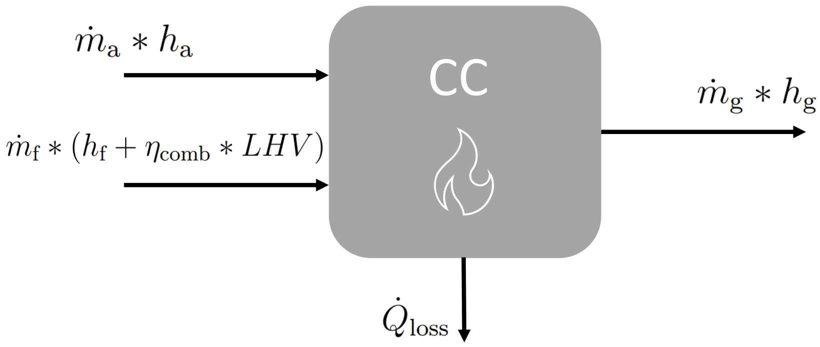

Figure 4.2: Inlet and outlet energy fluxes in the combustion chamber.

The only unknown in Equation 4.4 is the fuel mass flow. Indeed, the air inlet state has already been computed in the heat exchanger and the outlet gases temperature is fixed by the TIT. But the quantity of injected fuel also influences the composition of the flue gases. The most convenient way to solve that problem is to compute the air excess coefficient (λ). After dividing by the air mass flow, the equation reads:

$$h_{\mathrm{a}} + \frac{1}{\lambda m_{\mathrm{a1}}}(h_{\mathrm{f}} + \eta_{\mathrm{comb}} * LHV) = (1 + \frac{1}{\lambda m_{\mathrm{a1}}}) * h_{\mathrm{g}} + \frac{\dot{Q}_{\mathrm{loss}}}{\dot{m}_{\mathrm{a}}} \tag{4.5}$$

Isolating λ results in:

$$\lambda = \frac{1}{m_{\mathrm{a1}}} \frac{h_{\mathrm{f}} + \eta_{\mathrm{comb}} * LHV - h_{\mathrm{g}}}{\frac{\dot{Q}_{\mathrm{loss}}}{\dot{m}_{\mathrm{a}}} + h_{\mathrm{g}} - h_{\mathrm{a}}} \tag{4.6}$$

Knowing this parameter, the composition of the flue gases can be computed as well as their enthalpy and entropy. Since h_{g} depends on λ, an iterative process must be solved.

4.2.3 Turbine

After the combustion chamber, the hot flue gases enter the turbine where they are expanded to a sub-atmospheric pressure. The final pressure is defined by the fixed turbine expansion ratio. The outlet enthalpy of the flow is then determined using the enthalpy and entropy functions of Pyromat and the isentropic efficiency, defined as:

$$\eta_{\text{Si,T}} = \frac{h_{\text{in}} - h_{\text{out}}}{h_{\text{in}} - h_{\text{out,s}}} \tag{4.7}$$

4.2.4 Economizer

An economizer is added between the recuperator and the compressor with the purpose of recovering the remaining heat from the flow leaving the heat exchanger. The temperature of the latter is indeed still higher than 100°C which justifies the presence of such a component. The heat is this time recovered in the form of hot water as the engine must provide both heat and power (CHP unit). The cold water is injected at 15°C and 1.01 bar. The injection flow rate is adapted depending on the amount of recuperated heat in order for this water to be heated up to a satisfying temperature (between 70°C and 90°C for a domestic heating application [23]). The economizer is once again modelled using an effectiveness defined similarly as in the reference paper [8]:

$$\eta_{\text{WHX}} = \frac{\int_{T_{\text{gas,in}}}^{T_{\text{gas,out}}} c_{\text{p,gas}}(T)dT}{\int_{T_{\text{gas,in}}}^{T_{\text{water,in}}} c_{\text{p,gas}}(T)dT} \tag{4.8}$$

This effectiveness fixes the flue gases temperature at the outlet of the economizer because the inlet temperatures are known. To find the outlet water temperature, an energy balance is conducted on the entire system. As mentioned above, this temperature can therefore be adjusted depending on the injected water mass flow rate.

4.2.5 Compressor

The last step of the cycle is to bring the fluid back to atmospheric pressure. Similarly to the turbine, the isentropic efficiency is used, with the enthalpy and entropy functions, to compute the compressor outlet enthalpy:

$$\eta_{\text{Si,C}} = \frac{h_{\text{out,s}} - h_{\text{in}}}{h_{\text{out}} - h_{\text{in}}} \tag{4.9}$$

Since in our model the input is the turbine expansion ratio, the compression ratio must this time be initially computed based on the several pressure losses encountered in the cycle.

4.2.6 Pressure drops

Let us now say a few words about the modelling of the pressure drops. The way they are computed here is based on the experimental investigation on the MTT mGT [9]. When adapting our model to another engine, the pressure drop coefficients therefore need to be adapted. In this case, the two following correlations are used:

$$\Delta p = \underbrace{\frac{c_\mathrm{f} * L * \dot{V}^2}{2D * A^2 * R * T}}_{\Delta p_\mathrm{rel,p}} p_\mathrm{in} \tag{4.10}$$

$$\Delta p = \underbrace{\frac{c_\mathrm{f} * L}{2D * A^2}}_{\Delta p_{\mathrm{rel},\rho,\mathrm{V}^2}} \rho_\mathrm{in} * \dot{V}_\mathrm{in}^2 \tag{4.11}$$

The associated parameters are given in Table 4.3 below.

Table 4.3: Pressure drop coefficients for each component, coming from [8].

Type	**Component**	**Value**
$\Delta p_{\mathrm{rel},\rho,\mathrm{V}^2}$ [1/m^4]		
	Inlet	$9.22 \cdot 10^5$
	Combustion Chamber	$2.92 \cdot 10^6$
	Recup. (hot side)	$6.41 \cdot 10^5$
	Economizer	$1.85 \cdot 10^5$
	Pipe (Econ. → Comp.)	$1.57 \cdot 10^6$
	Outlet	$1.76 \cdot 10^6$
$\Delta p_\mathrm{rel,p}$ [%]		
	Recup. (cold side)	2.22

4.2.7 Miscellaneous losses

To go from the shaft power extracted by the turbine towards the effective electrical power generated, one must take into account several losses described by the correlation below (from [8]):

$$P_\mathrm{el,net} = (P_\mathrm{shaft} - 200) * 0.93 * 0.93 - 100 \text{ [W]} \tag{4.12}$$

This correlation includes the bearing losses (200 W), the generator and inverter efficiency (93% each) and the power demand of the auxiliaries (100 W). This correlation is once again only valid for the MTT mGT.

4.2.8 Heat losses

The heat losses are located mainly in the hot components. They are one more time computed using specific correlations and coefficients, only valid for the MTT mGT, from the papers of reference [8, 9]:

$$\Delta T = \gamma_{\Delta \mathrm{T}} * (T_{\mathrm{in}} - T_{\mathrm{amb}}) \tag{4.13}$$

$$\Delta \dot{Q} = \gamma_{\Delta \dot{\mathrm{Q}}} * (T_{\mathrm{in}} - T_{\mathrm{amb}}) \tag{4.14}$$

The associated heat loss coefficients are given in Table 4.4.

Table 4.4: Initial heat loss coefficients for each hot component, coming from [8].

Type	**Component**	**Value**
$\gamma_{\Delta \dot{\mathrm{Q}}}$ [W/K]		
	Combustion Chamber	3
	Recuperator	0.032
$\gamma_{\Delta \mathrm{T}}$ [K/K]		
	Pipe (Turb. $\rightarrow$ Recup.)	$6.8 \cdot 10^{-3}$

However, these coefficients come from an experimental test rig whose insulation can be improved [9]. Therefore, Agelidou and its coworkers assumed reduced heat losses in the numerical simulation equivalent to 50 W per kW of fuel power [8]. The presented heat loss coefficients might then be adapted to reach that value as discussed later.

4.3 IBC Validation

Before including the components related to the M-Cycle, the IBC model has to be validated. As mentioned a couple of times previously, the model is inspired by the work of Agelidou et al. [8] on the modified EnerTwin MTT mGT. The validation will accordingly be based on the same article.

In order to compare the results from our model with the reference data, the inputs should be identical to those in the paper. Their fixed parameters are the mass flow of air, the pressure ratio of the compressor, the efficiency of each component and the turbine outlet temperature (TOT). However in our model, we decided to fix the inputs in a slightly different way with two main differences. Firstly, the TIT is rather fixed instead of the TOT. This is justified by the fact that this latter is the highest temperature achieved during the combustion. Its maximum value is limited by the particular materials used in the design of the components. As the best performance is always reached when it is fixed to the highest possible value (one can consider the Carnot efficiency), we wanted to keep it as an input. Secondly, the expansion ratio of the turbine is initially fixed and then the compression ratio of the compressor is computed in order to offset for all the pressure drops and bring the pressure back to atmospheric condition. Doing it in the inverse way, as done in the reference paper, is similar but it increases a bit the computation time of the numerical model as the simulation follows the way of the flow (from the turbine to the compressor). The input values of each model are summarised in Table 4.5.

Table 4.5: Initial set of inputs used for the IBC model validation.

Inputs	**Symbol**	**Our model**	**Reference[8]**
Inlet air mass flow rate [kg/s]	$\dot{m}_{air}$	0.02	0.02
Combustion efficiency [%]	η_{comb}	99.5	99.5
Heat recuperator effectiveness [%]	η_{rec}	90.7	90.7
Economizer effectiveness [%]	η_{WHX}	92	92
Turbine isentropic efficiency [%]	η_{turb}	75	75
Compressor isentropic efficiency [%]	η_{comp}	75	75
Turbine outlet temperature [°C]	TOT	-	796.85
Turbine inlet temperature [°C]	TIT	971.85	-
Compressor pressure ratio [-]	Π_{comp}	-	2.7
Turbine pressure ratio [-]	Π_{turb}	2.3	-

The comparison of the results from each model using the mentioned set of parameters will be primarily presented. Thereafter, it is followed by the analysis of the effect of changing various parameters : the heat loss coefficients, the TIT and the turbine expansion ratio.

Using the set of values from Table 4.5 leads to the temperatures, pressures and mass flows displayed on Figure 10.1 in the appendix at all points of the cycle. The same figure also shows the power provided by the turbine, the required power of the compressor, and the power production of the generator.

Figure 4.3 allows to compare the temperature evolution between our model and the reference article. Despite a higher difference for the states before and after the compressor, the relative error between the two is lower than 1% in all other points. As is noticeable on the figure, the TOT reaches almost 800°C. Even if this is also what is achieved in the paper, it is worth noting that it represents a quite high value for a mGT cycle. As detailed in chapter 3, typical values for the TOT lie between 620°C and 680°C. Increasing it up to 800°C requires the use of much more expensive materials. As the scope of our work is limited to the assessment of the thermodynamic potential (and not the technological implementation) of the cycle under study, this is not a big issue at this stage. But this aspect should be considered in the design of an actual production unit.

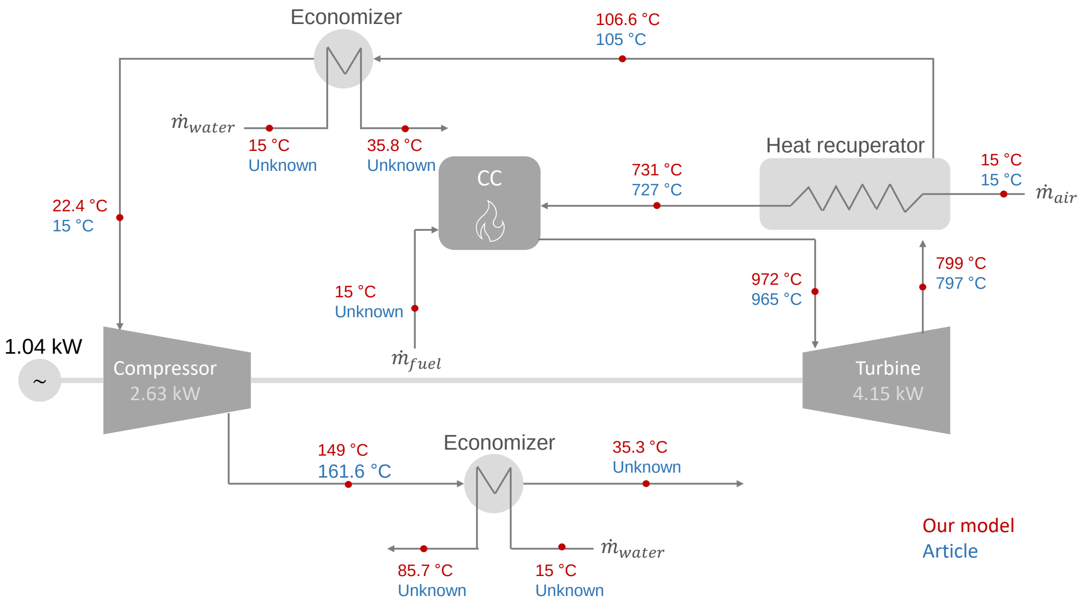

Figure 4.3: The temperature reached by our model in each state is close to that of the reference article [8].

It is also interesting to look at the pressure difference between our model and the reference article. As shown on Figure 10.2 in the appendix, it never exceeds 0.02 mbar.

Compared to the cycle presented on Figure 4.1, one could note the appearance of a second economizer after the compressor. This makes sense as the post-compression temperature is quite high (149°C in our model) relatively to the atmospheric temperature (15°C). It would therefore be worthwhile to take advantage of this remaining energy in the outgoing flow. What is proposed by Agelidou and its coworkers is to add a second economizer to increase the recovered heat and at the same time improve the cycle overall efficiency even further. As it is not clearly stated in the article, we have chosen the effectiveness of the second economizer so that our total recuperated thermal power is equivalent (with a relative deviation lower than 2%) to that of the article. This gives an effectiveness of 85% which is lower than that of the first economizer (which was 92%). It is indeed better to recover more heat in the first economizer as it decreases the CIT and thus lead to a better electrical power output. Nevertheless, being able to keep the same effectiveness of 92% for the second economizer would enhance the thermal power output and further increase the cycle overall efficiency.

In order to study the performance of our model, the computed efficiencies must be clearly defined. As the EnerTwin mGT is a CHP unit, two efficiencies are pertinent to look at : the electrical efficiency and the overall efficiency (also called 'cogenerative efficiency'). The first one is only focused on the electrical power produced by the cycle while the second one also takes the recovered heat as an useful output. To define them more rigorously, the electrical efficiency is defined as the electrical power produced divided by the fuel primary energy inserted in the cycle:

$$\eta_{\text{elec}} = \frac{P_{\text{el}}}{\dot{m}_{\text{fuel}} * LHV} \tag{4.15}$$

The product $\dot{m}_{\text{fuel}} * LHV$ is sometimes also called the primary energy flux and denoted by P_{prim}. The overall efficiency has a similar definition but the recovered thermal power is added to the numerator:

$$\eta_{\text{overall}} = \frac{P_{\text{el}} + P_{\text{th}}}{\dot{m}_{\text{fuel}} * LHV} \tag{4.16}$$

Actually, this last efficiency could have been defined as the sum of the electrical efficiency and a third one, the thermal efficiency. This latter is therefore defined as:

$$\eta_{\text{th}} = \frac{P_{\text{th}}}{\dot{m}_{\text{fuel}} * LHV} \tag{4.17}$$

Table 4.6 shows the comparison of the values obtained for the power outputs and efficiencies between our model and the reference paper. The two sets of results are pretty close with a maximum deviation of 2.52% for the primary energy flux. This latter will be discussed later with the effect of modifying the heat losses. Table 4.6 also contains the resulting TOT and compressor pressure ratio from our model, which are very close (with a deviation lower or equal to 0.25%) to the input value used for these parameters in the reference.

Table 4.6: The maximum relative deviation of the performance between our model and the reference is 2.52%.

Performance	**Our model**	**Reference[8]**	**Deviation [%]**
Electrical power [kW_e]	1.042	1.054	-1.14
Thermal power [kW_{th}]	4.11	4.14	-0.7
Primary power [kW]	6.45	6.617	-2.52
Electrical efficiency [%]	16.14	15.9	1.51
Overall efficiency [%]	79.83	78.5	1.69
TOT [°C]	798.85	796.85	0.25
Compression ratio [-]	2.696	2.7	-0.15

4.3.1 Effect of the heat losses

As mentioned in subsection 4.2.8, the heat losses were primarily computed using the heat loss coefficients coming from an experimental setup. Afterwards, they were assumed to account for 50 W per kW fuel power in the numerical investigation. To do so, the empirical coefficients presented in Table 4.4 have been modified. Firstly, the purpose was to reach the performance of the reference model with a relative deviation lower than 2% (Table 4.6). The considered heat loss coefficients used to get that set of results and their associated heat losses are displayed in Table 4.7. The total heat losses from that set of coefficients account for 60 W per kW fuel power. This latter value is quite different from the mentioned '50W per kW fuel power'. Also, the obtained primary energy flux features a relative deviation slightly higher than 2% compared to the reference. Choosing other heat loss coefficients might allow to reach different results closer to the reference from these two perspectives. Since the heat losses coming from the combustion chamber are dominating (accounting for 87% of the total heat losses with the coefficients from Table 4.7), we chose to focus on these to study their impact on the cycle in general.

Table 4.7: Adapted heat loss coefficients used with the initial set of inputs.

Type	**Component**	**Value**
$\gamma_{\Delta\dot{Q}}$ [W/K]		
	Combustion Chamber	0.46
	Recuperator	0.0107
$\gamma_{\Delta T}$ [K/K]		
	Pipe (Turb. → Recup.)	$2.27 \cdot 10^{-3}$

Increasing or decreasing the empirical heat loss coefficient of the combustion chamber obviously directly has a major impact on the heat losses but also a non-negligible impact on the primary energy flux. This latter could slightly change the electrical and overall efficiencies. Finally, the change in electrical power and recovered heat is negligible.

Table 4.8: Increasing the heat loss coefficient increases the primary energy while the electrical and thermal power outputs remain constant. This is associated with a slight decrease of the cycle efficiencies.

Combustion chamber				
	Heat loss coefficient [W/K]	0.38	0.46	0.67
	Heat losses [W]	268.5	337.5	487.5
Results				
	Primary energy [kW]	6.38	6.45	6.617
	Electrical power [kW_e]	1.042	1.042	1.042
	Thermal power [kW_{th}]	4.11	4.11	4.11
	Electrical efficiency [%]	16.33	16.14	15.75
	Overall efficiency [%]	80.69	79.83	78.03

The results from Table 4.8 confirm the previous statements. Each of the three last columns corresponds to the results obtained using a particular heat loss coefficient. The coefficients correspond respectively, column by column, to (i) a case where the heat losses amount to exactly 50 W per kW fuel power; (ii) the previous case with the initial set of parameters; and (iii) a case where the primary energy is the same as in the article. It is clear that increasing the heat losses leads to an equivalent increase in primary energy needed. Indeed as the maximum temperature of the cycle (TIT) is fixed, higher heat losses must be offset by a greater fuel mass flow and similarly a greater primary energy flux. Then as the electrical power and the recuperated heat remain (almost) constant, the change in primary energy impacts negatively both electrical and overall efficiencies. This shows the interest of having a good combustion chamber insulation.

4.3.2 Effect of the turbine expansion ratio

As a reminder in our model, the turbine expansion ratio is fixed as an input and then the compression ratio of the compressor is computed in order to go back to atmospheric pressure at the end of the cycle. But this is not the case in the reference article where the compression ratio is an input and its value has been optimised in order to maximize the electrical efficiency. As explained before, both approaches lead to similar compressor pressure ratio (with a relative deviation of 0.15%). Let us see now what is the impact of modifying the turbine expansion ratio on the cycle performance.

First of all, changing the expansion ratio obviously changes the compression ratio as well. If the expansion ratio increases, the flow is expanded to a lower pressure and then the compressor has to compress it more to go back to the atmospheric pressure. This thereafter impacts the electrical efficiency of the cycle. Indeed, increasing the turbine expansion ratio (from 1.6 to 2.3 for instance) involves a higher shaft power produced by the turbine (from 2.46 kW to 4.15 kW, see the red curve on Figure 4.5) for the same incoming energy in that component. But as the associated compressor pressure ratio is higher, its power required increases as well (from 1.46 kW to 2.63 kW, see the purple curve on Figure 4.5). Still, the absolute increase in shaft power is greater than that of the compressor resulting in an increased electrical power output (from 0.59 kW_e to 1.04 kW_e, see the blue curve on Figure 4.5). But the more the expansion ratio keeps increasing, the more this effect will saturate and the increase in electrical power output will become relatively low. Another consideration to take into account is the increase in primary energy flux with the turbine expansion ratio (see the green curve on Figure 4.5). The mentioned increase in shaft power produced by the turbine when increasing its expansion ratio goes in hand with less energy sent to the heat recuperator. Indeed, as the initial mass flow and the TIT do not change, the same energy level must be reached after the combustion chamber (and thus at the inlet of the turbine). But as the shaft power increases, the remaining fraction of the incoming energy that flows to the heat recuperator is lower, resulting in a lower heat recovery (from 16.9 kW to 15.4 kW) from that component to the combustion chamber. This latter must then be offset by adding more fuel. When starting to increase the turbine expansion ratio from its initial value, the relative increase in electrical power output is more important than that in primary energy needed. Therefore, the electrical efficiency increases. But as explained, the positive effect on the electrical power output tends to fade when increasing even more the expansion pressure ratio. This results in the existence of an expansion ratio, with an associated compression ratio, which maximizes the electrical efficiency. As illustrated on Figure 4.4, the optimal expansion and compression ratio are respectively equal to 2.37 and 2.79 and they lead to a maximal electrical efficiency of 16.17%. This maximal efficiency is though quite close to the one obtained with the initial set of input values.

Even though the curve for the electrical efficiency firstly increases, reaches a maximum and then decreases, this is not the case for the overall efficiency. This latter is always increasing with an increasing expansion ratio as depicted on Figure 4.4. This comes from the lower relative importance of the total losses in the cycle with respect to the injected primary energy. The previous analysis showed that this latter increases when increasing the expansion ratio. Part of this energy is used to increase the electrical power output as mentioned above. The remaining part will flow through the economizers resulting in more recovered heat as a thermal power output (see the yellow curve on Figure 4.5). Even though the exhaust losses increase due to the higher energetic content of the flow arriving at the second economizer, their relative importance with respect to the primary flux of energy still remains lower than with a lower expansion ratio. Regarding the evolution of the two efficiencies, it is not possible to maximize both of them. As our main interest relates to the electrical production, we chose to rather maximize the electrical efficiency.

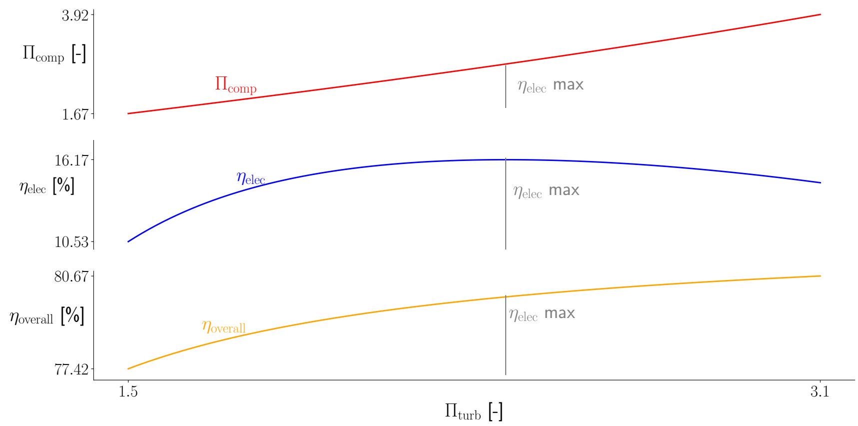

Figure 4.4: Increasing the turbine expansion ratio increases the compressor pressure ratio and the overall efficiency of the cycle. The electrical efficiency increases and then reaches a maximum before starting to decrease.

Finally, the evolution of the powers in the cycle is represented on Figure 4.5. All curves are increasing with an increasing expansion ratio but with different rates of growth coming from the previous explanations. It is now clear that the decreasing growth rate of the electrical power output compared to that of the primary energy flux explains the existence of a maximum for the electrical efficiency. On the other hand, the thermal power output increases faster and then combined with the increase in electrical power, it is higher than the increase in primary energy flux. This is the reason why there is no maximum for the overall efficiency. One could note that we have decided to neglect here the effect of changing the expansion and compression ratio on the turbomachinery components efficiency, which were kept constant. This will be included in the final M-SAB model when switching from the EnerTwin MTT mGT to the Turbec T100 mGT and including its turbomachinery maps.

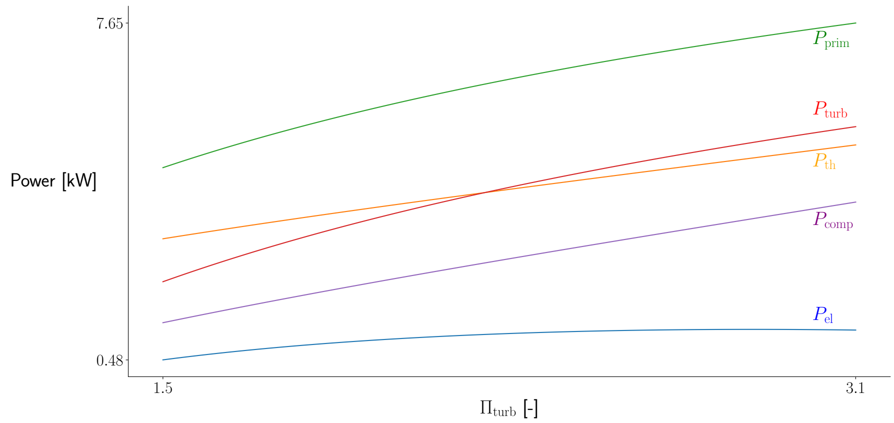

Figure 4.5: Increasing the turbine expansion ratio increases the electrical and thermal power outputs, the primary energy flux as well as the power produced and required by the turbine and compressor. Yet, the relative increase in electrical efficiency tends to fade when increasing the pressure ratio.

4.3.3 Effect of the TIT

The last parameter under study is the turbine inlet temperature. As specified before, it is the highest temperature reached in the cycle. Modifying the TIT impacts all the other temperatures in the cycle leading to several changes of other quantities.

First of all, a lower temperature goes in pair with a higher fluid density. According to Equation 4.11, this results in lower pressure drops. Then, the compressor pressure ratio almost linearly decreases with the TIT (see Figure 4.6). Still, the impact is obviously less significant than that of the turbine expansion ratio illustrated by the fact that decreasing the TIT by 50°C goes in pair with an absolute decrease of only 0.01 of the compression ratio, which requires only a similar change of the expansion ratio. The evolution of the heat losses is also depicted on the same plot. As the TIT is the highest temperature reached during the combustion, this has an impact on them. As a reminder, the dominant heat loss comes from the combustion chamber and is computed depending on the temperature gradient between ambient conditions and the highest combustion temperature. Consequently, the heat losses are proportional to the TIT and the relation appears to be almost linear. Both impacts of decreasing the TIT should be interesting in terms of performance as less power must be provided to the compressor and less heat is lost at the combustion chamber. However, other impacts will play at the same time as explained below.

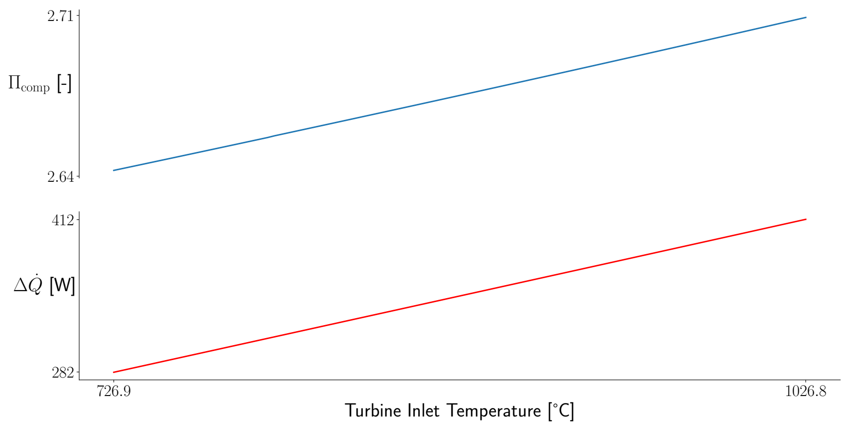

Figure 4.6: Decreasing the TIT decreases the compressor pressure ratio due to decreased pressure drops and decreases the combustion heat losses as the temperature gradient with the ambient conditions is reduced.

In terms of power (electrical, thermal and primary energy), decreasing the TIT decreases them all (see Figure 4.7). Concerning the thermal power output, decreasing the TIT leads to lower temperatures for the flow arriving to the economizers. As a result, less energy is recovered there. For the electrical power, the explanation is similar and the impact even bigger. Indeed, the TIT is the inlet temperature of the turbine. Therefore, decreasing it means that the incoming flow to the turbine has a lower energy content. Then, the turbine extracts less power and even though the required compressor power is slightly lower as explained before, the impact on the turbine is stronger. Finally, the primary energy increases with the TIT because it represents the energy needed to reach that higher temperature. This increase is accentuated by the higher heat losses.

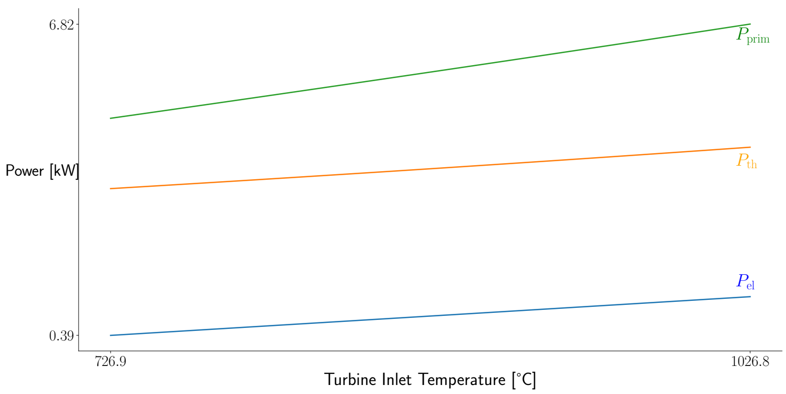

Figure 4.7: Increasing the TIT increases the energy arriving at the turbine and the economizers resulting in increased electrical and thermal power outputs. This also involves the combustion of more fuel.

Subsequently, the evolution of the electrical and overall efficiencies is shown on Figure 4.8. It shows that both efficiencies increase as the TIT increases but it is more pronounced for the electrical efficiency. This results from the analysis of the previous graph showing that the relative increase in electrical power is bigger than that of the thermal power. Regarding the fact that both efficiencies are increasing with the TIT, working with the highest possible temperature leads to a better performance. One must recall though that the TIT is limited by the highest temperature that the turbine and heat recuperator materials could withstand.

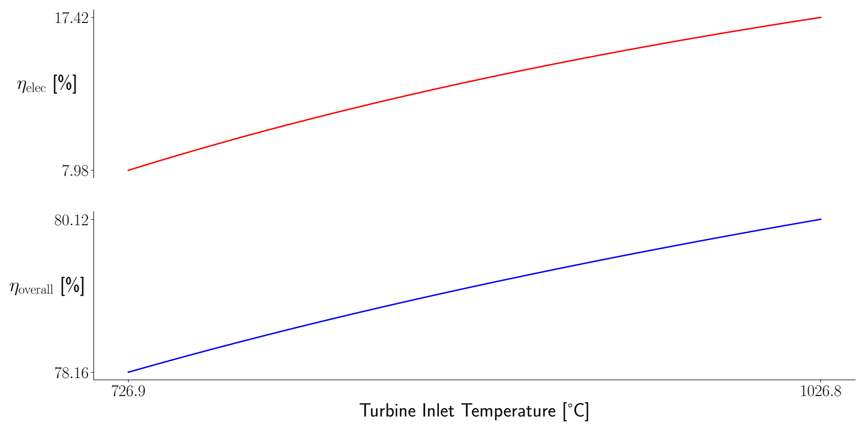

Figure 4.8: Increasing the TIT goes in pair with higher electrical and overall efficiencies.

Chapter 5

Maisotsenko Cycle

With the aim of substituting the conventional heat exchanger with the Maisotsenko recuperator, this latter must formerly be modelled. Based on the existing numerical studies from the literature, our own model has been developed. This chapter is intended to present the different assumptions taken as well as to confront the results of our model to another numerical implementation, the one from De Paepe et al. [10]. Similarly to the previous chapter, a few words primarily explain the characterisation of the working fluid before addressing the heat exchanger design.

5.1 Humid air properties

A fundamental aspect of the M-cycle modelling, which was not yet part of the IBC model, is the humid air characterisation. It is crucial to correctly assess the humid air enthalpy and entropy due to the injection of liquid water and its associated humidification.

5.1.1 Enthalpy

The humid air enthalpy has to be computed from its temperature T and its vapor content x_{v}. The following relation was used:

$$h_{\mathrm{ha}}(T, x_{\mathrm{v}}) = h_{\mathrm{da}}(T) + x_{\mathrm{v}}(h_{\mathrm{H_2O}}(T) + h_{\mathrm{lv}}) \left[\frac{\mathrm{kJ}}{\mathrm{kg_{da}}}\right] \tag{5.1}$$

where h_{ha}, h_{da}, $h_{\mathrm{H_2O}}$ and h_{lv} account respectively for the humid air, dry air, water and vaporisation enthalpies. The second and the third one were computed using the same ideal gas library of Python (Pyromat) as in the IBC model. It is correct to use this assumption for the gaseous water as it only accounts for its sensible enthalpy, since its vaporization enthalpy is taken separately. One should note that since all the species are considered as ideal gases, their enthalpy does not depend on their partial pressure. As indicated in the equation, we decided to work with enthalpies expressed per unit mass of dry air. It is more convenient to work with dry masses because they remain constant even if condensation occurs or if some water is injected and evaporated. The only change in dry mass flow that might appear is therefore situated at the combustion chamber. This also implies to express the absolute humidity (x_{v}) in mass of gaseous water per unit mass of dry air. Even if only the case of pure humid air was presented here, a similar reasoning is kept for the humid flue gases, based on their composition.

5.1.2 Entropy

The modelling of the entropy is a bit more complex because it also depends on the partial pressure of the different species (p_{air} and p_{H_2O}). The equation used to compute the entropy is the following:

$$s_{\text{ha}}(T, x_{\text{v}}, p) = s_{\text{da}}(T, p_{\text{air}}) + x_{\text{v}} * s_{H_2O}(T, p_{H_2O}) \left[\frac{\text{kJ}}{\text{kg}_{\text{da}}\text{K}}\right] \tag{5.2}$$

The dry air entropy was again approached using Pyromat, but the gaseous water entropy was computed with a water library of Python (XSteam) which also takes into account the entropy of vaporisation. Similarly to the enthalpy, the entropy is expressed per unit mass of dry air. A dead state had to be chosen in order to fix a reference entropy. We chose to take a state of humid air at 15°C, with the ambient relative humidity (60%) and with a sub-atmospheric pressure. The choice of the dead state pressure was influenced by the fact that in our M-SAB cycle, the fluid between the turbine and the compressor is at a lower pressure than the atmospheric one. As it will be explained in chapter 8, this choice allows to only have positive exergy fluxes, which is necessary to draw the Grassmann diagram of the cycle. Once again, a similar reasoning can be applied for the entropy of humid flue gases.

5.2 M-cycle modelling

In order to implement the Maisotsenko cycle, our work was inspired from the model described and developed by De Paepe et al. [10]. One must note that this article deals with a MBC as depicted on Figure 5.1. Still, the numerical implementation of the M-Cycle component can be done similarly. The difference with an IBC resides in the injected states. Indeed, the arriving cold flow will be at atmospheric conditions (initial state of the working fluid before entering the cycle) instead of coming from the compressor outlet. Simultaneously, the incoming hot flue gases flow will be at an equivalent temperature level but with a sub-atmospheric pressure. In order to ease the comparison with that model, the notation for each state inside the M-power unit is the same as indicated on Figure 5.1 and Figure 5.2.

The M-Cycle is divided into a lower and an upper part. The flux entering through the lower one (state 2) is cooled in a dry channel (until state 3). Once reaching the other side, part of the flow is sent to the upper part while the remainder flows in the opposite direction in a wet channel. The wet character of this channel arises from the injection of liquid water. This latter part of the flow is heated (until state 4) thanks to the heat released by the cooling of the flow from state 2 to 3. While being heated, the water in the wet channel (from 3 to 4) is evaporated in the flow. The parameter determining what portion of the flow is going back or to the upper part is called the split fraction.

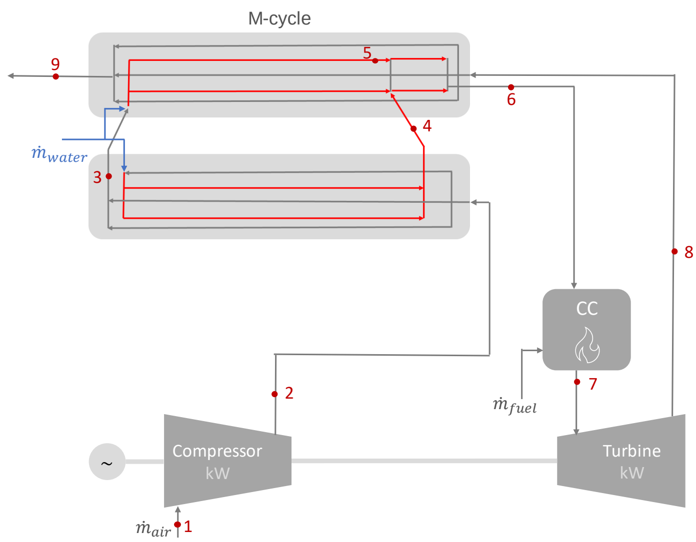

Figure 5.1: MBC scheme as studied in [10].

The portion of the flow introduced into the upper part is also mixed with liquid water and then heated (until state 5). The required heat is captured from the cooling of the flue gases flowing in the opposite direction through a dry channel (from state 8 to state 9). Shortly before the end, the two heated flows (states 4 and 5) are mixed and then further heated until the outlet of the saturator (state 6). One must note that a possible condensation might happen during the cooling of the flue gases (between states 8 and 9) if this latter is strong enough. In that case, the condensate should be removed from the flow at the end of the dry channel.

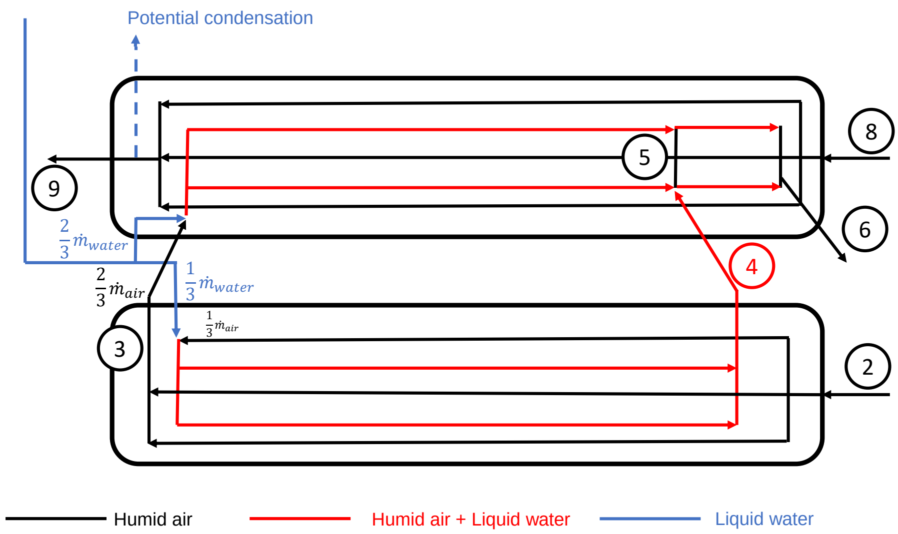

Figure 5.2: Schematic of the M-cycle and its associated state numeration.

As displayed on Figure 3.7, each part of the M-Cycle is characterised by an effectiveness. Concerning the lower part, the dew point effectiveness (ϵ_{dew}) is used. It reflects the difference between the actual cooled temperature reached in state 3 with the dew point temperature associated with state 2, representing the lowest temperature to which the fluid can ideally be cooled in this lower dry channel. A typical value for this effectiveness can be found in the literature and $\epsilon_{\text{dew}} = 0.8$ has therefore been chosen as done in [10]. Mathematically, it gives the following relation:

$$T_3 = T_2 - \epsilon_{\text{dew}} * (T_2 - T_{\text{dew},2}) \text{ [K]} \tag{5.3}$$

In the upper part of the M-Cycle, the effectiveness is called the wet-bulb effectiveness (ϵ_{WB}). The flow cooled through the upper part can, in the best case, reach the wet-bulb temperature of state 3. This effectiveness accounts then for the difference between this ideal temperature and the one actually reached. Once again, the value used for this effectiveness comes from the literature and is taken as $\epsilon_{\text{WB}} = 0.9$. Mathematically, it gives the following relation:

$$T_9 = T_8 - \epsilon_{\text{WB}} * (T_8 - T_{\text{WB},3}) \text{ [K]} \tag{5.4}$$

Now that the temperature in states 3 and 9 are fixed by the use of each effectiveness, it is possible to perform an energy balance on each part in order to find the different unknown states. But before, let us state the assumptions taken in our model, which are based on those from the work of De Paepe et al. [10]. The first one has to do with the split fraction of the flow and the injected water between the two parts. As shown on Figure 5.2, a distribution of 'one-third, two-thirds' is assumed for both the flow and the water. Concerning the pressure drops, it amounts to 3% in the cold side (between states 2 and 4) and to 40 mbar in the hot side (between states 8 and 9). No heat losses have been accounted inside the M-cycle as they will be all encapsulated as one single combustion chamber heat loss in the M-SAB cycle (see next chapter).

Firstly, the purpose of the energy balance of the lower part is to determine the temperature in state 4. To do so, the flow reaching this state is assumed to be saturated. It is then possible that a fraction of the injected liquid water does not evaporate. If this is the case, this latter stays in the flow and is sent to the upper part (when mixing states 4 and 5). It might then be further evaporated between the mixing point and the outlet of the saturator. The enthalpy balance reads:

$$\dot{m}_{\text{da},2} * h_2 + \dot{m}_{\text{H2O,ev}} * h_{\text{H2O,in}} = \frac{2}{3}\dot{m}_{\text{da},2} * h_3 + (\frac{1}{3}\dot{m}_{\text{da},2} + \dot{m}_{\text{H2O,ev}}) * h_4 \tag{5.5}$$

where $h_{\text{H2O,in}}$ is the enthalpy of the liquid water at the point of injection, $\dot{m}_{\text{da},2}$ is the cold dry air mass flow injected in state 2 and $\dot{m}_{\text{H2O,ev}}$ is the amount of water evaporated in the air in the wet channel from state 3 to state 4. One can note that the remaining liquid water that does not evaporate does not appear in the balance. This comes from the fact of neglecting its increase in temperature, assuming then the same state when leaving the lower part as when entering.

The unknowns in Equation 5.5 are h_4 and $\dot{m}_{\text{H2O,ev}}$. But both are related to a single parameter : the temperature T_4. Even if this is straightforward for the enthalpy which depends only on the temperature and the water content, $\dot{m}_{\mathrm{H2O,ev}}$ can be known by computing the difference between the amount of water needed to saturate the air at temperature T_4 and the initial amount of water present in state 2. By applying the Dalton's law for perfect gases, it reads:

$$x_{\mathrm{v,sat}}(T_4) = \frac{0.622 * p_{\mathrm{sat}}(T_4)}{p_4 - p_{\mathrm{sat}}(T_4)} \left[\frac{\mathrm{kg_{H2O}}}{\mathrm{kg_{da}}}\right] \tag{5.6}$$

$$\dot{m}_{\mathrm{H2O,ev}} = \frac{1}{3}\dot{m}_{\mathrm{da,2}}(x_{\mathrm{v,sat}} - x_{\mathrm{v,2}}) \left[\frac{\mathrm{kg_{H2O}}}{\mathrm{s}}\right] \tag{5.7}$$

Starting with a guess value for T_4, an iterative process is then conducted until convergence. In order to be physically correct and to avoid violating the second law of thermodynamics, one must check that the sign of the initial pinch of temperature, called 'cold pinch', is positive. This last parameter is expressed as the temperature difference between states 2 and 4. A positive sign therefore indicates that the outlet temperature of the heated flow must remain lower than the inlet temperature of the cooled flow. In the case of an IBC, the increase in enthalpy from state 3 to state 4 will be limited by the low temperature of state 2 (which is at atmospheric conditions and has not been compressed, and thus heated, by the compressor). This also impacts the cold pinch which is rather low (below 15°C, the minimal cold pinch used in [10], which is a typical value that should be at least reached). A more detailed discussion about this aspect will be held in the next chapter (see section 6.1) when introducing the M-power unit in the IBC.

Switching now to the upper part, it is possible to determine state 6 in terms of temperature and absolute humidity. The most important assumption taken here is that all the injected water (2/3 $\dot{m}_{\mathrm{H2O}}$) is evaporated in the flow between state 3 and state 5. Additionally, the remaining liquid water coming from state 4 will be fully evaporated when reaching state 6. In this way, all the injected water is finally evaporated in the flow going out from the M-Cycle. Moreover, the potential condensed water between state 8 and state 9 is assumed to be at a temperature of 15°C and is removed at the end of the channel. Therefore, the balance reads:

$$\begin{aligned}\frac{2}{3}\dot{m}_{\mathrm{da,2}} * h_3 + \dot{m}_{\mathrm{dg,8}} * h_8 + (\frac{2}{3}\dot{m}_{\mathrm{H2O}} + \dot{m}_{\mathrm{H2O,left}}) * h_{\mathrm{H2O,in}} + \frac{2}{3}\dot{m}_{\mathrm{da,2}} * h_4 = \\ (\dot{m}_{\mathrm{dg,8}} - \dot{m}_{\mathrm{cond}}) * h_9 + \dot{m}_{\mathrm{cond}} * h_{\mathrm{H2O,9}} + (\dot{m}_{\mathrm{da,2}} + \dot{m}_{\mathrm{H2O}}) * h_6\end{aligned} \tag{5.8}$$

where $\dot{m}_{\mathrm{dg,8}}$ represents the dry mass flow of flue gases coming from the turbine, $\dot{m}_{\mathrm{cond}}$ is the mass flow of potential condensed water and $\dot{m}_{\mathrm{H2O,left}}$ is the remaining portion of liquid water from state 4. Also, $h_{\mathrm{H2O,9}}$ is the enthalpy of the condensed liquid water.

The only unknown needed before being able to calculate h_6 (and therefore T_6) is the mass flow of potential condensed water ($\dot{m}_{\mathrm{cond}}$). With the knowledge of T_9 (from Equation 5.4), the maximum amount of water that could be withstood by the flue gases at the end of the upper channel can be computed. Assuming that the initial absolute humidity of the same incoming hot flow (state 8) is known, one can compare the two quantities. If this initial amount of water is higher than that associated with a saturated flow at temperature T_9, water condensation will take place. Mathematically, it reads:

$$x_{\mathrm{v,sat}}(T_9) = \frac{0.622 * p_{\mathrm{sat}}(T_9)}{p_9 - p_{\mathrm{sat}}(T_9)} \left[\frac{\mathrm{kg_{H2O}}}{\mathrm{kg_{dg}}}\right] \tag{5.9}$$

Then if $x_{\mathrm{v,sat}}(T_9) < x_{\mathrm{v,8}}$ (otherwise $x_{\mathrm{v,cond}} = 0$):

$$x_{\mathrm{v,cond}} = x_{\mathrm{v,8}} - x_{\mathrm{v,sat}}(T_9) \left[\frac{\mathrm{kg_{H2O}}}{\mathrm{kg_{dg}}}\right] \tag{5.10}$$

And this can be converted into a mass flow by multiplying it with the mass flow of dry air in the channel:

$$\dot{m}_{\mathrm{cond}} = x_{\mathrm{v,cond}} * \dot{m}_{\mathrm{dg,8}} \left[\frac{\mathrm{kg_{H2O}}}{\mathrm{s}}\right] \tag{5.11}$$

Now that the amount of condensed water is known, it only remains to isolate h_6 in the first balance. From h_6, the temperature T_6 can be known and the positive sign of the pinch of temperature at the inlet of the upper part ($T_8 - T_6$), called 'hot pinch' this time and denoted as ΔT, can be verified. In the work of De Paepe et al. [10], the latter was forced to have a value of at least 50°C and we chose to use the same minimal value in our model. The last missing parameter is the absolute humidity of water in state 6. It can be computed using the mass conservation of dry air ($m_{\mathrm{da,2}} = m_{\mathrm{da,6}}$) and knowing that all the injected water is evaporated. This reads:

$$x_{\mathrm{v,6}} = x_{\mathrm{v,2}} + \frac{\dot{m}_{\mathrm{H2O}}}{m_{\mathrm{da,2}}} \left[\frac{\mathrm{kg_{H2O}}}{\mathrm{kg_{da}}}\right] \tag{5.12}$$

In the M-saturator, three key parameters can be set as inputs. The two first ones are the injected water mass flow rate and the wet-bulb effectiveness. The dew point effectiveness has not been considered as a fundamental input in itself due to its limited impact on the cycle as detailed in chapter 7. But an alternative way to model the cycle is to fix rather the hot pinch of temperature instead of setting the wet-bulb effectiveness. In the present section only the first approach was explained, but the adaptation of the model in order to have the hot pinch as an input is not very complex. Nevertheless, all the three parameters can not be fixed at the same time. For instance, at a fixed injected water flow rate, fixing one of the two other parameters automatically sets the other one. Imposing both the pinch of temperature and the wet-bulb effectiveness (for a fixed quantity of injected water) would overconstrain the upper part of the M-saturator. The main difference between the two ways of fixing the inputs is that each determines one of the outlet state of the upper part. Indeed, the pinch of temperature sets the temperature in state 6 based on the TOT while the wet-bulb effectiveness fixes the temperature in state 9 as shown in Equation 5.4. As the temperatures in states 3 and 4 and the water content do not vary for the same injected water mass flow, it is not possible to respect the energy balance while choosing freely the two inputs. Still, as explained by De Paepe et al. [10], the M-cycle has a degree of freedom that other humidified heat exchangers do not have. Indeed, the latter always have an optimal amount of injected water corresponding to imposing the minimal pinch of temperature. Whereas the M-cycle offers an additional degree of freedom. Indeed, it can be seen as three different heat exchangers, therefore requiring the computation of each heat flux. Adding the amount of the injected water gives four unknowns to the system. The dew point effectiveness supplies one equation to determine the heat exchanged in the lower part while the wet-bulb effectiveness (or the hot pinch depending on what is fixed) determines the same quantity in the upper part. Adding the fact that the energy balance on the entire system must be respected, this makes a total of three equations. It is therefore possible to vary the amount of injected water in the system. In the following, the injected water flow rate will always be an input whereas either the wet-bulb effectiveness or the hot pinch will be fixed.

5.3 Results & Comparison

After modelling this particular humidified heat recuperator, it is important to be sure that our model gives coherent results. As it is based on the work from De Paepe et al. [10], the results of our model are now compared to those of the same paper. More precisely, the temperature deviation in every state of the M-saturator is computed and analysed. To make the comparison, the same M-Cycle inputs, corresponding then to a MBC, are used (see Table 5.1).

Table 5.1: Inputs used in our M-cycle model, coming from [10].

	Constant rotational speed		**Constant power output**	
	$\epsilon_{WB} = 0.9$	$\Delta T = 50°C$	$\epsilon_{WB} = 0.9$	$\Delta T = 50°C$
T_1 [°C]	15	15	15	15
T_2 [°C]	203.5	203.5	168.2	168.2
T_8 [°C]	700	696.3	739.2	734.6
p_2 [bar]	4.34	4.34	3.44	3.44
p_8 [bar]	1.05	1.05	1.05	1.05
$\dot{m}_{air}$ [g/s]	574	574	454	460
$\dot{m}_{water}$ [g/s]	147	153	117	117
$\dot{m}_{fuel}$ [g/s]	12.3	6.93	9.43	4.68
ϵ_{dew} [-]	0.8	0.8	0.8	0.8
ϵ_{WB} [-]	0.9	0.98	0.9	0.975

As shown in Table 5.1, the article provides four different sets of input parameters, each corresponding to a study case. Firstly, they are divided in two categories: constant rotational speed and constant power output. Then, each category is divided into either a fixed ϵ_{WB} or a fixed ΔT. As the purpose here is to compare exclusively the results of the M-power component, only the associated inputs are listed. The denomination of the cases used in the article is therefore not really adapted as neither the rotational speed nor the power output are involved in the M-Cycle model in itself. In the following, they are rather called respectively 'classical model' and 'model with boosted T_4' for the constant rotational speed and constant power output. The difference between the two is the use of additional assumptions for the cases associated with the 'model with boosted T_4'. Indeed, similarly to what has been done by De Paepe et al. in the article, the temperatures in states 4 and 5 are forced to be the same.

5.3.1 Classical model

The classical model corresponds to the one used to simulate the results without adding any new assumption from what has been presented so far. As for every case, all the injected water in the upper part is evaporated in state 5 and the air is there fully saturated. However in state 4, some liquid water still remains even though the air is also fully saturated. Table 5.2 lists the temperatures obtained with our model as well as the ones indicated in the reference article and the relative error between them.

Table 5.2: For the classical cases, the maximum relative deviation between our model and [10] is 3.52%.

	$\epsilon_{\mathrm{WB}} = 0.9$			$\Delta T = 50°\mathrm{C}$		
	Model	Article [10]	Deviation [%]	Model	Article [10]	Deviation [%]
T3 [°C]	64.95	64.8	0.24	64.95	64.8	0.24
T4 [°C]	95.88	93.2	2.88	95.88	93.0	3.01
T5 [°C]	106.96	104.8	2.06	107.76	105.7	1.95
T6 [°C]	367.87	381.3	-3.52	628.01	646.3	-2.83
T9 [°C]	111.06	110.7	0.33	58.64	57.9	1.28

The relative error gives an indication on the accuracy of our model. As this error is lower or equal to 3.5% in every state, it is rather accurate. Furthermore, as two numerical models are compared, the results might vary a bit depending on the assumptions taken and the way each model has been developed.

The heat fluxes that take place in the M-saturator are represented on Figure 5.3 and Figure 5.4 respectively for $\epsilon_{\mathrm{WB}} = 0.9$ and $\Delta T = 50°\mathrm{C}$, as well as the temperatures of every state. One can observe that a much larger quantity of heat is exchanged in the upper part for both cases. This makes sense as the initial hot flow in that part has the higher energy content (flue gases coming from the turbine). Also, more heat is transferred when fixing the hot pinch of temperature. This is linked to the associated higher wet-bulb effectiveness, which will be explained in the sensitivity analysis (see chapter 7). As the dew point effectiveness and the incoming cold flow properties do not change, the heat exchanged in the lower part is identical for both cases.

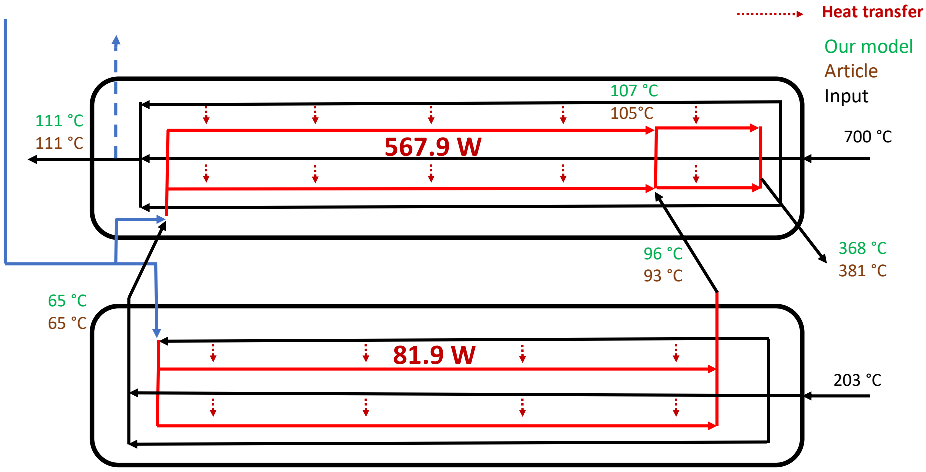

Figure 5.3: More heat is recovered in the upper channel thanks to the high energy content of the incoming flue gases ($\epsilon_{\text{WB}} = 0.9$).

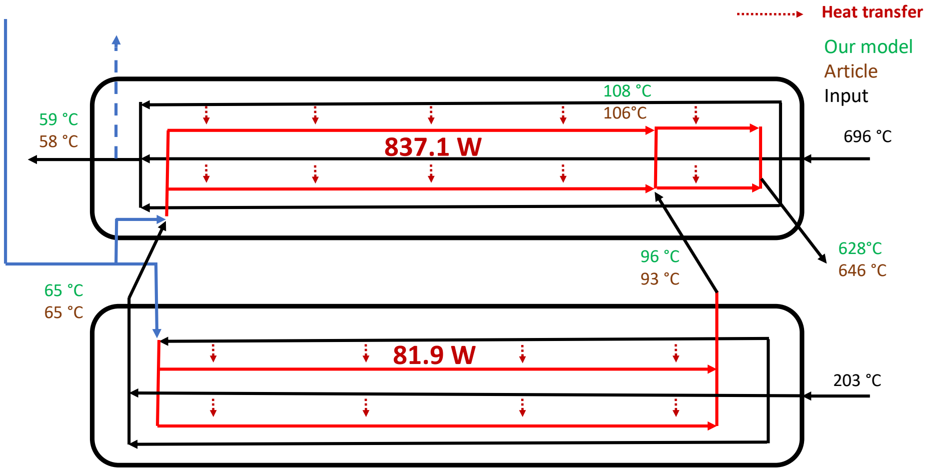

Figure 5.4: The case $\Delta T = 50°\text{C}$ is associated with a higher heat recovery compared to $\epsilon_{\text{WB}} = 0.9$ due to the associated higher wet-bulb effectiveness. Similarly to $\epsilon_{\text{WB}} = 0.9$, the heat recovered in the upper channel is higher.

5.3.2 Model with boosted T_4

Using the initial set of assumptions with the inputs corresponding to the two cases at constant power gives major deviations from the results of the paper [10]. In order to assess if our model was accurate for those cases as well, a meeting was taken with Prof. De Paepe to figure out the specific assumptions taken in these cases. This section is thus intended to show that our model was still able to give coherent results after being slightly adapted.

The major difference now is that the model is pushed to obtain equal temperatures in states 4 and 5. In order to achieve such a condition, one more assumption must be added : the air is fully saturated in state 4 (similar as before) and all the injected water in the lower part of the M-saturator must be evaporated. Indeed, the proportion of water and air in state 4 with respect to the total injected quantity for each flow is the same (both equal to 1/3) which is also the case in state 5 (but the proportion there is 2/3). But as all the injected liquid water from the upper part is evaporated in state 5, the only way to have the same temperature is to evaporate all the injected water from the lower part in state 4. This comes from the fact that the saturation temperature of the air only depends on its gaseous water fraction content. In other words, the temperature of state 4 is kind of boosted by evaporating all the liquid water, which explains the denomination of the corresponding cases.

Adding this assumption overconstraints the system of equations used before, which might violate the previously used energy balance on the lower part. Actually, the temperature in state 4 is imposed without checking that there is enough energy available in the lower channel to reach it.

In order to release one degree of freedom and to use the energy conservation, another assumption must be added : a fraction of energy from the hot flue gases in the upper part will be transferred to the flow in the lower part going from state 3 to state 4 (one heat flux is then added as represented on Figure 5.5 and Figure 10.3, in the appendix, respectively for $\epsilon_{\mathrm{WB}} = 0.9$ and $\Delta T = 50°\mathrm{C}$). This additional heat allows to give enough energy to evaporate all the water in state 4 and reach the imposed temperature. In order to satisfy the energy conservation in the lower part, the additional heat ($\dot{Q}_{\mathrm{add}}$) can be computed as:

$$\dot{Q}_{\mathrm{add}} = \frac{1}{3}\dot{m}_{\mathrm{da},2} * h_4 - (\dot{m}_{\mathrm{da},2} * h_2 + \frac{1}{3}\dot{m}_{\mathrm{H2O}} * h_{\mathrm{H2O,in}} - \frac{2}{3}\dot{m}_{\mathrm{da},2} * h_3) \tag{5.13}$$

Then, it has to be added in the energy conservation of the upper part as follows:

$$\begin{aligned} \frac{2}{3}\dot{m}_{\mathrm{da},2} * h_3 + \dot{m}_{\mathrm{dg},8} * h_8 + \frac{2}{3}\dot{m}_{\mathrm{H2O}} * h_{\mathrm{H2O,in}} + \frac{1}{3}\dot{m}_{\mathrm{da},2} * h_4 = \\ (\dot{m}_{\mathrm{dg},8} - \dot{m}_{\mathrm{cond}}) * h_9 + \dot{m}_{\mathrm{cond}} * h_{\mathrm{H2O},9} + (\dot{m}_{\mathrm{da},2} + \dot{m}_{\mathrm{H2O}}) * h_6 + \dot{Q}_{\mathrm{add}} \end{aligned} \tag{5.14}$$

The results associated with the situation described here are shown in Table 5.3. Again, all the relative errors are below 3.5%.

Figure 5.5 and Figure 10.3 (in the appendix) show the different heat exchanges that are taking place in the M-saturator for the two different fixed parameters. According to the new assumption, a fraction of the heat available in the flue gases (between 9% and 14% of the total heat transferred between states 8 and 9) is sent to state 4. The heat gained from the flow between state 2 and state 3 is also roughly equivalent to this additional heat transfer. Without this latter, only half of the energy required to evaporate all the injected water in the lower part would have been supplied. As the dew point effectiveness and the cold inlet temperature do not change between the two cases ($\epsilon_{\mathrm{WB}} = 0.9$ and $\Delta T = 50°\mathrm{C}$), nearly the same temperatures are reached in T_3

and T_4. The difference between the added heat exchange (respectively 57.9 W and 57.3 W, due to the slightly different inlet air mass flow) for each case is then very small. The same comments as for the classical model are still valid.

Table 5.3: For the cases with T_4 boosted, the maximum relative deviation between our model and [10] is 3.33%.

	$\epsilon_{\text{WB}} = 0.9$			$\Delta T = 50°\text{C}$		
	Model	Article	Deviation [%]	Model	Article	Deviation [%]
T3 [°C]	54.73	54.7	0.05	54.73	54.7	0.05
T4 [°C]	100.42	98.4	2.06	100.17	98.3	1.90
T5 [°C]	100.42	98.4	2.06	100.17	98.3	1.90
T6 [°C]	388.61	402	-3.33	665.80	684	-2.66
T9 [°C]	109.06	108.7	0.33	56.43	55.3	2.04

In practice, the additional assumption used to boost the temperature in state 4 might increase the complexity of the recuperator as it requires an additional heat exchange from the upper part to the lower part. We decided not to investigate much more on how this could take place in practice and to stick to the assumptions associated with the cases with the classical model.

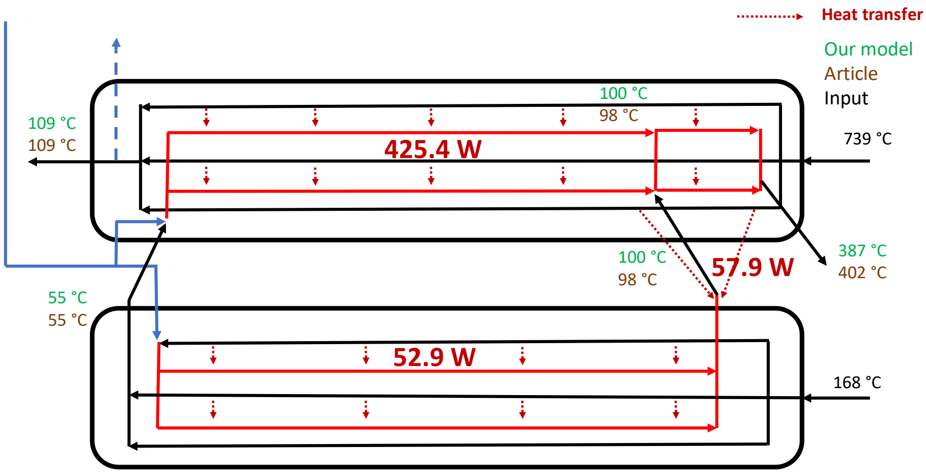

Figure 5.5: An additional heat transfer from the upper part towards the lower part is needed to evaporate all the injected water in the lower part (case with $\epsilon_{\text{WB}} = 0.9$).

Chapter 6

M-SAB cycle

Once the two separated models of the IBC and the M-Cycle are completed, they must be assembled together. In this sense, the conventional heat exchanger implemented in the IBC model must be replaced by the M-power component. But not only that, the merging also implies the introduction of a preheater. The reason and the way it is done constitute the first consideration addressed in this chapter. As mentioned in chapter 2, even though the IBC model was developed using the MTT mGT, the final model of the M-SAB cycle will rather be adapted to another mGT : the Turbec T100. Changing the engine requires several adjustments which are presented thereafter. This chapter finally describes the operating principle of our model and ends with an elementary analysis of its results giving a first perception of how the model reacts to different input parameters.

6.1 IBC : addition of a preheater

The fact of having an inverted cycle implies that the inlet of the heat recuperator is at ambient temperature. This is not the case for a BC thanks to the presence of the compressor which increases that mentioned temperature. When using a typical heat exchanger, a low inlet temperature is not a problem. On the contrary, it enhances the heat recovery. However when using the M-cycle as the heat exchanger, the heat used in the lower wet channel to increase the temperature of the backward flow (from state 3 to state 4, in the numeration associated with the M-power component displayed on Figure 5.2) comes from the incoming cold flow (state 2). But if this last flow is at ambient temperature, the heat exchange would be very limited. Moreover, as specified in the previous chapter, a positive cold pinch of temperature must be maintained between the cooled and heated flow at the inlet of the cold side. As mentioned in section 5.2, the typical minimal value considered for this parameter is 15°C [10]. This latter evolves with the inlet temperature of the M-cycle as represented on Figure 6.1. This graph was drawn using a typical inlet pressure (0.96 bar due to the pressure drop induced by the introduction of a preheater), relative humidity (60%) and injected mass flows (20 g/s of injected water in the M-Cycle and 130 g/s of air injected, which are typical mass flows as shown in section 6.3). The wet-bulb and dew point effectiveness were also kept at their value presented in chapter 5. As can be seen on the graph, the minimal inlet temperature which provides at least the required cold pinch is 51°C.

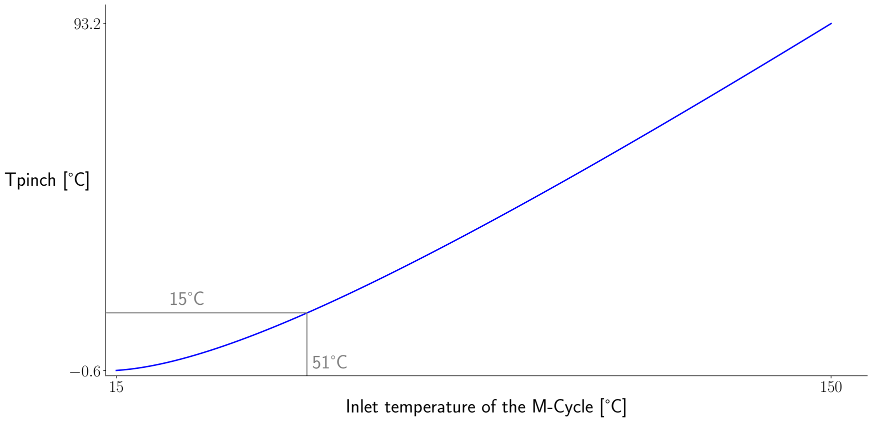

Figure 6.1: In order to guarantee a minimal cold pinch of 15°C, the cold inlet temperature of the M-Cycle must be of at least 51°C.

The latter concern is usually overcome in the literature with the addition of a solar preheater, as it was done by Mahmood et al. [30] and Khalatov et al. [14]. Nevertheless, this will not be the case in our model. The reason has already been mentioned in chapter 3 : adding a solar preheater goes in pair with a higher complexity and larger investment costs. But also relying on a renewable source of energy (the sun) declines one of the main strength of mGT cycles : their flexibility. Another solution has therefore been considered to deal with the essential need of preheating the initial flow. As highlighted in the analysis of the IBC model with the MTT mGT, a considerable quantity of heat is available after the compressor. This latter was in that model recovered in the second economizer. Our idea is now to use that remaining energy in order to preheat the air sent to the M-Cycle instead of increasing the amount of heat recovered as thermal power output. The resulting cycle is visible on Figure 6.2.

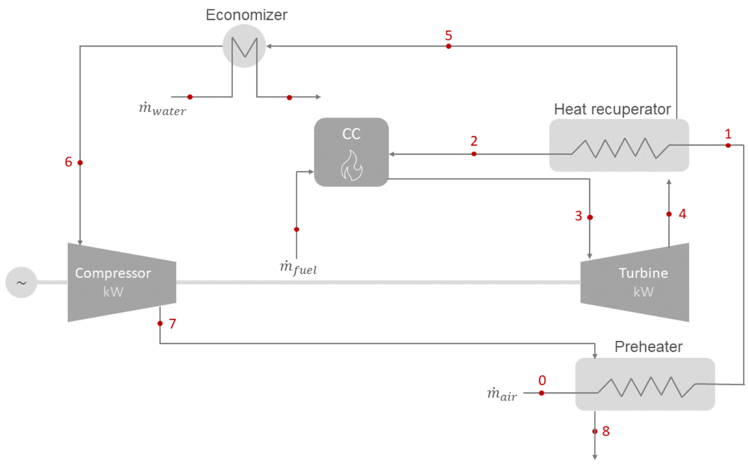

Figure 6.2: Modified schematic of the IBC with the introduction of a preheater.

The preheater is modelled as a gas-gas heat exchanger, like the heat recuperator of the IBC model. The pressure drops are also assumed to be the same and the preheater effectiveness is estimated at 90% (typical value for the effectiveness of a gas-gas heat exchanger [8, 29, 38]). Taking the results of the IBC model with the MTT mGT and replacing the second economizer by the preheater allows to reach a temperature of 155°C at the inlet of the heat exchanger (see Figure 10.4 in the appendix). This is then more than enough to respect the minimal cold pinch of 15°C.

6.2 IBC : Conversion from the MTT to the T100

As explained in the literature review, introducing humidity involves increased investment costs. Such investment is therefore not justified for small power units such as the MTT and its associated 1 kW_e electrical power output. The electrical efficiency reached with an IBC applied on that particular mGT accounts barely for a bit more than 16%. As a result, another mGT is used for the model of the M-SAB cycle : the Turbec T100. This mGT has been installed at the VUB laboratory. As already cited a couple of times, W. De Paepe, M. M. Carrero and other researchers in that university investigated the possibility and consequences of introducing humidity in it [5, 11, 35–37]. The paper from De Paepe et al. [10] previously used to model the M-Cycle is also a numerical investigation on that same installation. This justifies the use of that mGT in our final M-SAB cycle.

6.2.1 Specifications of the T100 mGT

Table 6.1 summarises the specifications of the T100 mGT. The power outputs correspond to those observed when the unit is operated in a conventional BC layout. Consequently, they might vary when running the same mGT in an inverted mode. One can notice the higher electrical power output and efficiency compared to the MTT ones. The isentropic efficiency of the compressor is found by using the compressor map as further explained in subsection 6.2.3 while the isentropic efficiency of the turbine is taken as a constant value equal to 85%. This is done according to what Marina Montero Carrero has described in her work [5].

Table 6.1: Specifications of the Turbec T100 mGT [5]. The higher electrical power output compared to the MTT mGT justifies the potential introduction of water in the cycle and the higher proportion of electricity generated with respect to the thermal power output makes more sense for a unit intended to promote the electrical production.

Specifications	**Value**
Nominal power output :	
Electricity [kW_e]	100
Heat [kW_{th}]	165
Electrical efficiency [%]	30
Thermal efficiency [%]	50
Isentropic efficiency :	
Compressor [%]	From the maps
Turbine [%]	85
Mechanical efficiency :	
Compressor [%]	99
Turbine [%]	99
Power electronics efficiency [%]	95
Generator efficiency [%]	99

6.2.2 Pressure drops & heat losses

Concerning the pressure and thermal losses considered in each component, they are listed in Table 6.2. Unlike the IBC model, they are now all computed using a relative pressure drop or heat loss coefficient. One can note that all the heat losses of the cycle are gathered as one single heat loss in the combustion chamber accounting for 5% of the input energy. The values are similar to those from the VUB research team [5] but some have been adapted to an inverted mode. For instance when running the T100 mGT in a BC configuration, the thermal heat losses equal 19 kW. But as the power outputs decrease when switching to an inverted mode, this value is not relevant anymore. In any case, the effects of varying the pressure drops and heat losses are analysed in the sensitivity analysis (see chapter 7).

Table 6.2: Relative pressure drop and heat loss coefficients for each IBC component.

Assumptions	**Value**
Combustion thermal losses	5% of the heat added
Relative pressure loss :	
Combustion chamber	5%
Economizer (gas side)	1%
Heat exchanger (cold side)	5%
Heat exchanger (hot side)	2%

6.2.3 T100 maps

Unlike for the MTT mGT, the turbine and compressor maps of the T100 mGT are now available to us. These maps allow us to determine the mass flow and isentropic efficiency depending on their operating point. This latter varies with the pressure ratio and the rotational speed of each turbomachinery component. In practice, dealing with turbomachinery maps requires to use reduced values for the mass flow and the rotational speed. These latter read:

$$\dot{m}_{\text{red}} = \frac{\dot{m}\sqrt{T_{\text{in}}}}{p_{\text{in}}} \tag{6.1}$$

$$N_{\text{red}} = \frac{N}{\sqrt{T_{\text{in}}}} \tag{6.2}$$

where T_{in} and p_{in} are taken as the inlet temperature and pressure of the related component while $\dot{m}$ and N are the real values of the mass flow and the rotational speed.

When working with turbomachinery maps, a choice has to be made between running the cycle with a fixed rotational speed or a fixed electrical load. As the electrical power output does not appear directly on the map while the rotational speed is a required information to find the operating point, fixing this latter seems more straightforward. The second option requires to have a control loop that changes the rotational speed in order to keep the load constant. Indeed, due to the use of the maps, fixing the electrical power output does not allow to compute the total mass flow through the turbine. But this mass flow is necessary in itself to know the electrical production of the cycle. The purpose of the additional loop is then to adapt the rotational speed based on the result given by the previous value to try to finally reach the requested power output. This would add a non-negligible running time to our model and might also make it unstable. As a result, all our simulations are performed at constant rotational speed.

Taking into account the compressor map adds also a technological limit well known in the turbomachinery field : the surge limit. This latter occurs when the reduced mass flow through the compressor becomes too low. As explained further in this section, keeping a fixed rotational speed makes the total mass flow relatively constant through the cycle regardless of the quantity of injected water. Therefore, when more water is introduced, it replaces some of the air that would have been present at a low water injection rate. If condensation occurs in the M-power unit or in the economizer (which is often the case as shown in section 6.3), the total mass flow through the compressor would be reduced. This would shift the operating point of this component closer to the surge limit. As far as condensation has started, injecting more water is then associated with a larger condensation and a lower surge margin. As the aim of our work is to study the thermodynamic potential of the M-SAB cycle (not necessarily applied to a particular machine), we have decided not to limit the injected water mass flow regarding the surge limit. As it is exposed in chapter 7, this parameter is still limited by other thermodynamic considerations. But these latter allow a higher maximal proportion of injected water with respect to the total mass flow (around 30% compared to a bit less than 20% for the surge limitation). Nevertheless, one must not forget to check that the surge limit is not exceeded when implementing the cycle in practice. Indeed, achieving the performance associated with a high water injection rate might require to change the compressor or to lower its surge limit.

The easiest way to avoid considering the surge limit of the compressor is to not use its map (except to compute the isentropic efficiency as specified below). As water injection moves the operating point closer to the surge limit and that our model is working with a fixed rotational speed, the iso-speed lines there are rather flat. Therefore, assuming in that region and after the surge limit that the compressor pressure ratio does not change with the reduced mass flow while keeping the same rotational speed is a legitimate assumption (see Figure 6.3). This compressor pressure ratio is instead computed based on a fixed turbine expansion ratio and the different pressure drops of each component. In other words, we have decided to avoid the iterative process used to match the compressor ratio given by the compressor map, depending on the fixed rotational speed and the computed reduced mass flow, with the one computed from the turbine expansion ratio and the pressure losses.

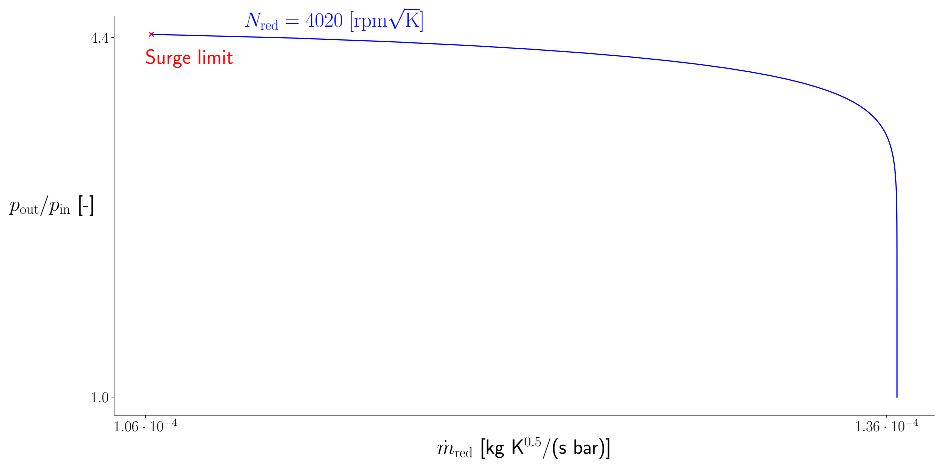

Figure 6.3: In the region close to the surge limit, it is legitimate to assume the iso-speed lines as rather flat.

The procedure used in our model is the following. The rotational speed, the turbine expansion ratio and the TIT are fixed. The reduced rotational speed is found using Equation 6.2 where T_{in} is the TIT. Using this result with the turbine expansion ratio allows to deduce the reduced mass flow from the turbine map. Knowing the turbine inlet pressure (by subtracting the pressure drop of the preheater, recuperator (cold side) and combustion chamber from the atmospheric pressure), the real mass flow through the turbine is found using Equation 6.1. As the turbine inlet pressure and temperature as well as the rotational speed and the turbine expansion ratio do not change, the total mass flow through the cycle is then constant regardless of the quantity of injected water. A small difference might appear due to the alteration of the flow characteristics (molecular weight and heat capacities varies with the amount of injected water) when using the modified reduced values presented below, but it remains rather limited. As mentioned in subsection 6.2.1, the isentropic efficiency of the turbine is taken as a constant equal to 85%. After computing every state (temperature and pressure) until the compressor, the reduced mass flow at its inlet can be known based on the total mass flow found before and again using Equation 6.1. The reduced rotational speed is also computed using Equation 6.2. These two information are enough to take away the isentropic efficiency of the compressor from its map. The assumption concerning the compressor pressure ratio has then no impact. In case of an injected water mass flow normally leading to the surge of the T100 compressor, the isentropic efficiency associated with the point where the surge arises is considered (and then modified as explained below).

The available maps used for the T100 mGT deal with pure air as the working fluid. But in reality, it is necessary to take into account the composition of the flue gases after the combustion chamber. In addition, our final cycle has to do with a fluid which potentially has a high water content due to liquid water injection inside the M-Cycle. The reduced values and the compressor isentropic efficiency must then be adjusted to take these considerations into account. Based on the book from Philip P. Walsh and Paul Fletcher [49], the paper from Reale et al. [50] and that of Parente et al. [51] the adapted reduced mass flow and rotational speed as well as the isentropic efficiency are expressed as:

$$\dot{m}_{\mathrm{red}} = \frac{\dot{m}\sqrt{T_{\mathrm{in}}}}{MW * p_{\mathrm{in}}} \tag{6.3}$$

$$N_{\mathrm{red}} = \frac{N}{\sqrt{\gamma * T_{\mathrm{in}} * R}} \tag{6.4}$$

$$\frac{\eta_{\mathrm{is}}}{\eta_{\mathrm{is}}^*} = \frac{\gamma - 1}{\gamma^* - 1}\sqrt{\frac{\gamma^* + 1}{\gamma + 1}\frac{1 - (\frac{1}{\Pi_{\mathrm{comp}}})^{\dfrac{\gamma^* - 1}{\gamma^*}}}{1 - (\frac{1}{\Pi_{\mathrm{comp}}})^{\dfrac{\gamma - 1}{\gamma}}}} \tag{6.5}$$

where MW is the molecular weight of the working fluid, γ is its ratio of specific heats, R is its specific gas constant and the apex '*' is related to pure air properties.

Taking these modifications into account for the IBC without the M-Cycle and its associated injection of liquid water slightly changes the operating point of the turbomachines. This results in a minor relative decrease of 0.5% of the total mass flow through the turbine and an absolute decrease of the compressor isentropic efficiency of 0.8%. Although the correction here is rather negligible (because the only difference comes from the composition of the flue gases), the injection of water into the M-SAB cycle will involve greater changes.

6.2.4 IBC performance with the T100 mGT

Now that the Turbec T100 mGT maps are included in our IBC model, it can be run to see how it works with this new mGT. The input parameters are listed in Table 6.3.

Table 6.3: Input values of the IBC model with the T100 mGT.

Inputs	**Value**
TIT [°C]	950
Turbine exp. ratio [-]	3
Rotational speed [rpm]	74000
Economizer eff. [%]	92
Heat exchanger eff. [%]	90
Preheater eff. [%]	90

The resulting performance is shown in Table 6.4 while the temperature, pressure and mass flow in every state are shown on Figure 10.5 in the appendix.

Table 6.4: The electrical power output and the electrical efficiency are higher than with the MTT mGT. The mass flow through the cycle is also increased.

Results	**Value**
Comp. ratio [-]	3.68
Mass flow	
Air [g/s]	157.9
Fuel [g/s]	1.5
Power	
Electrical [kW_e]	14.2
Thermal [kW_{th}]	38.3
Primary [kW]	61.4
Efficiency	
Electrical [%]	23.2
Thermal [%]	62.4
Overall [%]	85.6
Exergetic overall [%]	27.8

As expected, running the T100 mGT in an IBC configuration leads to much higher power outputs than with the MTT mGT (14.2 kW_e and 38.3 kW_{th} compared to 1.04 kW_e and 4.11 kW_{th}). The electrical efficiency is also improved by 7.3% in absolute points. One of the main reasons that could explain the increased power outputs is the greater total mass flow throughout the cycle (159 g/s compared to 22 g/s). As explained in subsection 6.2.3, this latter does not really fluctuate if the TIT, the rotational speed and the turbine expansion ratio remain the same. The shaft power produced by the turbine is therefore also unchanged when using the same mGT in the IBC alone. The main point to increase the electrical efficiency is then either to reduce the compressor work (by decreasing the CIT or inducing condensation in the economizer in order to decrease the mass flow through it) or to recuperate as much heat as possible from the flue gases to reduce the fuel consumption.

By now comparing the performance obtained when running the engine in an inverted mode compared to the conventional BC mode, several statements from the literature review can be confirmed. Firstly, the mass flow is much smaller (more than 4 times) when running the cycle in the inverted mode. But as the pressure level is sub-atmospheric, the volumetric flows remain nearly constant and therefore the isentropic efficiency of the turbomachinery components is preserved (at least the one for the compressor as the turbine isentropic efficiency is only considered as a constant). Secondly, the electrical efficiency of the IBC is smaller than that of the BC (23.2% compared to 30%). However, the introduction of the preheater, aimed at satisfying the cold inlet temperature pinch when replacing the heat recuperator with the M-Cycle, is probably not optimal to maximise the electrical efficiency if the plan was to keep an IBC alone. Finally, the thermal efficiency is higher than that of the initial layout (62.4% compared to 50%). As the increase in thermal efficiency is higher than the decrease of the electrical one, the overall efficiency also increases (85.6% compared to 80%). In an exergetic perspective, the inverted cycle is also less efficient as the exergetic overall efficiency is lower (27.8% compared to 35.7% [5]), mainly due to the lower electrical efficiency which has a major contribution as explained in chapter 8.

6.3 Merging of the two models

Now that the preheater is added to the IBC model and that the engine has been adapted, the introduction of the M-Cycle can be fulfilled. The final M-SAB cycle under study is shown on Figure 6.4.

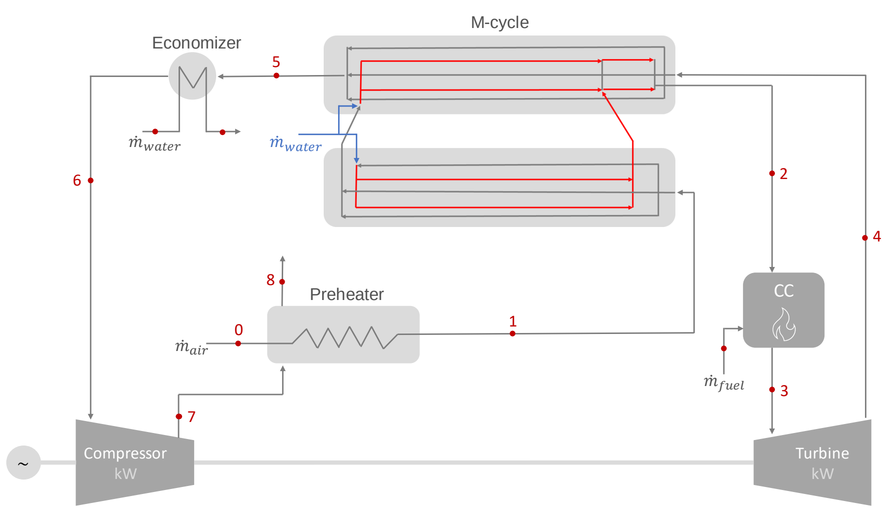

Figure 6.4: Final scheme of the M-SAB cycle.

Adding this component adds a new set of input parameters largely influencing the cycle performance: the wet-bulb effectiveness, the hot pinch of temperature and finally the mass flow rate of injected water. One should remember from section 5.3 that only two of those parameters can be fixed at the same time. In the following, either the wet-bulb effectiveness or the hot pinch is fixed simultaneously to the injected water flow rate. This latter provides a degree of freedom to our model. In order to get a first perception on the way the M-SAB cycle behaves, let us analyse two simulations respectively performed at $\epsilon_{\mathrm{WB}} = 0.9$ (typical value for a heat exchanger effectiveness) or $\Delta T = 50$°C (minimal value required for the hot pinch). The fixed injected water mass flow chosen here is 30 g/s as this constitutes a median value between the lower and upper limits of this parameter. These limits will be explained accurately in chapter 7 and the impact of varying the water injection rate will be largely investigated in the same chapter. The set of input parameters used to produce the coming results is shown in Table 6.5. The same values will be kept as boundary conditions for the sensitivity analysis coming in the next chapter.

Table 6.5: Boundary conditions of the M-SAB cycle.

Preheater		
	Inlet air temperature	15°C
	Inlet air pressure	1.013 bar
	Inlet air humidity	60%
	Effectiveness	90%
	Cold design pressure loss	5%
	Hot design pressure loss	2%
M-Cycle		
	Wet-bulb effectiveness	90%
	Dew point effectiveness	80%
	Feed water temperature	15°C
	Cold design pressure loss	3%
	Hot design pressure loss	40 mbar
Combustion Chamber		
	Design pressure loss	5%
	Heat loss	5% of added power
Turbine		
	TIT	950°C
	Mechanical efficiency	99%
	Expansion ratio	3
	Rotational speed	74000 rpm
Compressor		
	Mechanical efficiency	99%
General		
	Combined power electronics efficiency	94%

The results of the two simulations are listed in Table 6.6. As a comparison, the results of the IBC with the T100 mGT are also shown.

Table 6.6: Fixing $\Delta T = 50°C$ improves the electrical efficiency due to the condensation in the M-power component and the associated enhanced heat recovery. But the thermal power output is larger at $\epsilon_{WB} = 0.9$ since all the condensation occurs in the economizer. Still the total quantity of condensed water is relatively equivalent in both cases.

Parameter		$\epsilon_{WB} = 0.9$	$\Delta T = 50°C$	IBC
Efficiencies				
	Electrical [%]	19.1	36.2	23.2
	Overall [%]	86.6	78.4	85.6
	Compressor (isentropic) [%]	76.8	77.6	73.5
Power				
	Electrical [kW_e]	23.9	24.2	14.2
	Thermal [kW_{th}]	84.2	28.2	38.3
	Primary [kW]	124.8	66.9	61.4
	M-Cycle Recovery [kW]	126.3	179.6	-
Mass flow				
	Total [g/s]	151	151	159
	Condensed in M-Cycle [g/s]	0	17.5	-
	Condensed in Economizer [g/s]	28.4	10.4	0

The first observation between the M-SAB cycle and the IBC without the M-saturator is the appearance of water condensation. This has a major impact on the performance and comes from the injection of liquid water in the M-saturator, largely increasing the water content of the flow. Yet, it does not occur in the same components with $\epsilon_{WB} = 0.9$ or $\Delta T = 50°C$. Indeed, the case with $\Delta T = 50°C$ corresponds to the best heat recovery in this component (179.6 kW compared to 126.3 kW) and is associated with a significant quantity of condensed water there (17.5 g/s). Reaching it requires though to have a rather high wet-bulb effectiveness (value of approximately 98%) as it will be explained in detail in chapter 7. This is then associated with a lower temperature at the hot outlet of the M-cycle (32°C compared to 90°C as shown on Figure 10.6 and Figure 10.7 in the appendix). As the flow can contain less water at lower temperature, this justifies that condensation occurs more easily. Indeed, setting a 50°C pinch induces condensation in the M-saturator while setting a wet-bulb effectiveness of 90% does not. But not condensing in that first component does not mean a loss of energy. All the non-condensed water subsequently condenses in the economizer. So modifying the saturator performance parameters allows to change the distribution of the condensed water between the M-Cycle and the economizer. This constitutes then a trade-off between the heat recovery in each component. The effect of increasing one at the expense of the other is illustrated in the upcoming analysis of Sankey diagrams. Nevertheless, the total amount of condensed water in the cycle at a constant water flow rate remains relatively constant (around 28 g/s for both cases here). In fact, it only depends on the outlet temperature of the economizer, since this temperature is lower than the one at the M-cycle outlet. Even though the wet-bulb effectiveness has a slight impact, the related temperature does not vary by more than 5°C here.

Regarding the M-SAB cycle itself, a major difference between the two cases is the considerable increase in the electrical efficiency with ΔT = 50°C (+17.1% in absolute points). On the other hand, the associated overall efficiency is lower (-8.2% in absolute points). The main reason for this distinct behavior is the improved heat recovery in the M-Cycle due to the higher wet-bulb effectiveness and greater amount of condensed water. In order to understand the benefits of improved M-Cycle performance on the electrical efficiency, the energy fluxes along the cycle for each case are shown on their corresponding Sankey diagram (see Figure 6.5 and Figure 6.6). A first commonality between the two cases is the similar total energy level coming to the turbine inlet due to the similar energy level at the combustion chamber (with a relative difference of 3.8%). Actually, the latter depends mostly on the amount of injected water (which is identical for both cases) and its linked energy needed to be evaporated and heated up to the TIT. As the total mass flow through the cycle does not vary significantly, especially if the same quantity of water is injected, this results in the same shaft power produced by the turbine (50 kW). As the compressor power consumption does not vary importantly (23 kW), the same level of electrical power output is generated (24 kW_e). The main difference between the two cases comes then from the proportion of energy recovered in the M-Cycle. As this last is directly sent to the combustion chamber, it allows to decrease the amount of fuel burned. The more heat recovered, the more fuel saved. An improved electrical efficiency emerges then, for the case with ΔT = 50°C, from the fuel-saving ability due to the improved M-Cycle heat recovery. Even if it tends also to increase the overall efficiency (as the fuel injection rate is smaller), this latter decreases due to the highly reduced thermal power output. The higher proportion of energy recovered in the M-Cycle means simultaneously less energy sent to the economizer (43 kW with ΔT = 50°C compared to 104 kW with $\epsilon_{WB} = 0.9$), and accordingly less recovered heat in that component. The first message to be drawn from this discussion is that the improved heat recovery capacity of the M-Cycle allows some of the remaining heat from the flue gases to be used to reduce fuel consumption and increase electrical efficiency.

A particular point of attention noticeable on the Sankey diagrams is related to the input energy of the fuel. Indeed, the fuel contains hydrogen atoms which are transformed into water after combustion. If this water remains in a gaseous state, the amount of energy provided by combustion is the lower heating value (LHV). In case of a potential condensation of the created water, the energy provided rather corresponds to the higher heating value (HHV). The only difference between these two quantities is the energy associated with the latent heat of vaporization of the created water. Since a significant amount of water can condense in our cycle, allowing considerable heat recovery, this energy must come from somewhere in the Sankey diagram. This explains the presence of an additional energy flux named 'fuel water content'. Yet cycle efficiencies are still computed based on the fuel's LHV.

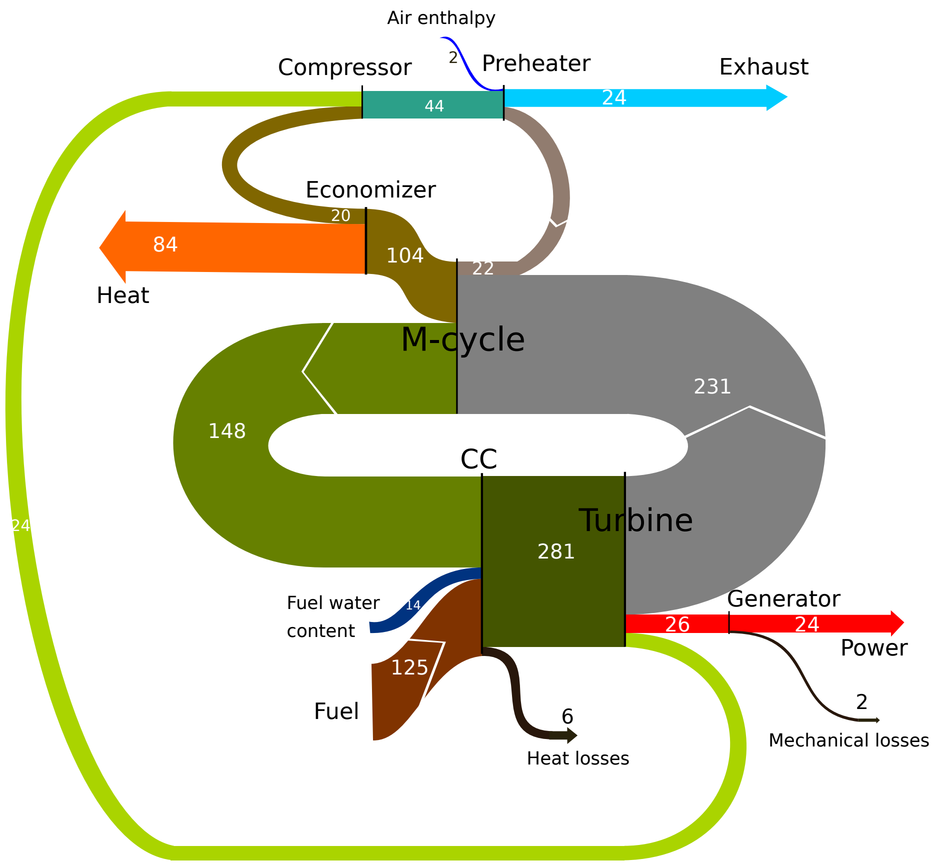

Figure 6.5: The case with $\epsilon_{\mathrm{WB}} = 0.9$ is associated with a high proportion of recovered heat in the economizer resulting in a favorable overall efficiency to the detriment of the electrical efficiency. The energy fluxes are expressed in kW.

Several observations can also be made with the IBC case which does not include the Maisotsenko saturator. First, the isentropic efficiency of the compressor has increased from 3% to 4% in absolute points. This comes from its modified expression (Equation 6.5) to account for the working fluid different from pure air. Even if the composition of the flue gases did not modify it that much, the injection of water with a significant proportion compared to the total mass flow induces a greater modification of the isentropic efficiency of the compressor. Second, the total mass flow is equivalent but not exactly the same (159 g/s compared to 151 g/s). As clarified above, the total mass flow for the M-SAB cycle remains in the same range of values but varies slightly with the injected water mass flow. This is once again due to the impact of the water on the modified reduced quantities used with the turbine map (Equation 6.3 and Equation 6.4). As mentioned earlier, no condensation occurs in the IBC model. This means that the mass flow passing through the compressor is not reduced and is exactly the same as through the turbine. Combining this consideration with the reduced compressor isentropic efficiency, the compressor power consumption exceeds that of the M-SAB cycle resulting in a lower electrical power output.

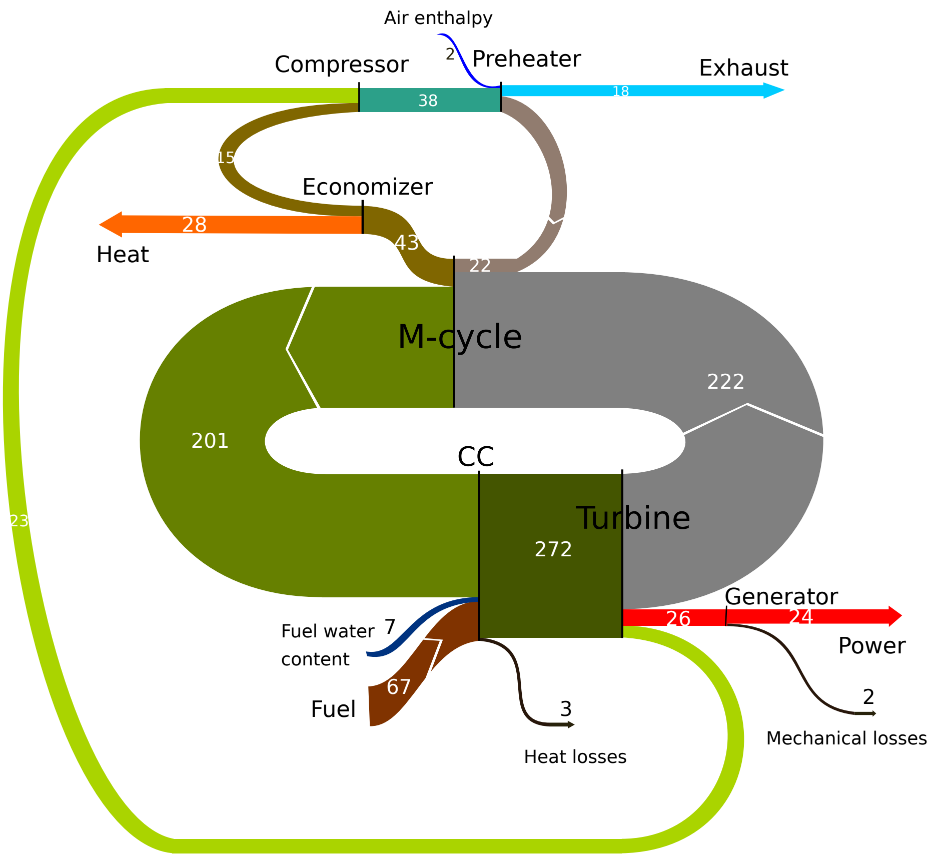

Figure 6.6: The case with $\Delta T = 50°C$ leads to an enhancement of the recovered heat in the M-Cycle resulting in a reduced fuel consumption and thus a better electrical efficiency. The amount of energy sent to the economizer is therefore reduced together with the thermal power output. The energy fluxes are expressed in kW.

Finally, a last remark is necessary concerning the TOT. As shown in Figure 10.6 and Figure 10.7 in the appendix and similarly to what has been achieved in the numerical model of the IBC with the MTT mGT, the temperature at the inlet of the heat recuperator exceeds the typical upper limit for mGT cycles (620°C to 680°C [21]). This latter is even bigger when increasing the amount of injected water. Indeed, it is associated with a higher heat capacity of the flow limiting the temperature reduction at the turbine. Even though particular materials can be used to resist to the higher temperature, they are also more expensive as detailed in chapter 3.

Chapter 7

Sensitivity analysis

This chapter aims to present and analyse the results produced by our final M-SAB cycle model. The impact of the most important parameters on the performance is shown and meticulously explained. This in-depth discussion will give the reader a broad understanding of the behaviour of the M-SAB cycle.

7.1 Preliminary considerations

In order to better perceive the behavior of the M-Cycle component as well as its influence on the performance of the IBC cycle, a sensitivity analysis was carried out. The studied parameters are the performance parameters of the M-power saturator (ϵ_{WB} and ϵ_{dew}), the initial conditions of the working fluid (T_{in} and ϕ_{in}), the design parameters (TIT, heat losses in the combustion chamber and pressure drops along the cycle) and the control parameters of the turbomachines (expansion ratio of the turbine and injected water mass flow). As explained in chapter 5, the particular configuration of the M-Cycle allows to fix a different water mass flow while keeping the other parameters identical. After having studied the effects of this parameter in itself on the cycle performance, the impacts of each other input are then studied while modifying this control parameter. The initial set of values used in every simulation is visible in Table 6.5. Similarly to the sensitivity analysis conducted by De Paepe et al. on the MBC [10], the simulations are made either at a fixed wet-bulb effectiveness of $\epsilon_{\mathrm{WB}} = 0.9$, either at a fixed hot pinch of $\Delta T = 50$°C. As mentioned in chapter 5, fixing one of these two parameters while imposing a water mass flow is enough to determine the other one. For the reasons specified in subsection 6.2.3, all the simulations are carried out at a constant rotational speed.

The amount of injected water has been varied between 20 and 50 g/s. This choice was made based on the minimum and maximum quantity of water that can be injected into the cycle. Indeed, injecting too little water can lead to a too low hot pinch of temperature of the upper part of the M-Cycle. As mentioned earlier, this parameter must be kept to a value higher than 50°C. Even if a lower margin could have been chosen while respecting the second law (which implies that the outlet temperature of the heated flow is lower than the initial temperature of the cooled flow), we have chosen to maintain this parameter at a minimum value of 50°C for all simulations. Consequently, the injected water mass flow must be above 10 g/s and 13 g/s when running the model respectively with $\epsilon_{\mathrm{WB}} = 0.9$ and $\epsilon_{\mathrm{WB}} = 0.98$. The physical reason behind this lower limit is that injecting more water makes it possible to limit the temperature reached by the heated flow at the outlet of the M-Cycle because the recuperated heat is partly used to evaporate the injected water. If the amount of injected water is too low, the increase in temperature might be too important to respect the minimum value of the hot pinch. Also, an assumption of our model was to consider that the flow is saturated when leaving the lower part (state 4 in the M-Cycle numeration). This assumption might not be respected if the amount of injected water is too low. But the definitions used for each effectiveness are inherently based on the fact that the heat exchange in the M-Cycle involves an evaporation process. It is then not correct to apply them if the quantity of injected water is not sufficient. In another perspective, the injected water in this lower part is the key element which allows an heat exchange. Without it, the cooled flow would simply not be able to reach its dew point temperature. As the advantage of the M-power saturator does not lie in such low range of injected water, we chose to perform all the simulations starting with 20 g/s.

In addition to the previous consideration regarding the injection of a minimum water mass flow, one may wonder what happens if no water is injected at all. Actually, this is not linked to a risk of damage to the heat recuperator [10]. This latter will in this case behave as a classical dry heat exchanger. Still, this component is not designed for that use as without water the lower part does not allow for any heat recovery and just increases the pressure drops. Also as specified in the previous paragraph, the way of using each M-Cycle effectiveness is based on several assumptions (presented in chapter 5) which are no longer respected. Although no rigorous calculation has been performed, the value of these parameters is expected to drop.

Concerning the maximal quantity of water that could be injected, it can be limited by two factors: once again the value of the hot pinch of temperature that must stay above 50°C or the need to keep a complete combustion. The first aspect relates to setting a high wet-bulb effectiveness (above 96%) which involves condensation inside the M-Cycle component (as discussed later on when analysing Figure 7.4). As previously presented, the total mass flow in our model is approximately constant. Thus, injecting more water considerably increases the proportion of water per unit air in the working flow. Thereafter when having such a high wet-bulb effectiveness, increasing the injected water mass flow increases the quantity of condensed water in the M-Cycle which improves the heat recovery of that component. Respecting the global M-Cycle energy balance consequently implies an increased outlet temperature of the heated flow which reduces the hot pinch. This issue is avoided when working at a fixed hot pinch by decreasing the wet-bulb effectiveness to keep the minimum value of 50°C (as shown on Figure 7.3). The second limitation deals with the reduced air excess coefficient (λ) when increasing the amount of injected water when the wet-bulb effectiveness is lower than 96% (no condensation in the M-Cycle). Indeed, if condensation does not occur in the M-power component, more injected water is associated with a higher fuel consumption to evaporate all the water and reach the fixed TIT. But since the total mass flow does not change much, the added water actually replaces some of the air. Both effects tend to decrease the mass of air per mass of injected fuel, therefore decreasing the air excess coefficient. The maximum quantity of water is then reached when this parameter becomes lower than 1, which means that there is not enough air to burn the injected fuel. The upper limit of the water mass flow varies then with the wet-bulb effectiveness. For the hot pinch limitation, the highest analysed wet-bulb effectiveness (98%) is associated with a maximum water mass flow of 48 g/s. Whereas the complete combustion faces a limit of 47 g/s when increasing the TIT (see Figure 7.16) with $\epsilon_{\mathrm{WB}} = 0.9$. We then decided to do all the simulations up to a value of 50 g/s (except those with an upper bound lower than this value). As the total mass flow set by the turbine is about 150 g/s, the maximum mass flow of injected water already constitutes one third of the working flow. On top of the two mentioned thermodynamic aspects, another consideration limiting the amount of injected water in practice is the compressor surge. As justified in subsection 6.2.3, we decided not to account for this technological phenomenon in our model. Indeed, this would have restricted the upper bound of water injectable and limit the range of our study of the thermodynamic potential of the cycle. Nevertheless, this must be taken into account in the design process.

A last point of attention that the reader must keep in mind when looking at values of the thermal power output and the overall efficiency is about their exergy content. Indeed, the exergetic version of these quantities highly depends on the temperature at which the heat is recovered in the economizer. This latter definitely varies with the amount of heat recovered by the M-Cycle. As a matter of fact, increasing the wet-bulb effectiveness involves a lower hot outlet temperature of the flue gases at the end of the upper channel (see Equation 5.4). As this temperature corresponds to the inlet temperature of the economizer, it is also the highest temperature attainable by the cooling water (case of an ideal economizer). Therefore, the exergy content of the thermal power output decreases when increasing the wet-bulb effectiveness. It is therefore also associated with a significant decrease in overall efficiency when going from the energetic to the exergetic value. In order to have a first intuition, the inlet temperature of the economizer reaches approximately 90°C for $\epsilon_{\mathrm{WB}} = 0.9$ (depending slightly on the amount of injected water) while it reaches only about 32°C for $\Delta T = 50$°C (which is associated with a much higher wet-bulb effectiveness). A more detailed exergetic analysis is conducted in chapter 8 but it is still important to be aware of this aspect when going through this chapter.

7.2 Impact of the injected water mass flow

As a first analysis the impact of the injected water flow rate for the two mentioned cases ($\epsilon_{\mathrm{WB}} = 0.9$ or $\Delta T = 50$°C) is shown on Figure 7.1 and Figure 7.2. Even though this parameter will still vary when investigating the impact of the other parameters, a particular focus on its effect is taken here. Increasing the amount of injected water increases the electrical power output for both cases. This must be related to the fact that the total mass flow is fixed by the turbine. The injected water then replaces a proportion of the air present at a lower injection rate. But the total quantity of water that condenses before the compressor, thus in the economizer and the M-Cycle, is driven by the outlet temperature of the economizer. This latter fixes indeed the maximal water content, reached when saturating the flow. That temperature depends on the economizer effectiveness but also on the wet-bulb effectiveness of the M-Cycle which fixes the outlet temperature of that component and so the inlet temperature of the economizer. Increasing the injected water mass flow while keeping each effectiveness constant leads therefore to more condensation. This results in a decreased mass flow going through the compressor and accordingly less work needed by that component. As the shaft power does not vary much, a higher proportion of it is converted into electricity.

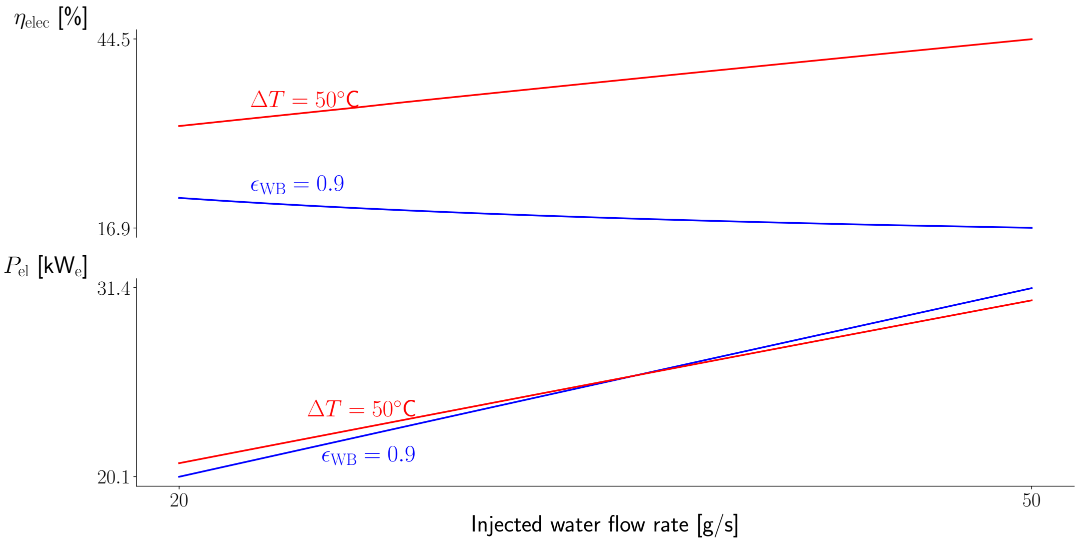

Figure 7.1: Injecting more water increases the electrical power output for both cases due to a higher quantity of condensed water before the compressor, reducing its power consumption. The case with $\Delta T = 50°C$ is also associated with an increasing electrical efficiency while this latter decreases with $\epsilon_{WB} = 0.9$. The difference comes from the improved M-Cycle heat recovery with $\Delta T = 50°C$ thanks to the presence of water condensation in that component.

The fact of having a slightly higher electrical power production at a fixed hot pinch (20.9 kW$_e$ compared to 20.1 kW$_e$ at $\epsilon_{WB} = 0.9$) when the water injection rate is low (20 g/s) is linked to the higher associated value of the wet-bulb effectiveness (98.43% as shown on Figure 7.3). Indeed, it decreases the outlet temperature of the M-Cycle and then also the outlet temperature of the economizer. As a result, more water condenses accentuating the effect described before. But one can see that the growth rate of the curve at a fixed wet-bulb effectiveness of 90% when increasing the water injection flow rate is higher. It results in a larger electrical power output (31.4 kW$_e$ compared to 30.6 kW$_e$) when the water flow rate reaches 50 g/s. This is linked to the fact that more water present in the cycle requires more energy to evaporate all of that water and reach the fixed TIT. The typical wet-bulb effectiveness of 90% is not sufficient to cause condensation in the M-Cycle and increase the heat recovery, so the fuel flow rate increases. As it will be explained when investigating the behavior of the cycle with a fixed and high wet-bulb effectiveness, increasing the heat recovery in the M-Cycle by generating condensation leads to a large fuel saving capacity as the flow recovering the heat is sent to the combustion chamber. Therefore, the case with $\epsilon_{\mathrm{WB}} = 0.9$ involves a higher fuel consumption than the case with $\Delta T = 50$°C. As burning more fuel is associated with a greater creation of water due to the combustion, the total water content of the flow after the combustion chamber is higher (0.72 $\mathrm{kg_{H20}/kg_{dg}}$ compared to 0.6 $\mathrm{kg_{H20}/kg_{dg}}$ when fixing ΔT). This finally increases the quantity of condensed water and decreases the mass flow through the compressor. The second effect of increasing the water content after the combustion chamber has a greater impact than the first one (higher wet-bulb effectiveness) when increasing the injected water mass flow. In the meantime, the first effect is less pronounced due to the decrease of the wet-bulb effectiveness at fixed hot pinch when injecting more water (explained when analysing Figure 7.3).

Injecting more water at a fixed wet-bulb effectiveness of 90% decreases the electrical efficiency (from 21.3% to 16.9% when increasing the injected water from 20 to 50 g/s). Although the electrical power output grows (from 20.1 $\mathrm{kW_e}$ to 31.4 $\mathrm{kW_e}$), the mentioned increase in primary flux is higher (absolute increase of 90.9 kW) resulting in a decreasing electrical efficiency. The trend is opposite for the curve at a fixed hot pinch. The main difference comes from the ability of condensing in the M-power saturator. Indeed, adding water while condensing in that component enhances the heat recovery thanks to the greater amount condensed and its associated high latent heat release. As this energy is recovered in the M-Cycle, it is used to decrease the amount of fuel needed (the absolute primary energy increase accounts only for 3.1 kW now compared to 90.9 kW in the previous case). The combined effect of increasing the electrical power output and reducing the primary flux leads to a significant increase in electrical efficiency (from 31.8% to 44.5% respectively for 20 g/s and 50 g/s of water injection).

Contrarily to the electrical power output, the heat recovered by the economizer as a useful thermal power output increases with the water injection rate only for the case with the fixed wet-bulb effectiveness (see Figure 7.2). The main difference lies once again in the absence of condensation in the M-Cycle (compared to the case with the fixed hot pinch). Indeed when increasing the water injection rate from 20 to 50 g/s, the total energy needed at the combustion chamber to evaporate all the water and reach the TIT is larger (from 251 kW to 358 kW) while the heat recovery in the M-Cycle barely changes (from 146 kW to 152 kW). Consequently, the fuel mass flow rate must increase leading to a higher primary flux (from 94.4 kW to 185.3 kW). But as the added energy coming from the fuel is not recovered in the M-Cycle due to the absence of condensation, this energy is recovered in the economizer under the form of useful thermal output (the quantity of condensed water in the economizer goes from 16.2 g/s to 53.1 g/s while the thermal power output rises from 52.9 $\mathrm{kW_{th}}$ to 147 $\mathrm{kW_{th}}$). Meanwhile with $\Delta T = 50$°C, increasing the injected water flow rate increases the quantity of condensed water in the M-power unit. This added condensation would have occurred in the economizer instead if no condensation was possible before. Thereafter, the energy flux sent by the M-Cycle to the economizer is much lower for the hot pinch case (38.65 kW compared to 161.6 kW at $\epsilon_{\mathrm{WB}} = 0.9$, values computed with a water mass flow of 50 g/s). This results in a greater heat recovery in the M-Cycle towards the combustion chamber to decrease the fuel mass flow rate, heat which is then not recovered by the economizer as a thermal power output.

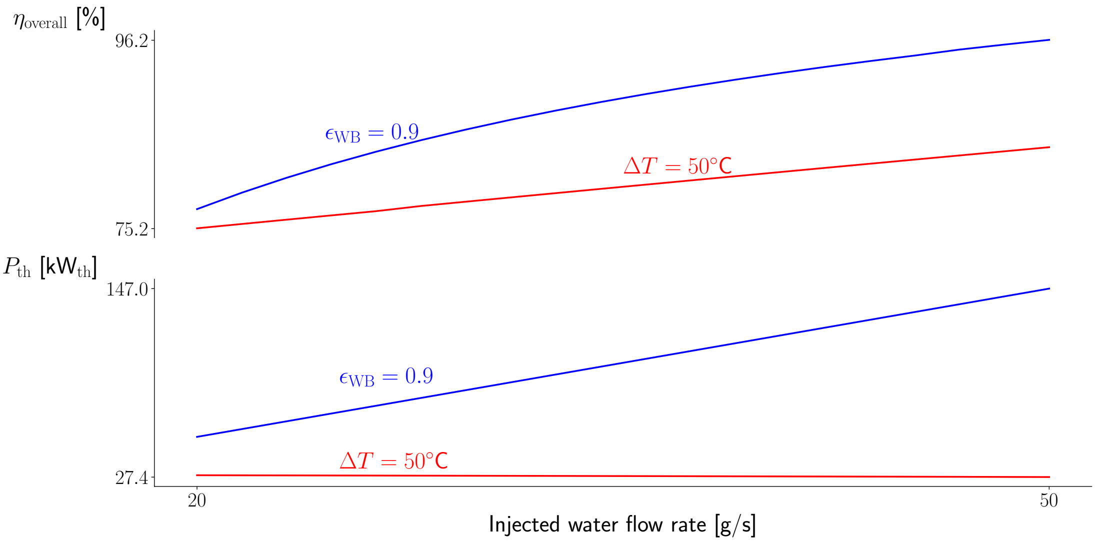

Figure 7.2: Increasing the injected water mass flow increases the thermal power output only for $\epsilon_{\text{WB}} = 0.9$ due to the prominent condensation in the economizer. This latter occurs in the M-Cycle instead with $\Delta T = 50°\text{C}$, not increasing the thermal power output. Contrarily, the overall efficiency increases for both cases as the total quantity of condensed water until the end of the cycle is increased, resulting in reduced exhaust losses.

Concerning the overall efficiency, Figure 7.2 shows an increase with the water injection flow rate for both curves. When analysing the overall efficiency, two perspectives could be taken. One could firstly look at the useful output fluxes (electrical and thermal) compared to the amount of primary flux injected, dictated by the fuel mass flow rate. The second option is to check how the losses evolve compared once again to the primary power flux. The different energy losses throughout the cycle are the heat losses at the combustion chamber (always considered as 5% of the added primary flux except when studying their impact), the mechanical losses of the turbomachinery components (dictated by their mechanical efficiency which is kept constant) and the exhaust losses. As the proportion of the two first losses compared to the injected energy at the combustion chamber will be rather constant, the evolution of the proportion of exhaust losses is a good indicator of how the overall efficiency of the cycle evolves.

As already explained before, injecting more water involves a higher proportion of water in the total mass flow. Consequently, the quantity of condensed water (either in the M-Cycle or in the economizer depending on the case) is higher. The resulting mass flow after the economizer is thus reduced, leading to lower exhaust losses. Let us illustrate this statement case by case. Firstly when keeping the wet-bulb effectiveness constant and injecting more water, the combined increase in electrical and thermal power output (respectively +11.3 kW_e and +94.1 kW_{th} when increasing the water injection flow rate from 20 to 50 g/s) is higher than the increase in primary flux (+90.9 kW for the same water mass flows). Taking the other perspective, the increased proportion of water per unit air in the flow after the combustion chamber (0.72 kg_{H20}/kg_{da} at 50 g/s of injected water compared to 0.19 kg_{H20}/kg_{da} at 20 g/s) due to the water injection results in a higher fraction of the flow condensed in the economizer. Consequently, the remaining energy after this component is lower resulting in lower exhaust losses (16.8 kW compared to 27 kW at a lower water injection rate). Combining the lower exhaust losses with more primary power injected means an increase in overall efficiency. Secondly, at a fixed hot pinch, it has been shown that increasing the injected water mass flow from 20 to 50 g/s results in an increase in electrical power production (+9.7 kW_e) and a slight decrease of the thermal power output (-0.8 kW_{th}). Also the heat recovery in the M-Cycle allows to keep the increase in primary flux at only +3.1 kW (compared to +90.9 kW for the previous case). Combining everything leads to an increase in overall efficiency.

This first analysis already shows the balance between the heat recovered in the economizer as a thermal power output and the heat recovery in the M-power component, used to improve the electrical performance of the cycle, depending on the M-Cycle performance parameters.

As presented in chapter 5, fixing either ϵ_{WB} or ΔT with a particular water mass flow is enough to determine the third parameter. During the analysis of the first two graphs was also mentioned the fact that increasing the water injection rate at fixed hot pinch is linked to a decrease of the associated wet-bulb effectiveness. This evolution is displayed on Figure 7.3. All the elements needed to understand this behavior have already been discussed. Indeed, the minimal value chosen for the pinch induces condensation in the M-Cycle. Injecting more water increases then the quantity of condensed water there, enhancing the heat recovery from the flue gases. As more heat is transferred to the cold flow, its outlet temperature should increase (even though part of the heat recovered is used to evaporate the injected water). But the TOT does not change much (only by 14°C between the two extreme values of the water mass flow) compared to the variation of the mentioned outlet temperature if the wet-bulb effectiveness stays equal to 98.43% as it is initially for a water mass flow of 20 g/s (increase of 43°C when injecting 30 g/s more water). So limiting its increase in order to keep the hot pinch at a constant value of 50°C requires to degrade the M-Cycle performance by decreasing the wet-bulb effectiveness. Nevertheless, this latter remains at a considerably higher value than the other effectiveness (90%) used to compare the two cases.

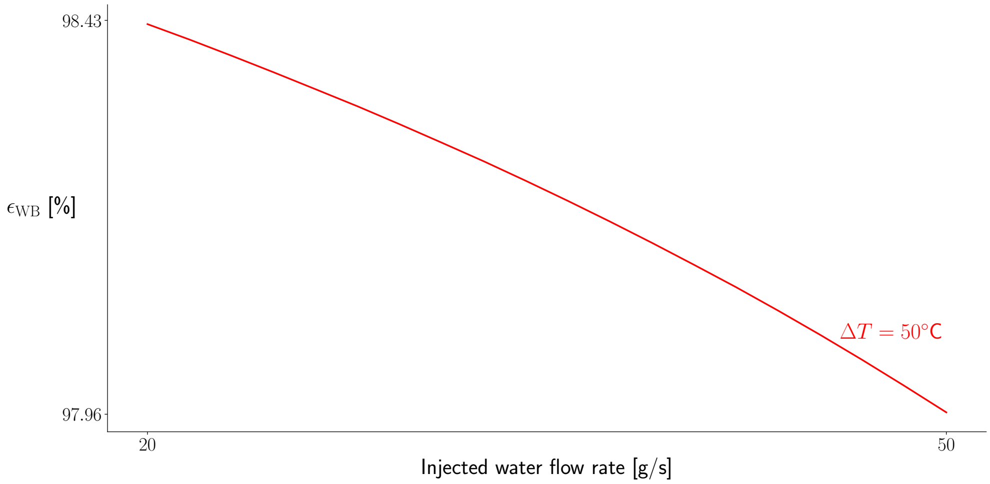

Figure 7.3: Keeping $\Delta T = 50$°C when injecting more water requires to deteriorate the wet-bulb effectiveness. The improved M-Cycle heat recovery due to the larger water condensation would be indeed too high to respect the minimal value of the hot pinch while keeping the same effectiveness. Still, the value of ϵ_{WB} associated with $\Delta T = 50$°C lies around 98%.

7.3 M-Cycle performance parameters

Wet-bulb effectiveness

The first parameter to be analysed is the wet-bulb effectiveness of the M-Cycle. We decided to vary it from 80% to 90% then to 95% followed by three increments of 1% until 98%. According to Equation 5.4, it fixes the outlet temperature of the flue gases in the upper part of the M-Cycle. This has a major impact on the heat recovery in this component. As observable on Figure 7.4, the impact on the electrical power output is rather limited, especially compared to that of the injected water mass flow. This latter parameter is indeed the main driver of the electrical power output as explained in the previous section. The purpose of increasing the M-Cycle performance parameter is to improve the waste heat recovery. This gained heat is then used to decrease the fuel mass flow rate needed to reach the fixed TIT, but not to increase the production of electricity in an absolute perspective. The difference between the curves at $\epsilon_{\mathrm{WB}} = 0.8$ and $\epsilon_{\mathrm{WB}} = 0.95$ (2.3 $\mathrm{kW_e}$ at 20 g/s of injected water) comes from the increased water condensation in the economizer before the compressor (17.4 g/s at $\epsilon_{\mathrm{WB}} = 0.95$ compared to 12.6 g/s at $\epsilon_{\mathrm{WB}} = 0.8$) resulting in a lower compressor work (26.4 kW compared to 28.8 kW) and an associated higher electrical production for the same shaft power. As already explained before, this comes from the reduced outlet temperature of the M-Cycle due to the higher wet-bulb effectiveness which results in turn to a lower outlet temperature of the economizer (18.2°C compared to 26.7°C).

Although increasing the wet-bulb effectiveness is not beneficial in an electrical power output perspective, its impact on the electrical efficiency is more important. Similarly to the blue curve of Figure 7.1, the electrical efficiency decreases when injecting more water at a low ϵ_{WB}. This observation can now be linked to the quantity of condensed water in the M-Cycle (see Figure 7.4) which is null before having a high enough effectiveness of 96% (as well as a sufficient amount of injected water). By increasing this parameter, the outlet temperature reached by the hot flow of the M-Cycle is decreased, bringing it closer to the saturation curve. It is clear that as far as condensation has started in the M-power component, the electrical efficiency starts to increase with the injected water mass flow. Water condensation is associated with a significant heat release. Therefore, the more water condenses the better the heat recovery. This investigation confirms what has been stated in section 6.3: modifying the M-Cycle performance parameter influences the component in which condensation occurs, but not really the total amount condensed in the entire cycle, and therefore dictates if the cycle is used to promote a production of heat or electricity.

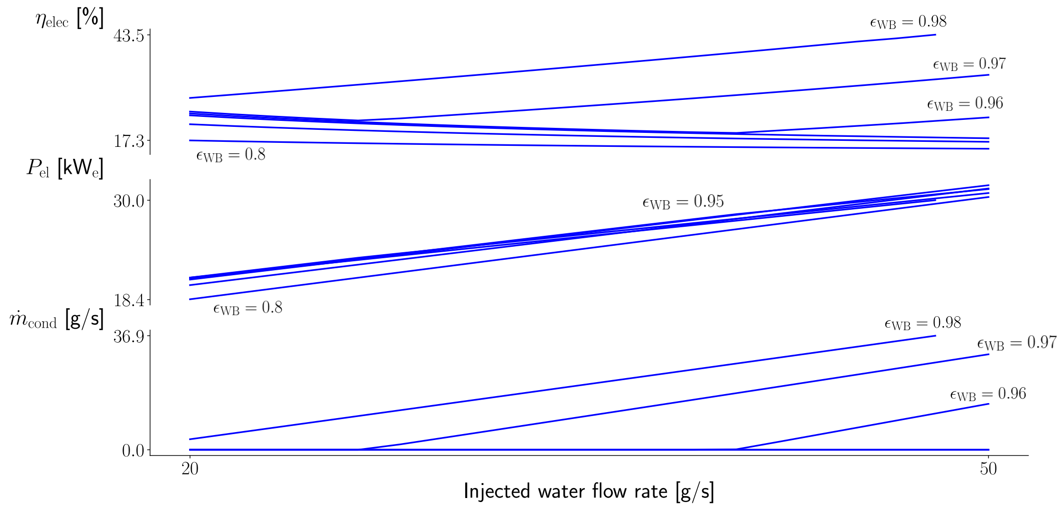

Figure 7.4: The wet-bulb effectiveness has a very slight impact on the produced electrical power, which depends mainly on the injected water mass flow. But it has a major impact on the electrical efficiency which starts to be improved when condensation arises in the M-Cycle (with at least $\epsilon_{WB} = 0.96$).

To summarize the main effect of condensing in the M-Cycle, let us look at some numbers from our simulations. When keeping the same fixed water mass flow of 50 g/s and increasing the wet-bulb effectiveness from 96% to 97%, the quantity of condensed water in the M-Cycle increases from 14.9 g/s to 30.9 g/s which increases the recovered heat from 181.1 kW to 221.6 kW. This results then in a decrease of the primary energy from 136.1 kW to 91.9 kW leading finally to an increase in electrical efficiency from 23% to 33.6%. Regarding this increase, a small variation of the wet-bulb effectiveness could deteriorate considerably the performance of the mGT cycle. This implies an insensible design of the saturator as mentioned by Pr. De Paepe [10] and discussed in chapter 9.

Now when keeping the same wet-bulb effectiveness of 97% but increasing the water mass flow from 40 g/s to 50 g/s, the quantity of condensed water and recovered heat in the M-Cycle increases respectively by 13.3 g/s and 37.8 kW. Meanwhile, the primary flux decreases by 6 kW and the electrical power output increases by 3.1 kW_e (thanks to the effect of adding more water). Everything mixed leads to an absolute increase in electrical efficiency of 5.3%. What should be learned from that observation is that when working with a wet-bulb effectiveness inducing condensation in the M-Cycle, the best electrical efficiency is reached when injecting the most water as possible.

The maximal electrical efficiency reached on Figure 7.4 is 43.5% with a wet-bulb effectiveness of 98% and an injected water mass flow of 48 g/s. In this case, the upper limit of injected water is reached. Indeed, further increasing the water injection rate would improve even more the heat recovery in the M-power component leading to a too high temperature at the cold outlet of the M-Cycle to respect the minimal value of 50°C for the hot pinch. The reader might now wonder the constraints linked to having such a high effectiveness of 98%, this is precisely discussed in section 9.3.

The evolution of the thermal power output (see Figure 7.5) is directly linked to the potential water condensation in the M-Cycle. The effect of increasing the water mass flow while keeping a wet-bulb effectiveness too low to induce condensation has been already explained (see section 7.2). However, the increasing tendency is not noticeable anymore as far as condensation in the M-saturator has started. Indeed, more energy is recovered in the M-Cycle which thus sends a less energetic flow to the economizer (which contains also a reduced proportion of water) resulting in a lower heat recovery in that component. The same explanation goes to justify the decreasing trend of the thermal power output when increasing the wet-bulb effectiveness at a fixed water flow rate.

Concerning the overall efficiency, increasing the injected water mass flow while keeping a constant wet-bulb effectiveness increases it with a different rate of rise depending on whether condensation in the M-saturator has started or not. The evolution without condensation has been already highlighted and explained in the previous section. Once condensation occurs in the M-Cycle, the primary energy flux decreases. Even if a similar impact on the reduced exhaust losses is observable as without condensation, the decrease of their relative importance with respect to the amount of energy injected is lower which explains the reduced growth rate.

When keeping the same water flow rate (for instance 40 g/s) and increasing the wet-bulb effectiveness from 80% to 95%, the overall efficiency increases from 88% to 94% (due to the lower outlet temperature of the economizer resulting in more condensed water and less exhaust losses) and then decreases to 82.3% when the upper value of 98% is set for the wet-bulb effectiveness (as explained above). The maximal overall efficiency accounts for 97.5% and is reached with a wet-bulb effectiveness of 95% and water injection flow rate of 50 g/s. Even though this energetic overall efficiency is quite high, the reader must not forget that its exergetic version might be significantly reduced (see chapter 8).

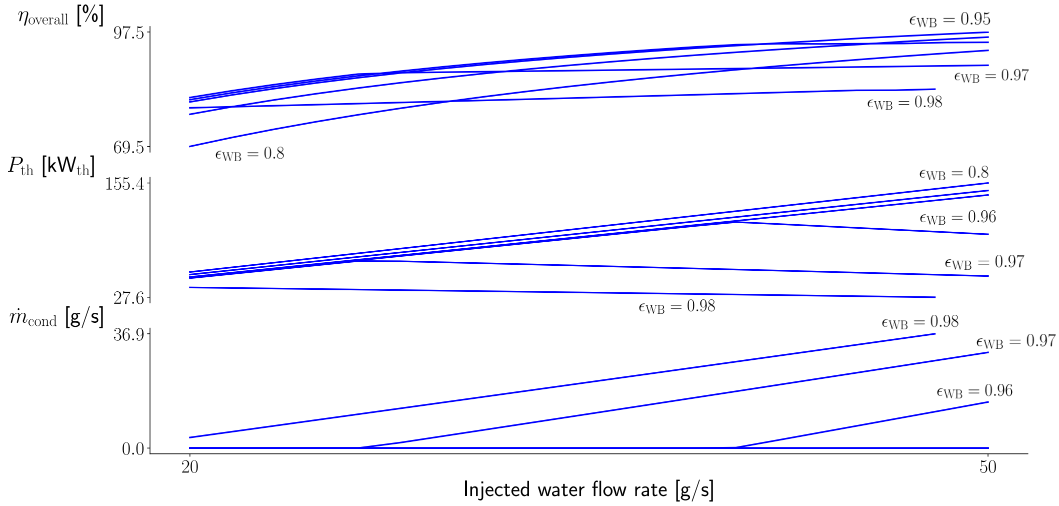

Figure 7.5: Increasing the wet-bulb effectiveness reduces the thermal power output, especially when condensation in the M-Cycle has started, due to the lower amount of energy sent to the economizer. Yet, it increases the overall efficiency until the start of condensation in the M-saturator. Once that phenomenon is reached, the overall efficiency decreases when increasing the wet-bulb effectiveness.

Dew point effectiveness

The second parameter under study is the other performance parameter of the M-Cycle: the dew point effectiveness. This latter has a less significant impact on the performance of the mGT cycle than its counterpart (see Figure 7.6 and Figure 7.7). The first observation which is valid for both graphs and that has been also highlighted in the sensitivity analysis of De Paepe et al. [10] is that the dew point effectiveness does not impact at all the behavior of the cycle when running it with a constant hot pinch. Indeed, the only direct influence of the studied parameter is on the final temperature of the cold flow in the lower part of the M-Cycle (T_3 in Equation 5.3). This latter influences in its turn the hot outlet temperature of the upper part of the M-Cycle. Indeed, the lower T_3 (M-Cycle notation) involves a lower $T_{WB,3}$ which is the minimal temperature achievable by the flue gases (with a wet-bulb effectiveness equal to 1, see Equation 5.4). But actually, fixing the hot pinch is already a sufficient information to determine the total amount of energy exchanged in the M-Cycle. It can be computed from the global energy balance on the component as the two inlet fluxes are known and the specified hot pinch fixes the hot flux going to the combustion chamber. Then regardless of the dew point effectiveness, it does not change the global impact of the M-power component on the cycle. However, the distribution of the heat exchanged in each part of the component is modified. As an example when increasing the dew point effectiveness from 80% to 95% (with a water mass flow of 50 g/s), the temperature T_3 in the M-Cycle decreases from 40.7°C to 15.1°C which means that more heat is exchanged in the lower part. The energy balance in the upper part is also adjusted with an increased heat exchange in the cold section (between states 3 and 5 according to the M-Cycle notation from Figure 5.2) and decreased one in the other section. Additionally, varying the dew point effectiveness with a fixed hot pinch modifies the wet-bulb effectiveness. Taking the same parameters as before, the increase of the dew point effectiveness makes the wet-bulb effectiveness going from 98% to 96.7%. Being able to design the M-power component with the highest dew point effectiveness as possible allows to decrease a bit the high wet-bulb effectiveness needed to improve the electrical performance of the mGT cycle. This consideration is part of the reasoning presented in section 9.3.

When keeping $\epsilon_{WB} = 0.9$, the reduced T_3 (and $T_{WB,3}$) due to the increased dew point effectiveness leads to a lower hot outlet temperature of the M-Cycle according to Equation 5.4. Taking a dew point effectiveness of 80% and 95% with a water mass flow of 50 g/s gives respectively 91.4°C and 82.9°C for the mentioned temperature. As a result, the heat recovered in the M-Cycle goes from 136.2 kW to 137.9 kW which decreases the primary flux needed from 185.3 kW to 183.6 kW. As a result the electrical efficiency increases by 0.2% in absolute points. The impact of this second M-Cycle performance parameter is thus quite limited. This already small effect is marginally increased by the very small increase in electrical power output (+0.1 kW_e) due to the slightly lower outlet temperature of the economizer (increasing the quantity of condensed water and thus reducing the compressor power consumption) following the decreased hot outlet temperature of the economizer.

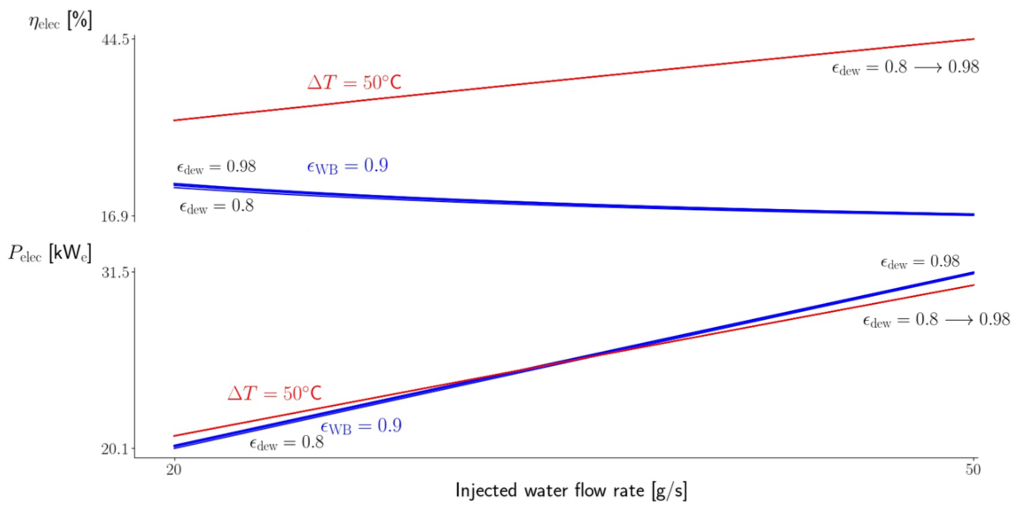

Figure 7.6: When keeping $\Delta T = 50$°C, the dew point effectiveness has no impact at all on the electrical performance. Yet at $\epsilon_{WB} = 0.9$, an increased dew point effectiveness marginally increases the electrical power output and efficiency due to a lower hot outlet temperature of the M-Cycle.

Analysing the same change in the dew point effectiveness (from 80% to 95%) with $\epsilon_{\text{WB}} = 0.9$, the thermal power output decreases from 147 kW_{th} to 145.8 kW_{th}. This comes from the slightly increased heat recovery in the M-Cycle leading to less energy sent to the economizer but also less fuel needed. Combining the small increase in electrical power output and the decrease of the fuel mass flow rate with the decrease of the thermal power output leads all in all to a slight increase of 0.3% in absolute points of the overall efficiency.

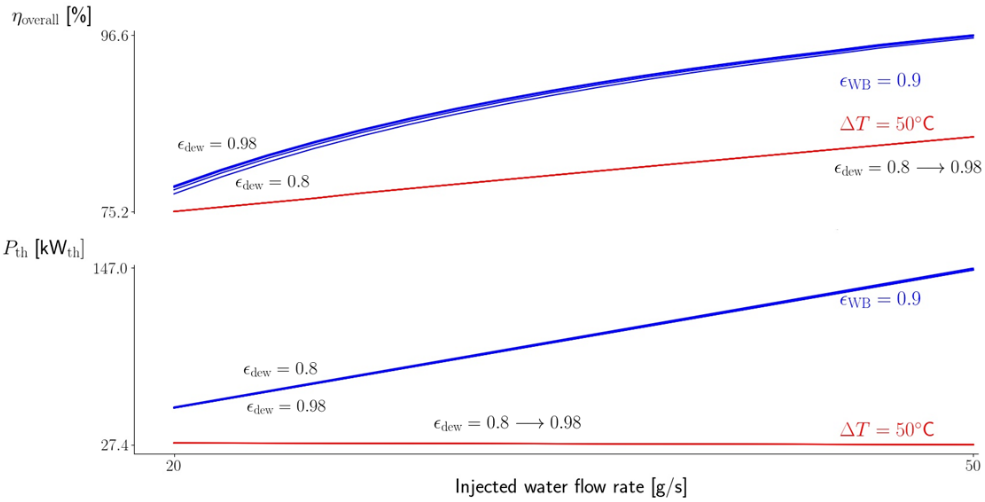

Figure 7.7: When keeping $\Delta T = 50°\text{C}$, the dew point effectiveness has no impact at all on the thermal performance. Yet at $\epsilon_{\text{WB}} = 0.9$, an increased dew point effectiveness marginally increases the overall efficiency due to a lower hot outlet temperature of the M-Cycle.

7.4 Initial conditions of the flow

Two variations of the inlet flow conditions are now investigated starting with its inlet temperature followed by its relative humidity.

Inlet air temperature

The main impact of changing the inlet air temperature on the electrical performance of the cycle is due to its associated initial water content. Indeed, this quantity is dictated by both the relative humidity and the inlet temperature. Keeping one of these two parameters fixed while increasing the other involves a bigger water content of the starting working fluid. This statement comes from the higher ability of humid air to carry water when its temperature is higher. Still, the influence of the inlet air temperature on the electrical performance of the M-SAB cycle is minimal as shown on

Figure 7.8. Four different temperatures were tested from 5°C to 20°C with increment of 5°C. Comparing the two extreme values for the case with $\epsilon_{WB} = 0.9$ and a water mass flow of 20 g/s shows the slight increase of the initial water content from 3 g_{H2O}/kg_{da} to 9 g_{H2O}/kg_{da} when increasing the inlet temperature. This results in a very small increase of the quantity of condensed water in the economizer from 15.9 g/s to 16.4 g/s. Accordingly, the compressor work decreases by 0.1 kW while the electrical power output increases by 0.1 kW_e. The impact of these marginal variations is though quite insignificant for the electrical efficiency. When fixing the hot pinch of temperature, this impact is slightly increased (the difference goes from 0.1% to 0.3%) thanks to a small decrease of the fuel needed by increasing scarcely the heat recovered in the M-Cycle. Having initially more water as a gaseous state is theoretically beneficial in terms of electrical efficiency as it enhances the heat recovery when condensing the extra water due to the release of the heat of vaporisation. Contrarily as when injecting liquid water and evaporating it in the flow, this extra energy is free as it is already present in the initial air. Yet, the discussion held here deals with narrow variations of the initial water content and the other variables, which could be qualified as negligible. This confirms what has been stated in the literature review concerning the insensitivity of the IBC to atmospheric conditions, especially compared to a BC. In that case, the main impact relies on the inlet conditions of the compressor which is the first component faced by the flow in that configuration.

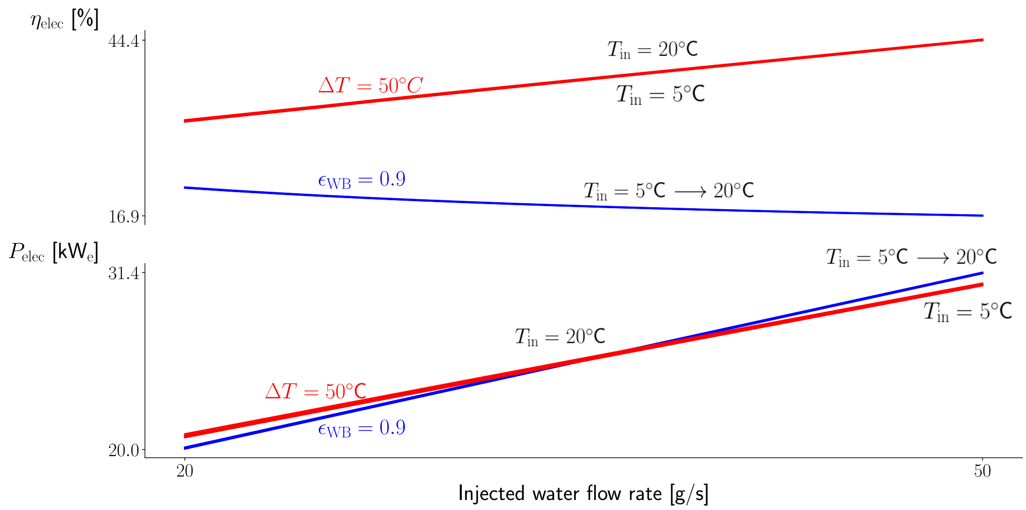

Figure 7.8: The inverted configuration makes the electrical performance of the M-SAB cycle almost insensitive to a variation of the inlet air temperature.

Apart from the minor effect of having more condensation (in the economizer or in the M-Cycle depending on the case) due to the increased initial water content, the initial energy content of the flow is also higher (with an enthalpy difference of 29.1 kJ/kg_{da} due to the increased temperature and water content). The global energy level along the cycle is therefore fairly more elevated. As the considered initial temperature of the cooling water does not change (15°C), the gap between the hot and cold flow in the economizer is higher. This results in a bit more heat recovered in that component (from 27.3 kW_{th} to 29.5 kW_{th} respectively with T_{in} = 5°C and 20°C and for ΔT = 50°C). Simultaneously, the increased water content is associated with a slight increment of the flow heat capacity. This implies to burn more fuel, yet that aspect is mitigated by the greater heat recovered in the M-Cycle and the lower difference between the initial temperature of the flow and the TIT. The relative increase in primary energy flux (from 65.7 kW to 65.8kW) is then lower than that of the thermal power output. Linking both observations explains the higher overall efficiency (from 73.2% to 76.7%) when increasing the inlet air temperature (from 5°C to 20°C) as it can be seen on Figure 7.9. This result is greater for the fixed hot pinch case as more heat is recovered in the M-Cycle limiting a bit more the increase in primary energy compared to the fixed wet-bulb effectiveness case (for which the absolute increase in overall efficiency is only of 1.9%). Moreover, it is also attenuated when increasing the water mass flow due to the lower relative importance of the initial water content compared to the amount of injected water.

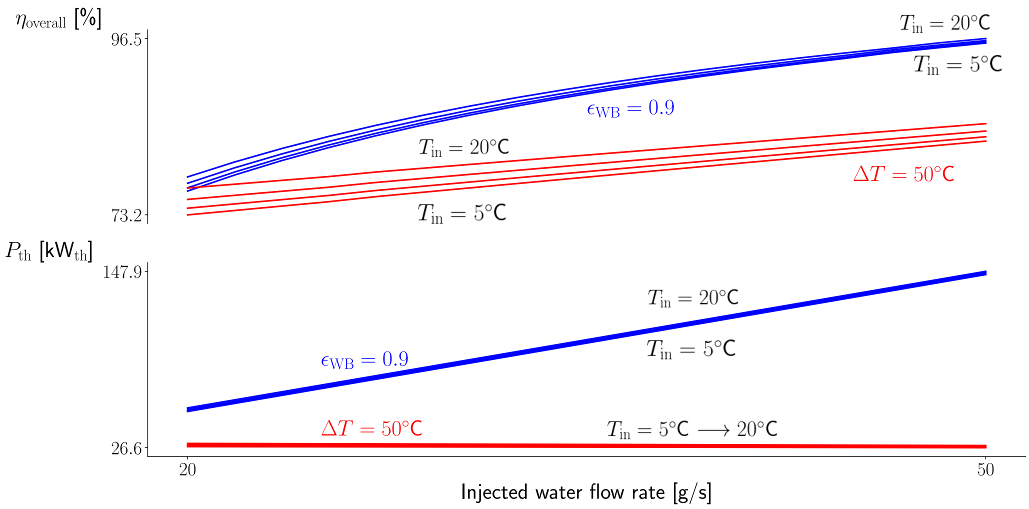

Figure 7.9: Increasing the inlet air temperature increases the overall efficiency, with a higher effect at low injected water mass flow and for a fixed hot pinch. The impact on the thermal power output is rather limited.

Inlet air relative humidity

The effect of changing the second parameter describing the inlet flow conditions, which is the air relative humidity, is similar to that of the inlet air temperature (see Figure 7.10).

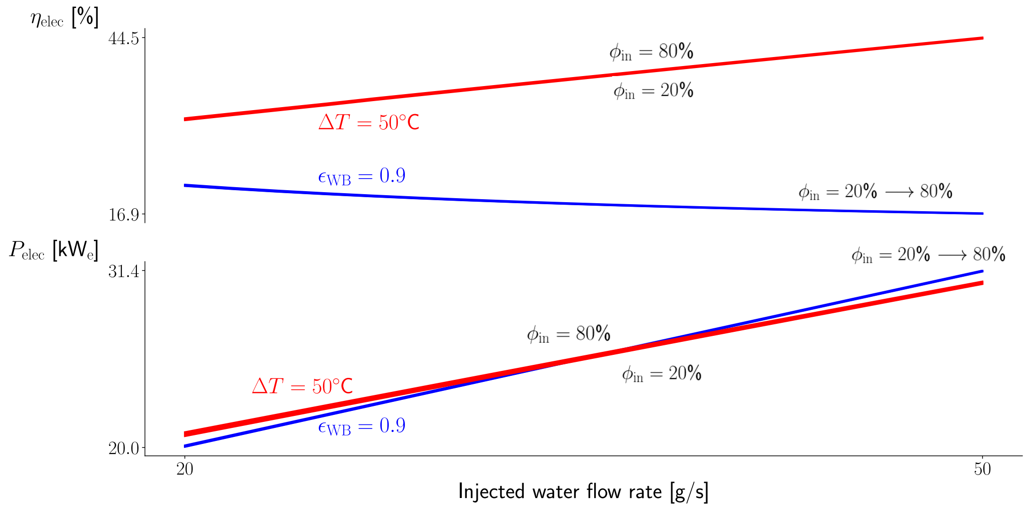

Figure 7.10: The inverted configuration makes the electrical performance of the M-SAB cycle almost insensitive to a variation of the inlet air relative humidity.

Indeed, increasing it means more water contained in the air initially. Once again a set of four values was used starting at $\phi_{in} = 20\%$ until $\phi_{in} = 80\%$ with steps of 20%. Comparing the water content using the two extreme values in the same conditions as for the inlet air temperature ($\epsilon_{WB} = 0.9$ and water injection flow rate of 20 g/s), the difference is similar: it goes from 2 g_{H2O}/kg_{da} to 8.5 g_{H2O}/kg_{da}. The effect of changing the inlet air relative humidity on the electrical performance is thus quantitatively very close to that of the inlet air temperature for the same reason.

Correspondingly to the electrical performance, changing the inlet air relative humidity has the same impact on the thermal power output and the overall efficiency as changing the inlet air temperature (see Figure 7.11). Indeed, the increased initial water content of the flow goes in pair with a higher initial energy. Still, this increase is lower (+16 kJ/kg_{da}) than when changing the temperature as only the water content has a contribution while the temperature also had one before (less difference between the initial temperature and the TIT). This is though offset by the slightly improved performance of the preheater when it features a lower cold inlet temperature (so compared to the case with $T_{in} = 20°C$).

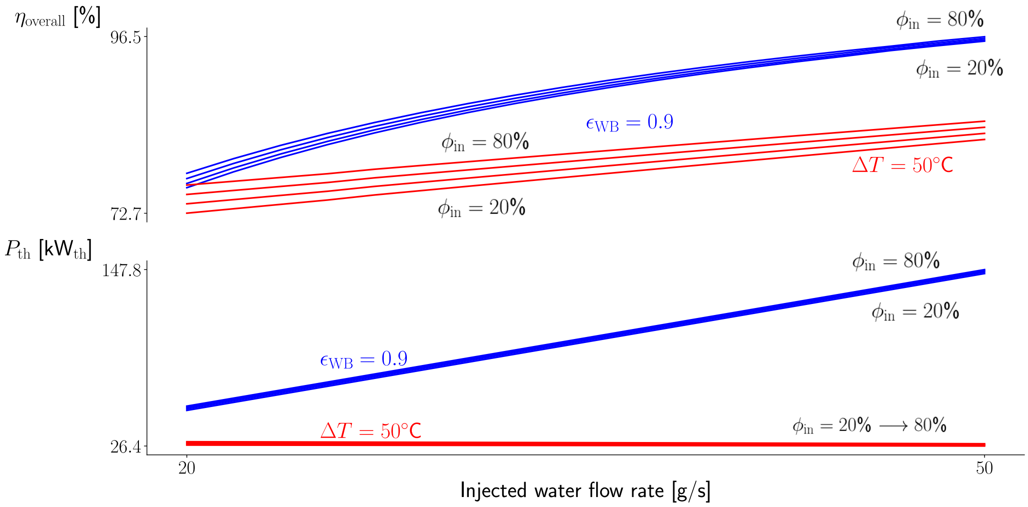

Figure 7.11: Similarly as for the inlet air temperature, increasing the inlet air relative humidity increases the overall efficiency, with a higher effect at low injected water mass flow and for a fixed hot pinch. The impact on the thermal power output is once again rather limited.

7.5 Design parameters

Even if our work is particularly focused on the study of the thermodynamic potential and not the design of a real unit in itself, it would be interesting to know how different parameters related to that aspect impact the performance of the cycle. We have decided to focus here on the heat losses, the pressure drops and the TIT.

Heat losses

One of the assumptions taken when adapting our model to the Turbec T100 mGT was to assume all the heat losses gathered into a single one located at the combustion chamber. The value of this latter was at first chosen equal to 5% of the added primary energy. We have here decided to investigate the effect of increasing or decreasing it by 3%.

Similarly to what was shown in the IBC model validation (see section 4.3), modifying this value directly impacts the injected fuel mass flow rate. The variation of the heat losses is actually exactly equal to that of the primary energy flux regardless of the fixed parameter (ϵ_{WB} or ΔT). The increased fuel injection flow rate when facing higher heat losses is then only used to offset their augmentation. This induces obviously a decrease of the electrical and overall efficiencies (see Figure 7.12 and Figure 7.13). Taking an injected water flow rate of 50 g/s, the increase in heat losses (and so in primary energy flux) when increasing the heat loss coefficient from 5% to 8% accounts for 6 kW and 2.3 kW respectively for $\epsilon_{\text{WB}} = 0.9$ and $\Delta T = 50°\text{C}$. The difference between the two cases comes from the much higher initial quantity of energy needed when fixing the wet-bulb effectiveness (185.3 kW compared to 68.9 kW at fixed ΔT) due to the non-condensation in the M-Cycle that does not allow a decrease of the quantity of fuel needed. One must then compare the relative increase in heat losses with respect to the primary energy: +3.2% for $\epsilon_{\mathrm{WB}} = 0.9$ compared to +3.5% for $\Delta T = 50°\mathrm{C}$. This results in the same order to an absolute decrease of the electrical efficiency of 0.5% and 1.4%.

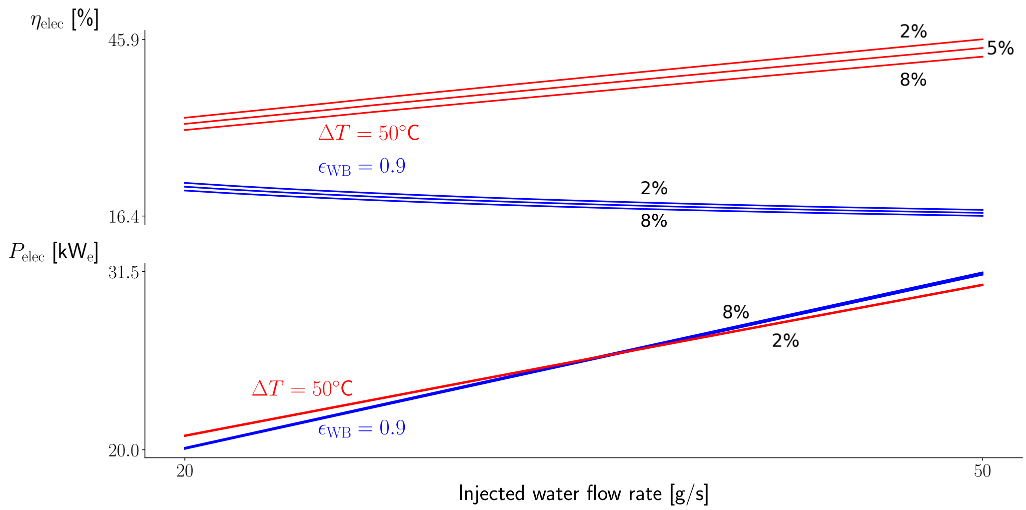

Figure 7.12: Increasing the heat losses in the combustion chamber requires the injection of more fuel which decreases the electrical efficiency. The impact on the electrical power output is negligible.

Yet, a side effect of the increased quantity of injected fuel is the creation of more water during the combustion. The increased water content in the flow after the combustion chamber slightly amplifies the condensation in the economizer or the M-Cycle (depending on the case under study) resulting in a lower mass flow through the compressor, an accordingly a lower compressor power consumption and thus a small increment of electrical power output. The last consideration must yet be considered as a side effect regarding its relatively low importance as illustrated on the graphs.

For the same reason as the marginal increase in electrical power output, enhancing the condensation in the economizer (considering then the case with a fixed wet-bulb effectiveness) goes in hand with an increase in thermal power output. Once again, this effect is rather negligible.

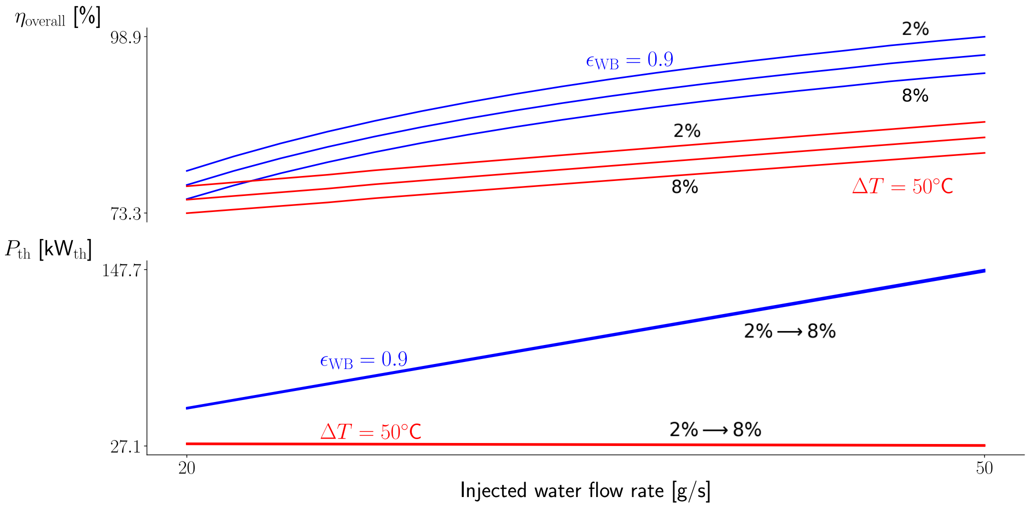

Figure 7.13: Increasing the heat losses in the combustion chamber requires the injection of more fuel which decreases the overall efficiency. The impact on the thermal power output is negligible.

Pressure drops

The second design parameter, estimated based on the values taken from the Turbec T100 mGT in a BC configuration [5], is the pressure loss in each component. More precisely, the impact of varying the relative pressure drops coefficient by ±25% for the components featuring a significant pressure drop is studied. These are the combustion chamber, the cold side of the M-Cycle and both sides of the preheater. Their main influence lies on the electrical power output. Two effects are involved in this observation. On one side, increasing the pressure drops goes in pair with a higher compressor pressure ratio, which tends to increase its power consumption. On the other side, higher pressure drops decrease the total mass flow through the cycle (according to Equation 6.3 with a lower turbine inlet pressure). So for the same amount of injected water, less air travels inside the cycle which increases the proportion of water per unit air in the working flow. An equivalent quantity of condensed water before the compressor (or even slightly increased as less air is present which means that it can contain a lower absolute quantity of water) leads thus to a decrease in the mass flow passing through it, and accordingly to a lower power consumption. The second consideration is the most significant at higher injected water mass flows.

Consequently when looking at a water injection flow rate of 20 g/s and with $\epsilon_{\text{WB}} = 0.9$, the two effects are counterbalanced and lead to a similar compressor work (respectively 27 kW and 27.1 kW with the lowest and highest pressure drops). But the increase in total mass flow when the pressure drops are lower (161 g/s compared to 150 g/s) is associated with a higher shaft power (50.8 kW compared to 47.6 kW, as more fluid flows trough the turbine). As a result, the electrical power output is higher

(21.7 kW_e in comparison with 18.6 kW_e) as shown on Figure 7.14. Another effect of having a higher total mass flow is the increase in primary energy flux (+4 kW between the previously considered cases) as more fluid needs to be heated up to the TIT. Yet, the relative increase in electrical power output (16.67% in this case) is more meaningful than that of the primary energy flux (4.3%) leading to an increase in electrical efficiency (of 2.4% in absolute points) as shown on Figure 7.14.

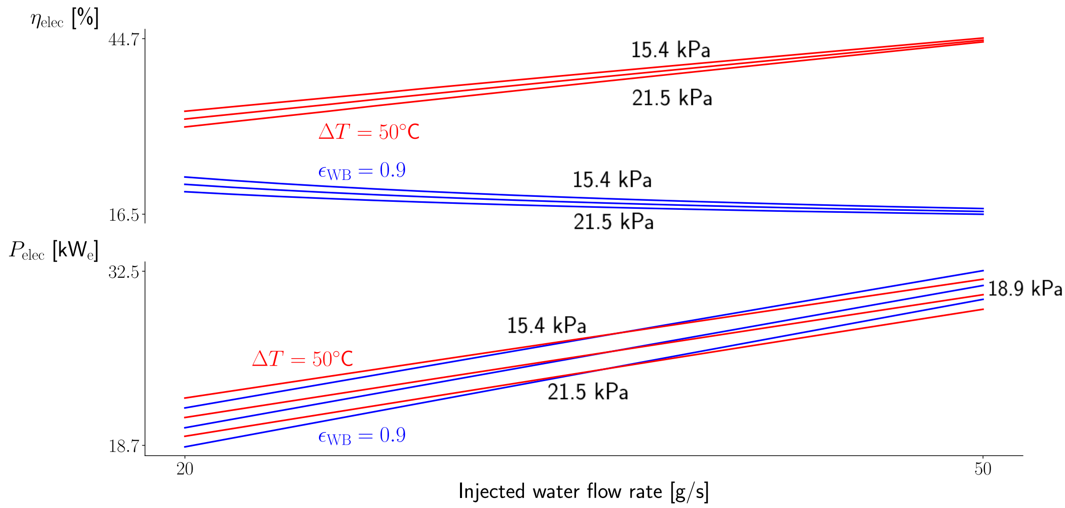

Figure 7.14: Increasing the pressure drops decreases the electrical performance of the M-SAB Cycle due to a higher compressor power consumption. Yet, this decrease tends to fade when increasing the injected water mass flow. The total decrease of pressure throughout the cycle due to the pressure drops is mentioned on each curve.

When injecting more water in the cycle (up to 50 g/s), the effect of the decreased total mass flow and its associated higher proportion of water per unit air on the compressor required work becomes more important. As a consequence, the compressor work is now lower for the case with the higher pressure drops (16.7 kW compared to 17.5 kW). Nevertheless, the increase in shaft power induced by the higher total mass flow with less pressure drops remains larger (52.8 kW compared to 49.5 kW) than the increase in compressor work. Therefore, the electrical power output is then still higher with the decreased pressure drops (32.5 kW_e compared to 30.3 kW_e). But this leads to a more nuanced increase in electrical efficiency. Even though only the results with $\epsilon_{WB} = 0.9$ were discussed here, the discussion is also valid with $\Delta T = 50°C$.

Following the interpretation of the last graph, the impact of the pressure drops mainly relates to the shaft power and its division between the compressor power consumption and the effective power produced. This has therefore no impact on the thermal power output as displayed on Figure 7.15. However, they impact the overall efficiency due to the same reasons explained before. Indeed, having lower pressure drops increases the overall efficiency when the injected water mass flow is low. The more this latter increases, the closer the curves get. This comes from the increased electrical efficiency while the thermal efficiency slightly decreases (as the thermal power output stays constant while the primary energy flux features a modest increase). As the increase in electrical efficiency is attenuated when increasing the injected water, the same behavior is observed for the overall efficiency (see Figure 7.15).

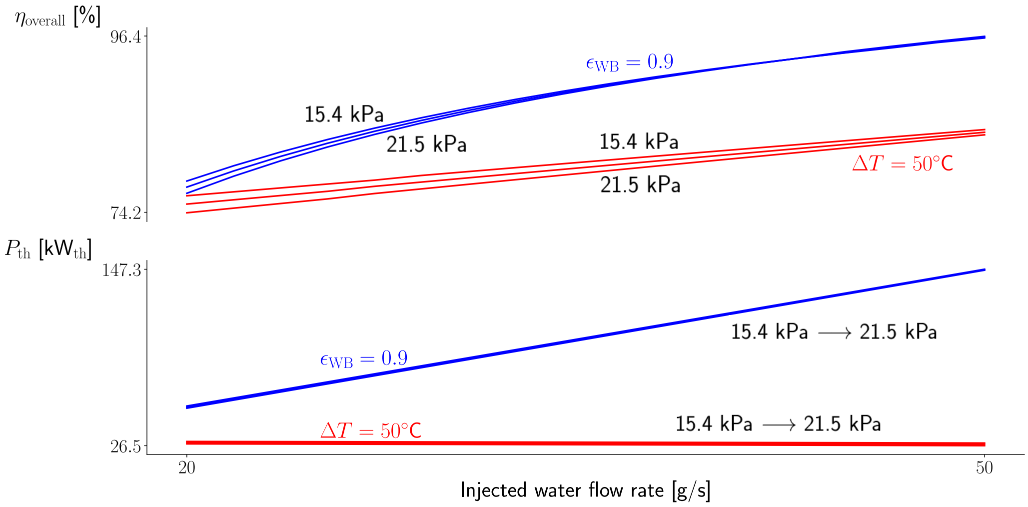

Figure 7.15: Increasing the pressure drops has no impact on the thermal power output while it decreases the overall efficiency. Once again, this decrease becomes limited at higher injected water mass flows. The total decrease of pressure throughout the cycle due to the pressure drops is mentioned on each curve.

Turbine Inlet Temperature

The last design parameter is the TIT. It has been described as the maximum temperature reached in the cycle and is limited by the choice of the materials of different components. The value chosen for all the simulations (except the ones analysed here) was 950°C, in harmony with the mGT literature. Still, it would be interesting to see the effect of a possible increase of this parameter to 1050°C and 1150°C associated with more robust and expensive materials (as highlighted in the literature review). As expected by the Carnot efficiency, increasing the TIT goes in pair with a greater electrical production and electrical efficiency (see Figure 7.16). Two effects are taking place justifying that statement. The first one is the increased energy content at the inlet of the turbine resulting in a higher shaft power production. Indeed, for the same pressure difference (fixed by the expansion ratio) if the initial enthalpy of the fluid at the turbine inlet is higher, the resulting enthalpy extraction is larger too. This can be explained graphically by the diverging behavior of the isobars in a h-s diagram. As a result, the difference between the shaft power produced by the turbine and the required power of the compressor increases to the profit of the electrical power output.

The second effect of increasing the TIT is related to its influence on the total mass flow through the cycle. According to Equation 6.3, this latter is reduced. The effect is therefore similar as when increasing the pressure drops: the proportion of water per unit air is higher resulting in a lower mass flow through the compressor reducing its power consumption. Let us analyse case by case the effect of increasing the TIT from 950°C to 1150°C for an injected water mass flow of 20 g/s. The total mass flow goes from 155.5 g/s to 144.5 g/s regardless of the fixed parameter (ϵ_{WB} or ΔT).

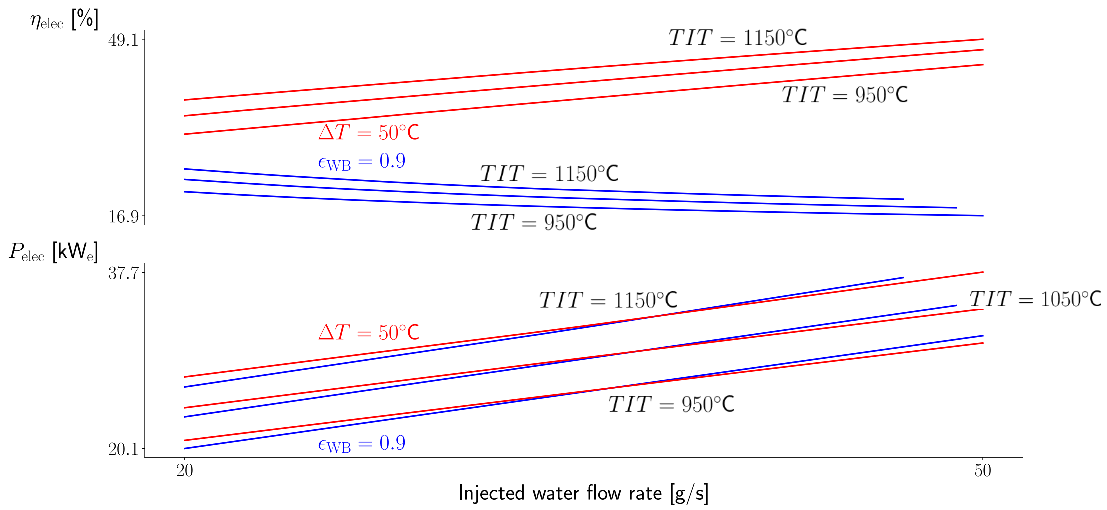

Figure 7.16: Increasing the TIT increases considerably the electrical performance of the M-SAB cycle thanks to an increased shaft power and a reduced total mass flow. However, it reduces the upper limit of the maximal quantity of water that can be injected when keeping $\epsilon_{WB} = 0.9$ due to a too low air excess coefficient.

For the case with $\Delta T = 50°C$, despite the reduced total mass flow, the energy content at the turbine inlet is higher by 30 kW for the TIT of 1150°C. The resulting shaft power increase reaches 4.6 kW. In addition, a higher TIT implies a higher TOT, which is linked to an increased energy content (+26 kW) of the flue gases at the inlet of the M-Cycle. The heat recovered in the M-Cycle is thus enhanced by 25 kW. As a result of the increased water content in the flow after the combustion chamber (199 g_{H2O}/kg_{da} compared to 180 g_{H2O}/kg_{da}) due to the smaller quantity of air with a higher TIT, the mass flow through the compressor is lower resulting in a lower compressor work (26.2 kW compared to 24 kW). Combining this last point with the increased shaft power results in a significant boost of the electrical power output (from 20.9 kW$_e$ to 27.3 kW$_e$). Even though the amount of injected fuel must increase to reach the higher TIT, it is limited by the better heat recovery in the M-saturator (the primary energy flux only increases of 5.8 kW). The electrical efficiency is then also promoted to 38% compared to 31.8%.

The case with $\epsilon_{\mathrm{WB}} = 0.9$ is similar to the other one with the difference that less heat is recovered in the M-Cycle resulting in a larger increase in primary energy flux (+8.7 kW compared to +5.8 kW with $\Delta T = 50$°C). As the increase in electrical power output is equivalent (+6.2 $\mathrm{kW_e}$ compared to +6.4 $\mathrm{kW_e}$ at a constant ΔT), the increase in electrical efficiency is slightly lower in this case (+4.1%). One can note the narrowed increase in electrical efficiency when injecting more water due to the reduced relative importance of the increased proportion of water in the flow when increasing the TIT.

A noticeable difference between the curves at fixed wet-bulb effectiveness for each TIT is the different maximum quantity of water that can be injected. As it has already been exposed in the beginning of this section, the upper limit of the injected water flow rate can be reached when the air excess coefficient (λ) becomes lower than 1. This will be the case when increasing the TIT and keeping at the same time $\epsilon_{\mathrm{WB}} = 0.9$. Indeed, it decreases the total mass flow through the cycle (decreasing consequently the amount of air in the flow) while it increases the amount of injected fuel. The upper limits are therefore 49 g/s and 47 g/s for respectively a TIT of 1050°C and 1150°C.

As shown on Figure 7.17, contrarily to the electrical power output, the thermal power output does not change much when increasing the TIT of 200°C (+2.7 $\mathrm{kW_{th}}$ at $\epsilon_{\mathrm{WB}} = 0.9$ and +1 $\mathrm{kW_{th}}$ at $\Delta T = 50$°C, both for a water injection rate of 20 g/s). Indeed, the increased shaft power and reduced compressor power consumption does not influence directly the heat recovered in the economizer. Concerning the overall efficiency, its increase when rising the TIT comes mainly from the associated higher electrical efficiency. The thermal efficiency is indeed slightly decreasing due to the combination of the limited increase in thermal power output and the increase in primary energy flux. Looking at a water injection of 20 g/s, where the increase in overall efficiency is the highest, the electrical efficiency increases of 4.1% and 6.2% respectively for $\epsilon_{\mathrm{WB}} = 0.9$ and $\Delta T = 50$°C while the thermal efficiency decreases of 2.2% for both cases. When increasing the amount of injected water, the increase in overall efficiency becomes more nuanced similarly as for the electrical efficiency. This is especially true for the curves at fixed wet-bulb effectiveness which tends to reach an upper value of the overall efficiency already close to 100%. In another point of view, rising the TIT results in a lower total mass flow through the cycle for an equivalent energy level at the combustion chamber. As the final temperature at which the flow is cooled does not change much with the TIT, the relative importance of the exhaust losses is reduced for a higher TIT. This results in a higher overall efficiency.

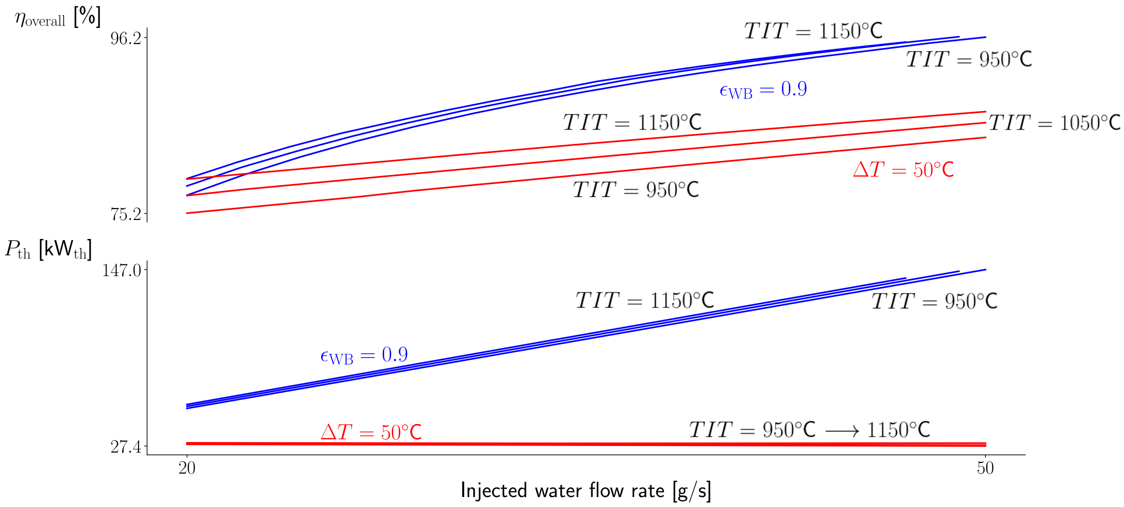

Figure 7.17: Increasing the TIT has a limited impact on the thermal power output. Yet, it increases slightly the overall efficiency, mainly due to the increase in electrical efficiency.

7.6 Control parameter

The last parameter investigated is the expansion ratio of the turbine. It is considered as a control parameter due to the assumption taken in subsection 6.2.3. Indeed, both the rotational speed and the turbine expansion ratio are used as input parameters. But as the rotational speed is kept constant in all simulations here, the pressure ratio constitutes the only control parameter under study. The following results have been simulated using three values: 2.7, 3 and 3.3. Three general effects of increasing the turbine expansion ratio are firstly that it increases the compressor pressure ratio, secondly that the shaft power produced is larger and thirdly that the total mass flow through the cycle is higher. The third consideration comes from the computation of the total mass flow thanks to the turbine map. Indeed, by following an iso-speed line and increasing the pressure ratio, the associated reduced mass flow is higher. As mentioned before, expanding to a lower sub-atmospheric pressure enhances the shaft power produced by the turbine. Even though the associated compressor pressure ratio increases as well, the increase of the produced turbine shaft power is higher than the increase in compressor power consumption. This can be once again justified by the diverging behavior of the isobars in a h-s diagram. Indeed, the enthalpy gap between two pressures is higher at high temperature. Taking for example a water injection of 20 g/s and increasing the ratio from 2.7 to 3.3, the shaft power increases of 9.8 kW and 9.7 kW respectively for $\epsilon_{\text{WB}} = 0.9$ and $\Delta T = 50°$C while the compressor work increases of 6.9 kW and 6.8 kW. The electrical power output increases then respectively by 2.5 kW$_\text{e}$ and 2.6 kW$_\text{e}$ (see Figure 7.18).

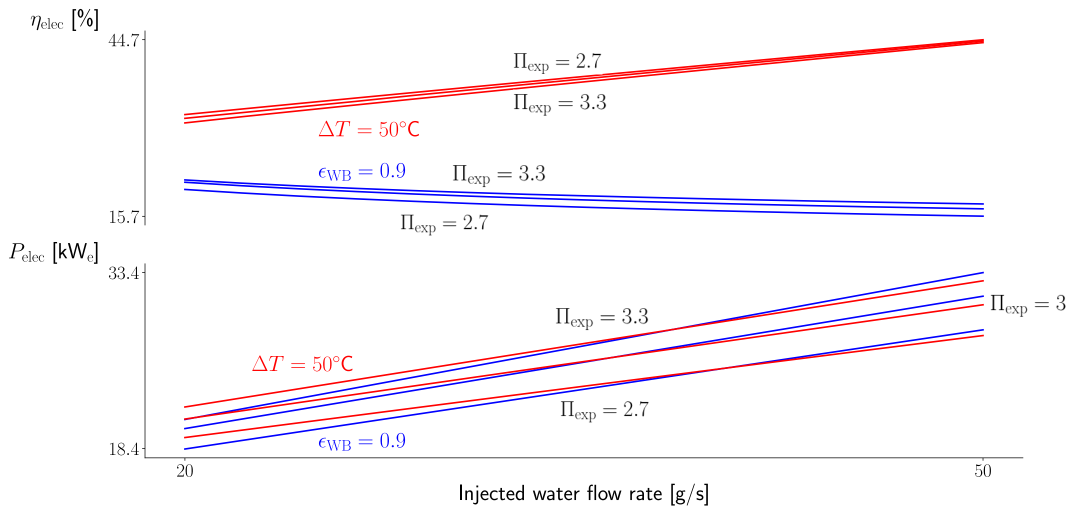

Figure 7.18: Increasing the turbine expansion ratio increases the electrical power output for both cases due to the larger shaft power produced by the turbine. Yet, it is associated with an increase in electrical efficiency only for $\epsilon_{\text{WB}} = 0.9$. The difference for the case with $\Delta T = 50$°C is that a lower expansion ratio allows condensation in the M-Cycle to start at a higher temperature. Indeed, the electrical efficiency mainly depends on the amount of condensed water in this case.

Nevertheless, the influence on the electrical efficiency is quite different depending on the case considered (see Figure 7.18). Let us then investigate each case separately, comparing two ratios of 2.7 and 3.3 but keeping the same water mass flow of 20 g/s. Starting with $\Delta T = 50$°C, increasing the turbine expansion ratio is not beneficial for the electrical efficiency in that case. Indeed, the pressure at the outlet of the M-Cycle is evidently higher with the lower pressure ratio (28.85 kPa compared to 22.88 kPa). Accordingly, condensation in the M-Cycle starts at a higher temperature and the quantity of condensed water is then enlarged (8.2 g/s instead of 5.7 g/s). The heat recovery in the M-Cycle is thus improved at a lower turbine expansion ratio (151.8 kW compared to 143.3 kW) explaining the better electrical efficiency (32.4% compared to 31%). Concerning the case with $\epsilon_{\text{WB}} = 0.9$, the trend is opposite due to the non-condensation in the M-Cycle. Indeed, as the heat recovery in that component does not change much (from 144.3 kW to 146.6 kW when increasing the pressure ratio), the fuel consumption is not drastically reduced as it would be the case when improving the M-Cycle heat recovery. It is therefore more interesting for the electrical efficiency to extract as much energy as possible with the turbine (which is the case with a higher pressure ratio) in order to increase the electrical power output. Our model shows an increase of 1.6% for the electrical efficiency when increasing the expansion ratio from 2.7 to 3.3.

As displayed on Figure 7.19, the turbine expansion ratio has a very slight impact on the thermal power output at $\Delta T = 50°C$. In that case a lower expansion ratio means that more heat is recovered in the M-Cycle as inspected just above, so less energy is sent to the economizer (40.9 kW compared to 48.2 kW, keeping for the analysis a water mass flow of 20 g/s and two expansion ratios of 2.7 and 3.3) which produces in its turn less thermal power output (26.9 kW_{th} compared to 29.6 kW_{th}). Concerning the case with $\epsilon_{WB} = 0.9$, due to the absence of condensation in the M-Cycle, the energy content of the flux sent to the economizer is pretty similar (75.4 kW compared to 76.1 kW respectively at low and high pressure ratio). Then similarly to what has been pointed out for the M-Cycle, the effect of having a higher pressure at the outlet of the economizer at a low expansion ratio (28.56 kPa compared to 22.65 kPa) enhances condensation in that component (17.3 g/s compared to 15 g/s). The thermal power output is thus somewhat higher at a lower pressure ratio (55.7 kW_{th} compared to 50 kW_{th}).

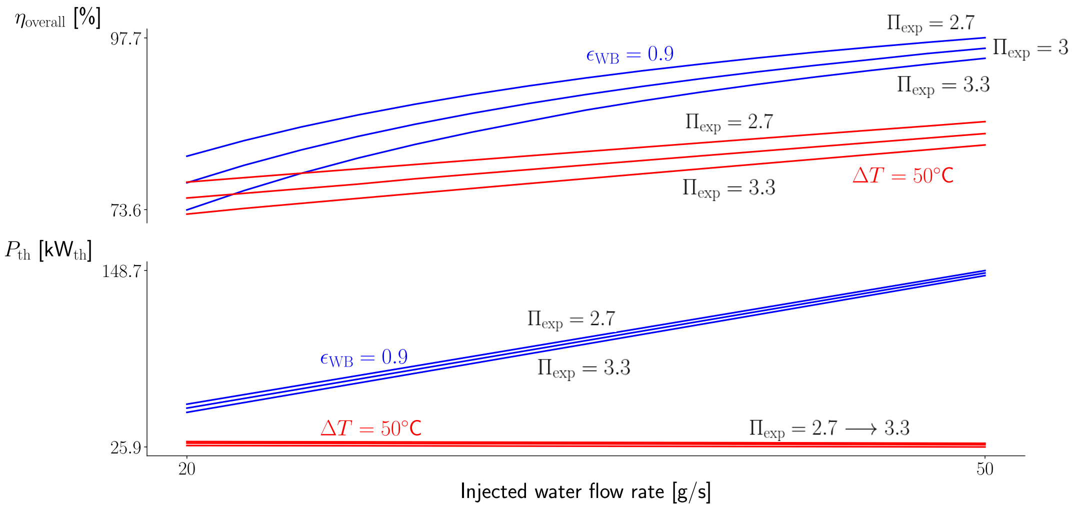

Figure 7.19: A lower turbine expansion ratio is associated with a small increase in thermal power output at $\epsilon_{WB} = 0.9$ due to the larger condensation in the economizer. The impact with $\Delta T = 50°C$ is limited. Yet, the overall efficiency is higher with a lower pressure ratio for both cases as seen by the reduced exhaust losses.

The fact of having a higher overall efficiency is once again linked to the same reasons discussed until now: the amount of condensed water and the proportion of water per unit air. A lower expansion ratio is associated with both a lower total mass flow and a larger amount of condensed water (in the economizer or the M-Cycle depending on the case). The remaining energy flux going to the end of the cycle and finally to the exhaust is then ineluctably declined leading to fewer exhaust losses (22.9 kW compared to 31.2 kW, with the same parameters as used above and with $\epsilon_{WB} = 0.9$). As their relative variation is more significant than that of the primary energy flux, the overall efficiency is higher when the expansion ratio is lower (81.1% compared to 73.6% still with $\epsilon_{\mathrm{WB}} = 0.9$). As shown on Figure 7.19, the effect is similar with $\Delta T = 50°\mathrm{C}$ for the same reason.

Chapter 8

Exergetic analysis

As every engineer specialised in thermodynamics knows, all the energy fluxes do not have the same quality. In the case of the M-SAB cycle, the quality (or exergy) of the heat recovered as useful thermal power output depends on its temperature. For instance, heating water to 30°C is not very useful while reaching a temperature of 80°C allows the water to be used, for example in district or domestic heating [23]. A second law analysis must then be conducted to assess the usefulness of our thermal output energy flux, to identify where exergy is destroyed in the cycle and contrast the energetic overall efficiency with its exergetic counterpart. The current chapter starts by defining the exergy and its associated dead state. This latter is indeed particular due to the sub-atmospheric pressure level encountered in the inverted configuration. A concise exergy study is then conducted for different cases, varying the wet-bulb effectiveness and the injected water flow rate. The associated Grassmann diagrams are used to illustrate the different observations.

8.1 Exergy definition & dead state

The exergy is related to the second law of thermodynamic as entropy is also taken into account in its definition, which is displayed on Equation 8.1.

$$e = h(p, T) - h(p_0, T_0) - T_0 * (s(p, T) - s(p_0, T_0)) \qquad (8.1)$$

The subscript '0' refers to the dead state, where the level of exergy is considered as null. As mentioned in the humid air entropy modelling (see subsection 5.1.2), it is taken as a state of humid air at 15°C, a relative humidity of 60% and a sub-atmospheric pressure. It is now time to justify this choice for the pressure of reference. The dead state commonly taken when conducting exergetic analysis corresponds to the atmospheric conditions, or the initial state of the working fluid if this latter is different. However, using that reference in a sub-atmospheric cycle might lead to a negative exergy content for several states. Indeed, lowering the pressure below 1.01 bar involves an increase in entropy. Consequently, it could be that a state with a relatively low temperature level, hence limiting the enthalpy h, and at the same time with a sub-atmospheric pressure, which increases the term $T_0 * s$, features a negative exergy content. This is for example the case of the states between the outlet of the heat recuperator and the inlet of the compressor. Sketching the Grassmann diagram is thus impossible due to the negative sign of several fluxes.

In order to solve that issue, the reference conditions must be changed. More precisely, the pressure of reference is shifted from the atmospheric pressure to the lowest pressure reached in the cycle. By doing that, every state features a positive exergy content which allows to sketch the Grassmann diagram.

Nevertheless, this choice has a detrimental impact on the interpretation of the fluxes on the Grassmann diagram. Indeed, the change of reference increases the value of all the fluxes that are expressed relatively to it. For example, the exergy content of the exhaust gases is bigger in the new reference as they are at atmospheric pressure. Another example is the introduction of a non-zero exergy flux corresponding to the initial exergy of the flow at atmospheric conditions, which was null in the previous reference. On the contrary, certain particular fluxes are expressed as a fixed amount of exergy. They result from a difference between two exergy states and consequently remain unchanged regardless of the dead state. This is the case for instance of the electrical power output. The electricity produced comes from the turbine and compressor work which depend on the exergy difference between the two states before and after each component. These two states both vary due to the change of reference but in an identical way, not affecting the difference between them. As a result, the exergy content of the electrical power output is constant regardless of the new reference pressure. One might thus take care when comparing the fluxes between them.

8.2 Exergy analysis

Let us now analyse the exergy fluxes and losses for four different cases. To ease the comparison and limit the number of simulations, we decided to restrict our study to cases with a fixed wet-bulb effectiveness. Still, it would be interesting to contrast the results of two cases with and without condensation in the M-cycle. Two different values for ϵ_{WB} are thus taken: 90% and 98%. For each value, it would also be relevant to observe the impact of increasing the amount of injected water. Therefore, this leads to two cases per wet-bulb effectiveness with a water mass flow going from 20 g/s to 50 g/s or 48 g/s respectively for 90% and 98%. The energetic efficiencies (electrical and overall) as well as the exergetic efficiencies associated with the mentioned cases are listed in Table 8.1.

Table 8.1: $\epsilon_{\text{WB}} = 0.98$ is associated with a higher exergetic overall efficiency mainly coming from the contribution of the electrical efficiency. The exergetic contribution of the thermal efficiency to the overall efficiency is much higher at $\epsilon_{\text{WB}} = 0.9$.

	$\epsilon_{\text{WB}} = 0.9$		$\epsilon_{\text{WB}} = 0.98$	
$m_{\text{H}_2\text{O}}$ [g/s]	20	50	20	48
η_{elec} [%]	21.3	16.9	27.9	43.6
η_{overen} [%]	77.4	96.2	79.1	83.6
η_{elex} [%]	20.4	16.2	26.7	41.7
η_{thex} [%]	2.7	5.9	1.2	1.1
η_{overex} [%]	23.1	22.1	27.9	42.8

In the previous table, η_{elex} corresponds to the exergetic version of the electrical efficiency. As the exergy content of a fixed amount of electricity is assumed to be identical to its energy content, the only difference with the energetic efficiency is that it is computed based on the exergy content of the fuel (e_{c}) instead of the LHV. As the exergy-to-energy ratio of the fuel is slightly above 1, the exergetic electrical efficiency is a bit decreased. A similar explanation goes for η_{thex} representing the exergetic thermal efficiency, with the difference that the exergy content of the recovered heat varies much more than its energy content. Depending on the temperature to which the cooling water is heated in the economizer, the gap between the two might be significant.

Before starting the analysis of the previous efficiencies using the Grassmann diagrams, a difference with the Sankey diagrams (presented in section 6.3) must be highlighted. As observable on the following figures, the fuel exergy is represented as a single flux feeding the combustion chamber. Whereas it was divided in two fluxes in the Sankey diagrams: the fuel energy content (LHV) and the latent heat of vaporization of the water produced by the combustion of the fuel (due to its atoms of hydrogen). In an exergetic point of view, this differentiation does not make sense anymore since in the computation of the fuel exergy, its water contribution is already calculated in a liquid reference (unlike the LHV in the energy case). Indeed, the fuel exergy can be defined as the energy obtained by direct chemical conversion at ambient temperature [52]. As water is liquid at ambient temperature, this justifies that the contribution present on the Sankey diagrams does not appear in the Grassmann diagrams.

A first major observation from Table 8.1 is that the contribution of the exergetic thermal efficiency is highly reduced at high ϵ_{WB}. This is linked to the exergy content of the recuperated heat in the economizer. As observable on Figure 8.1 and Figure 8.2, it accounts for up to 11 kW_{th} with $\epsilon_{\text{WB}} = 0.9$. On the other hand, with the higher wet-bulb effectiveness of 98% (see Figure 8.3 and Figure 8.4), this flux is very small (barely 1 kW_{th}). It is linked to the improved M-Cycle heat recovery resulting in less energy transferred to the economizer. The temperature of the flow arriving in that component is therefore much lower (about 32°C compared to 90°C with ϵ_{WB} $= 0.9$ as shown on Figure 10.6 and Figure 10.7 in the appendix), which limits the outlet temperature of the cooling water. Heating water up to 32°C is in this way not associated with a high exergy content. As shown in the previous chapter, $\epsilon_{\text{WB}} = 0.98$ is however associated with a boosted electrical efficiency (both energetic and exergetic), especially at high water injection. This analysis confirms then that improving the M-Cycle heat recovery performance enhances the electrical efficiency of the M-SAB cycle. But it also gives a new information : the simultaneous heat recovered in the economizer in that case has almost no interest due to its too low temperature. The cogenerative character of the mGT is therefore questioned if the wet-bulb effectiveness is too high. But since the main purpose is to find a solution to improve the electrical efficiency when the heat demand is low, this is not a real problem.

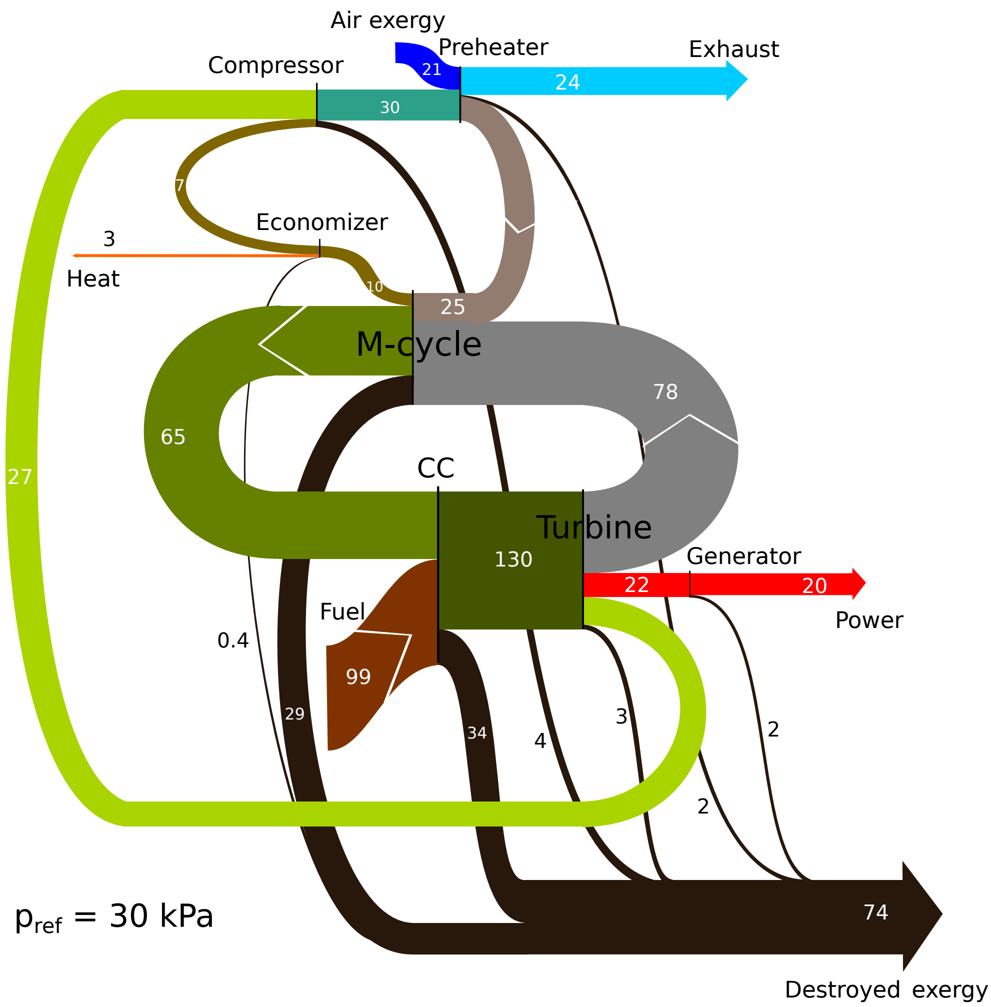

Figure 8.1: With $\epsilon_{WB} = 0.9$ and $\dot{m}_{H_2O} = 20$ g/s, the M-cycle losses are considerable and a small amount of useful heat is recovered. The exergy fluxes are expressed in kW.

Secondly, adding more water with $\epsilon_{WB} = 0.9$ makes the electrical efficiency drop by 4.4% absolute points due to the non-condensation in the M-Cycle. Even though in an energetic point of view the overall efficiency increases thanks to the larger amount of heat recovered in the economizer, its corresponding exergetic contribution is limited. As a consequence, the exergetic overall efficiency decreases.

Additionally, the main exergy loss in the cycle regardless of the case is located at the combustion chamber. It also represents a higher loss in absolute value than the energetic heat loss noticeable on the Sankey diagrams. Indeed, the loss of exergy at the combustion chamber results from two contributions : the exergy content associated with the heat loss (rather low) and the losses due to the chemical conversion of the fuel. This second contribution explains the increase of the exergetic combustion loss (approximately one third of the fuel exergetic content as noticeable on the following Grassmann diagrams) compared to the energetic equivalent (approximately 5% of the primary energy). The consideration mentioned here also appears on the Grassmann diagram of the exergetic analysis conducted by De Paepe et al. [10] and Marina Montero Carrero [11].

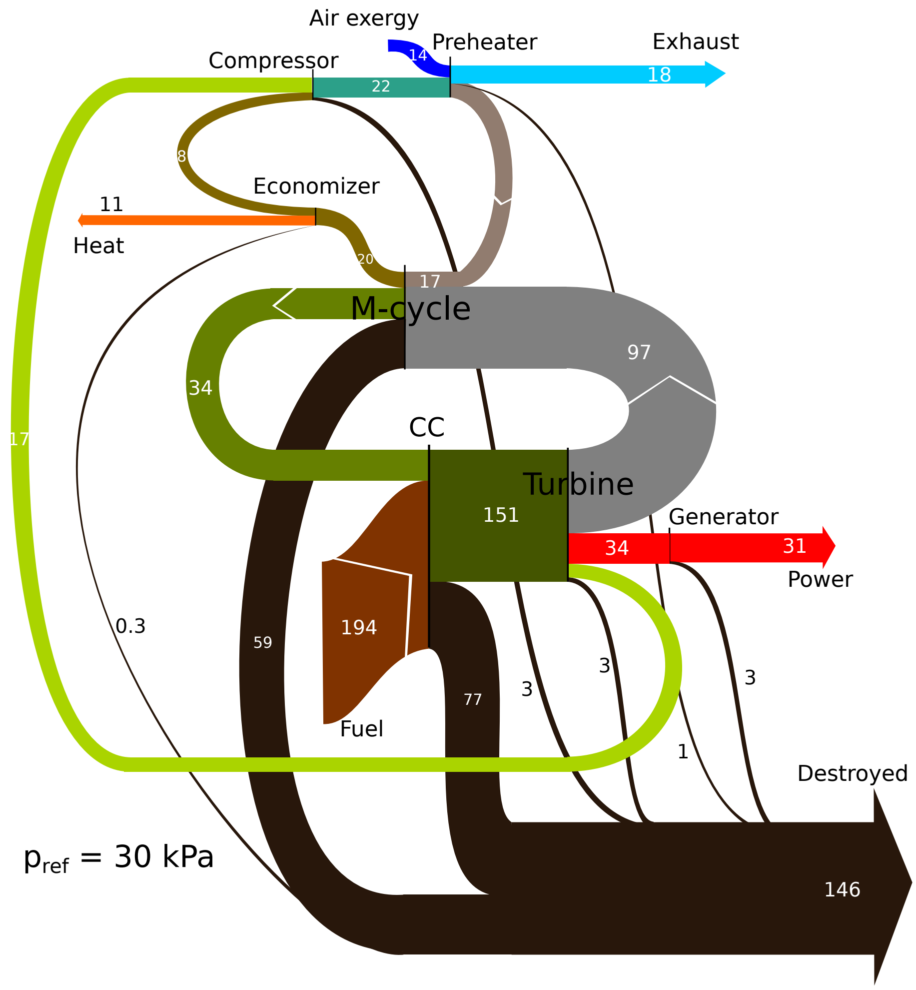

Figure 8.2: With $\epsilon_{WB} = 0.9$ and $\dot{m}_{H_2O} = 50$ g/s, the M-cycle losses are huge but a higher amount, compared to a reduced amount of injected water, of useful heat is recovered. The exergy fluxes are expressed in kW.

Another observation that could be made is related to the M-cycle exergy losses. In a heat exchanger, the higher is the pinch of temperature between the cold and the hot fluid, the more exergy is destroyed. For instance looking at the upper part of the M-cycle, both the hot and the cold pinch of temperature are lower with a higher wet-bulb effectiveness. As an illustration with $\dot{m}_{H2O} = 20$ g/s, the hot and the cold pinch of the M-saturator upper part $T_8 - T_6$ and $T_9 - T_{WB,3}$ (not to be confused with the earlier mentioned cold pinch $T_2 - T_4$, all of those in the M-cycle notations) decrease respectively from 182°C to 94°C and from 70°C to 14°C when increasing ϵ_{WB} from 90% to 98%. For the cold pinch, it is due to the lower hot outlet temperature determined by the wet-bulb effectiveness according to Equation 5.4. For the hot one, it is because the high wet-bulb effectiveness induces condensation in the M-cycle which results in a higher cold outlet temperature, therefore closer to the TOT. This can be seen when comparing two Grassmann diagrams with the same amount of injected water but a different wet-bulb effectiveness (for example Figure 8.1 and Figure 8.3 corresponding to $\dot{m}_{H_2O} = 20$ g/s). Indeed, the exergy loss in the M-Cycle accounts for 29 kW and 18 kW respectively for $\epsilon_{WB} = 0.9$ and $\epsilon_{WB} = 0.98$.

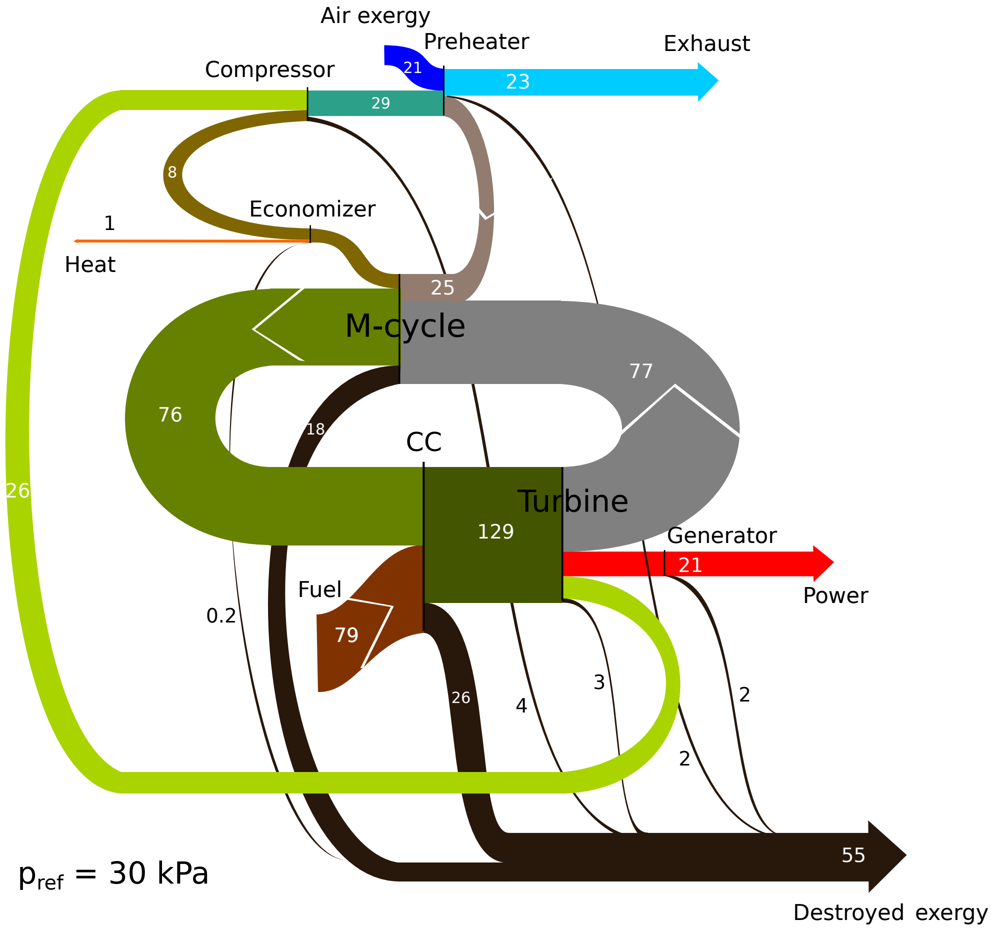

Figure 8.3: With $\epsilon_{WB} = 0.98$ and $\dot{m}_{H_2O} = 20$ g/s, the M-cycle losses are relatively small but nearly no useful heat is recovered. The exergy fluxes are expressed in kW.

A similar explanation justifies the increased M-cycle losses (18 kW compared to 7 kW) when decreasing the amount of injected water from 48 g/s to 20 g/s and keeping the wet-bulb effectiveness of 98%. Less injected water means less condensation in the M-Cycle (only 3 g/s compared to 37 g/s), so less heat recovered (139 kW compared to 236 kW) and thus a higher hot pinch of temperature (94°C compared to 50°C) leading to more losses as explained before. The trend when decreasing the water injection rate (from 50 g/s to 20 g/s) but this time when keeping a lower wet-bulb effectiveness of 90% is opposite. As no condensation occurs in the M-Cycle, injecting more water limits the increase in cold outlet temperature of the M-cycle because more water has to be evaporated. Thus the hot pinch of temperature is higher and so do the exergetic losses.

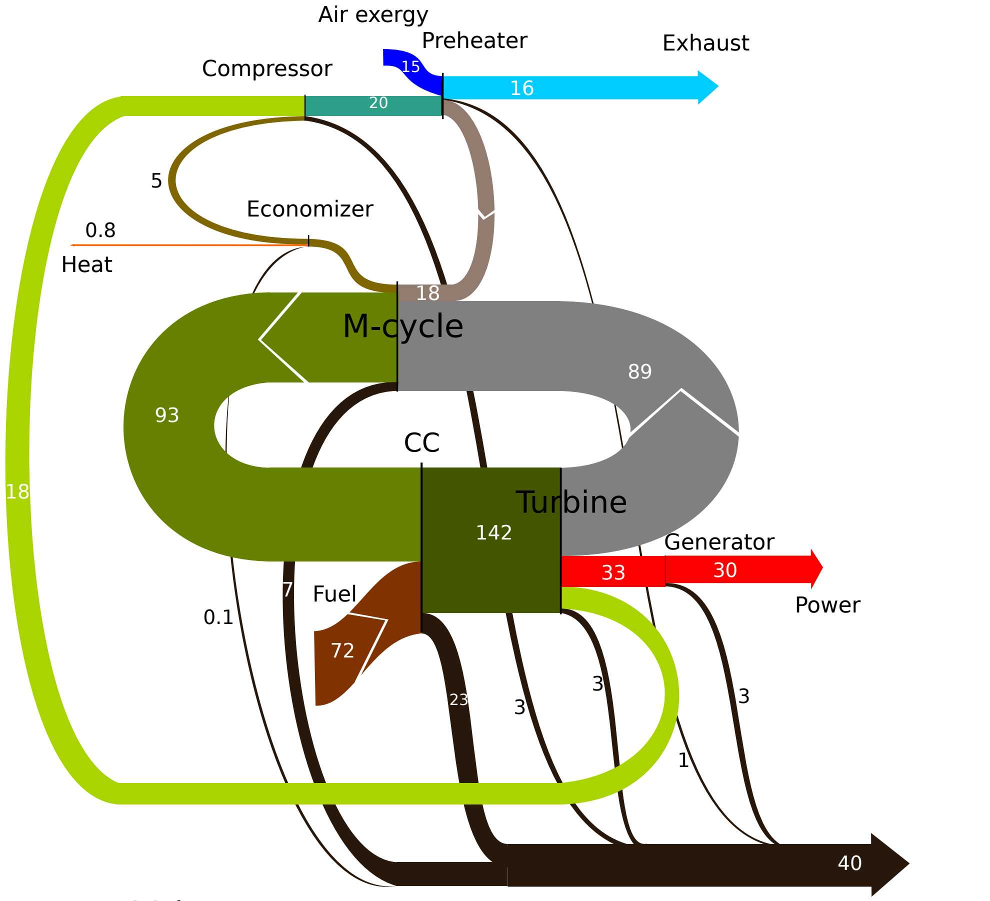

p_{ref} = 30 kPa

Figure 8.4: With $\epsilon_{WB} = 0.98$ and $\dot{m}_{H_2O} = 48$ g/s, a considerable amount of electricity is produced. In addition, the M-cycle losses are modest. The exergy fluxes are expressed in kW.

Finally, one should note the non-negligible size of the exergy fluxes corresponding to the initial air injected in the preheater and to the exhaust losses. As pointed out in the beginning of this chapter, it is the drawback of taking a sub-atmospheric pressure as reference. For that reason, these fluxes should not be compared to those corresponding to the recovered heat in the economizer or the effective electrical power output. These latter constitute indeed an invariable amount of exergy regardless of the pressure of reference. However, a better comparison would be to correlate them to the resulting flux obtained when subtracting the initial air exergy content to the exhaust losses. Doing so, the 'real' exergy content of the exhaust losses is quite small (only a few kW), and comparing it to that of the electrical or thermal power output makes now more sense. In this way, it is clear that the electricity produced (between 20 kW_e and 31 kW_e) represents much more exergy than what is lost at the exhaust (up to 4 kW).

Chapter 9

Comparison with other technologies

This chapter aims to point out the best performance of our M-SAB model, compare it to what is achieved by other commercial technologies providing the same range of power outputs and evaluate the constraints linked to an excellent heat exchanger effectiveness.

9.1 M-SAB performance

Following the sensitivity and exergetic analysis, the impact of the main parameters on the M-SAB cycle performance is now well established. We decided to compare here the results achieved by our model with two different values for the wet-bulb effectiveness. Indeed, this parameter significantly drives the design of the M-saturator as it will be described in section 9.3. The two considered values are 90% and 98%. The first one is rather common regarding what has been achieved in the literature [8,29,38] while reaching the second one constitutes a more complex technical challenge. With the purpose of identifying the set of input parameters maximising the efficiency (electrical or overall depending on what is requested) for each wet-bulb effectiveness, a detailed optimisation should be conducted. However, it is not part of our work. The same set of boundary conditions as used in the sensitivity analysis is therefore conserved. The only parameter which varies is the injected water mass flow.

Increasing or decreasing the amount of injected water will promote either the heat or the electricity production. This constitutes then a flexibility of the M-SAB cycle against the variation of the demand throughout the year. The power outputs and efficiencies of the M-SAB cycle for the two values of the wet-bulb effectiveness each tested with a low and a high water mass flow are shown in Table 9.1.

Table 9.1: The highest M-SAB cycle electrical efficiency of 43.5% is achieved with a high wet-bulb effectiveness and the maximum amount of injected water.

ϵ_{WB} [-]	$\dot{m}_{\mathrm{H2O}}$ [g/s]	Oriented	P_{elec} [kW$_{\mathrm{e}}$]	P_{th} [kW$_{\mathrm{th}}$]	η_{elec} [%]	η_{overen} [%]	η_{overex} [%]
0.9	20	Electricity	20.1	52.9	21.3	77.4	23.1
0.9	50	Heat	31.4	147	16.9	96.2	22.1
0.98	20	Heat	21	38.5	27.8	79	27.9
0.98	48	Electricity	30	27.6	43.5	83.5	42.8

As already mentioned in the sensitivity analysis, increasing the water injection at ϵ_{WB} = 0.9 decreases the electrical efficiency and increases the thermal power output and the overall efficiency. But in an exergetic approach, decreasing the electrical efficiency to increase the thermal efficiency is associated with a degradation of the exergy as shown by the slightly decreasing overall exergetic efficiency. Yet, as pointed out from the exergetic analysis, the exergy content of the thermal power output associated with this ϵ_{WB} is adequate for the heated water to be used in a district or domestic heating application.

For a ϵ_{WB} of 98%, it is the opposite : adding more water increases the electrical efficiency. Nevertheless, as shown in the exergetic analysis, the exergy content of the thermal power output is so low that this latter can not be used. Therefore, with such an effectiveness this unit can not be considered as a CHP unit since it would be difficult to use heat at a such low temperature. In this case, the overall energetic efficiency is misleading and should not be compared to the ones of other technologies. Moreover, there is no interest to inject smaller quantities of water with this effectiveness since it induces a lower electrical efficiency. The unit is thus here intended to produce electricity with the highest electrical efficiency as possible. In order to enable this cycle to produce useful heat again while producing electricity, no water should be injected at all. In that case, the M-Cycle would behave as a dry heat exchanger, losing its high heat recovery capacity. Also, the classical assumptions taken in our modelling would not be verified meaning that the considered value for the effectiveness might drop significantly. A complete characterisation should be conducted to assess exactly the consequences of running the M-SAB cycle without water injection. But it can be expected that the electrical efficiency falls considerably. Still, if it is possible for the M-power unit to feature a 98% wet-bulb effectiveness, the M-SAB cycle should be run as often as possible with the highest possible water injection rate (therefore producing only electricity). A potential solution to deal with a simultaneous heat and electricity demand would be to have another unit intended to produce, with a high thermal efficiency (such as a boiler with an efficiency generally between 85% and 95% [53]), all the required heat. This should be the subject of an in-depth economic study aiming at developing the most profitable unit in that perspective.

9.2 Comparison

It is now time to measure if the M-SAB cycle performance could be competitive with that of other small-scale CHP units. The technologies of comparison should produce an equivalent range of electrical power output as our model, which lies between 20 $\mathrm{kW_e}$ and 35 $\mathrm{kW_e}$. A panel of systems was therefore selected with different commercial applications whose electrical production reaches up to 100 $\mathrm{kW_e}$ for the majority with still a couple of bigger systems reaching about 300 $\mathrm{kw_e}$ as the upper limit. Three different types of engine appear to be relevant : other mGT applications, Stirling engines and ICE. The different CHP units with their associated electrical power output and efficiencies (electrical and overall) are listed in an ascending order and by technologies in Table 9.2. Only the electricity-driven performance of the M-SAB cycle is included in the same table. Indeed, the current obstacle towards a larger commercial development of mGT applications comes from their limited electrical efficiency. Therefore, the purpose of the comparison is to examine if the M-SAB cycle could help overcoming this barrier.

Table 9.2: Performance of a panel of commercial CHP units generating a comparable electrical power output. The electrical efficiency of the M-SAB cycle with $\epsilon_{\mathrm{WB}} = 0.98$ is the highest among the units listed here. However, if the effectiveness drops to 90%, the electrical performance declines drastically.

			P_{elec} [kW$_\mathrm{e}$]	η_{elec} [%]	η_{overen} [%]	Reference
M-SAB	$\boldsymbol{\epsilon_{\mathrm{WB}} = 0.9}$	$\boldsymbol{\dot{m}_{\mathrm{H20}} = 20}$ **g/s**	**20.1**	**21.3**	**77.4**	-
M-SAB	$\boldsymbol{\epsilon_{\mathrm{WB}} = 0.98}$	$\boldsymbol{\dot{m}_{\mathrm{H20}} = 48}$ **g/s**	**30**	**43.5**	**83.5**	-
Type of engine	Manufacturer	Model				
mGT						
	EnerTwin	MTT	1	15.9	78.5	[8]
	Capstone Turbine Corporation	C30	30	26	up to 90	[17]
		C65	65	28	up to 90	[18]
	Ansaldo Energia	AE-T100	100	30	-	[20]
	Capstone Turbine Corporation	C200	200	33	up to 90	[19]
Stirling						
	Stirling Danmark	-	31	9.2	90	[54]
	Stirling Biopower/ Qalovis	FleXgen G38	38	29	78	[55]
	Shangai MicroPowers Ltd.	4R90GZ	50	28-32	>85	[56]
	247 Energy	247-LNG-CPP-140	140	38.6	69.2	[57]
ICE						
	Yanmar	CP25WE-TNB	25	33.3	85	[58]
	Tedom	Micro 30	30	30.9	91.6	[59]
	Yanmar	CP35D1-TNUG	35	32.5	88	[58]
	Tedom	Micro 55	55	34.2	95.4	[59]
		Cento 80	83	35	85.9	[59]
		Cento 100	106	36.4	85.6	[59]
	Innio	Jenbacher Type2	294-330	38.8	up to 90	[60]

The analysis is pretty direct: the T100 mGT in a M-SAB configuration can be competitive in terms of electrical efficiency only if a sufficient wet-bulb effectiveness is reached. Indeed with $\epsilon_{\mathrm{WB}} = 0.98$, the electrical efficiency reaches 43.5%, which is the highest electrical efficiency from all the units catalogued here. This value could even be decreased by some absolute percentage points while staying competitive with the other technologies with a similar capacity. Therefore, this would allow to decrease the restrictive value of 98% of the wet-bulb effectiveness. Nevertheless, the drop of this M-Cycle performance parameter must remain small since achieving a high electrical performance requires to have condensation in the M-Cycle which is only the case if the wet-bulb effectiveness is higher than 96% (see Figure 7.4). In addition, the variation of the electrical efficiency with the wet-bulb effectiveness when this latter is higher than 96% is considerable which might limit the allowed drop in effectiveness to stay competitive with the other technologies. As an illustration, the electrical efficiency already drops to 33.6% with $\epsilon_{\mathrm{WB}} = 0.97$.

However, if designing a heat recuperator with such a high effectiveness (see the discussion held below in section 9.3) presents a too big challenge, the profitability of the M-SAB cycle, and therefore the potential existence of a commercial unit of this type, is to reconsider. What is certain is that the common value of 90% for the effectiveness leads to a too poor electrical efficiency (21.3% when the mass flow is such that the unit promotes the production of electricity). Even if this value allows the CHP unit to have flexibility regarding the injected water mass flow (to promote either electricity or heat production), the associated electrical efficiency is too modest to justify an investment in that technology. One should rather invest in an efficient mGT from an electrical point of view combined with a boiler delivering the needed heat at a high thermal efficiency.

9.3 Design requirements for a high ϵ_{WB}

As already specified several times, reaching the good electrical performance of the M-SAB cycle implies the recuperator to feature a not least wet-bulb effectiveness of 98%. Indeed, the main asset of the M-saturator is its great heat recovery when water condensation occurs. As presented in the sensitivity analysis, this requires to have a minimum wet-bulb effectiveness of 96%. This value leads though to notably inferior performance compared to 98%. Actually, once condensation has started, the behavior of the cycle is highly sensitive to a change of the wet-bulb effectiveness. As already highlighted by De Paepe et al., this requires a saturator design which avoids fluctuations of the wet-bulb effectiveness, called *Robust Design* [10]. As discussed in the sensitivity analysis, increasing the dew point effectiveness allows to reach a slightly lower wet-bulb effectiveness while keeping the same performance. Yet, this latter still constitutes a technological challenge. The number of existing technologies able to reach such an attribute is rather limited. Additionally, the studied devices must be compatible with the design of the Maisotsenko saturator, which is often not the case. As an illustration, Onufrena et al. [61] designed a compact counter flow heat exchanger reaching an effectiveness of 96.5% by adding copper mesh material. Nevertheless, their application aims to be used in cryocoolers with a range of temperature and pressure varying respectively between 4.5K and 290K and between 1 bar and 10 bar. The temperature and pressure levels reached in the M-power unit are then not compatible. Moreover, the typical effectiveness encountered in the different papers used in our work mostly lies around 90% [8, 29, 38].

Let us first come back to the definition of a heat exchanger effectiveness. According to Incropera et al., it is defined as 'the ratio of the actual heat transfer rate to the maximum possible heat transfer rate' [62]. This latter could in principle be achieved in an infinitely long counterflow heat exchanger. In order to compute the effectiveness with more convenience, it is usually expressed in terms of two parameters : C_r and NTU. The first one is the ratio of the heat capacity rate, defined as the product of the mass flow with the heat capacity, between the hot and cold fluid with always the higher value at the denominator. The number of transfer units (NTU) is a dimensionless parameter defined as:

$$NTU = \frac{UA}{C_{\min}} \tag{9.1}$$

where U is the overall heat transfer coefficient, A is the heat exchange surface area and $C_{\min}$ is the lowest heat capacity rate between the hot and cold fluid.

As the Maisotsenko heat exchanger is actually in a counterflow configuration and in view of the fact that condensation takes place (which gives $C_r = 1$, assuming then a sufficiently high wet-bulb effectiveness), the ϵ-NTU relation reads:

$$\epsilon = \frac{NTU}{1 + NTU} \tag{9.2}$$

Regarding the previous relation, our target effectiveness implies to increase the NTU as much as possible. According to Equation 9.1, three parameters could be modified. $C_{\min}$ is dependant on the mass flow and heat capacity of the hot flow to be cooled, it is therefore a rather difficult parameter to play on in our case. The other parameters are more related to the design of the heat exchanger in itself. Two options are then possible : either improving the heat transfer coefficient or increasing the heat exchange contact area.

First of all, the overall heat transfer coefficient can be improved using either active or passive methods. The difference between the two is the need of an external source of power for the active methods. The passive methods rely rather on geometric modifications or injection of additives to the fluid. Bhatnagar et al. [63] listed different alternatives of each method. Active methods include for example fluid or surface vibration, suction of the fluid, introduction of an electrostatic field, etc. However, this category of techniques is not really suited to our mGT application unless the required external power consumption does not decrease too much the electrical efficiency of the cycle. The passive methods might constitute a more relevant alternative such as modifying the surface roughness, inducing swirl in the flow or injecting additives to the fluid. The authors of the paper particularly focus their analysis on the last two methods. The swirl flow method intends to increase the turbulence by creating vortices near the walls to improve the heat transfer rate. The second method consists of adding nanoparticles in a liquid to upgrade its thermal conductivity. But as our application deals with gaseous flow inside the heat exchanger, this method is not applicable. Still, even if the passive methods do not involve any power consumption, they go in pair with a drawback : increased pressure drops. As an example, increasing the surface roughness or making the boundary layer more turbulent are indeed methods enhancing the heat transfer but they also increase the friction factor which is one of the main driver of the pressure losses. As underlined in the sensitivity analysis when looking at the impact of the pressure drops, increasing them decreases the electrical performance of the M-SAB cycle. A trade-off must thereafter be found between the reachable effectiveness and the degradation of the electrical efficiency due to the use of such methods.

The other mentioned solution towards a higher effectiveness is to simply enlarge the heat exchange surface. Nevertheless, as highlighted by Musgrove et al. [64] this implies also an increase in pressure drops. More than finding a trade-off between heat exchanger effectiveness and pressure drops level, a trade-off between the size of the system and its efficiency must be met. If the size of the heat exchanger has to vary, another factor will be involved : the cost of the installation. The bigger the heat exchanger, the higher its investment costs. But the installation still needs to be economically profitable.

Regarding the current discussion, reaching the target value of the M-Cycle effectiveness represents a technological challenge that implies choices. Undoubtedly, different trade-off will need to be reached. Regardless of the solution used to enhance the effectiveness (passive methods or increase of the heat exchange area), this has to be optimised with the increase of the pressure drops, directly influencing the electrical efficiency. When increasing the heat exchange surface, a compromise between the size of the installation and its related cost has also to be found. A detailed thermo-economic analysis of the M-SAB cycle might help to assess the real feasibility of this system, but this goes beyond the scope of our work.

Chapter 10

Conclusion

The purpose of our work was to develop a numerical model of the Maisotsenko sub-atmospheric inverted Brayton cycle in order to evaluate its thermodynamic potential, regarding the installation of small-scale decentralised power units. In this way, the specific M-saturator has been implemented and introduced in an IBC model previously validated. The results analysed in the sensitivity analysis show that an electrical efficiency of 43.5% is reached when the wet-bulb effectiveness is fixed at 98% (corresponding to a hot pinch of approximately 50°C for the M-saturator). Such parameter allows indeed to boost the heat recovery by decreasing sufficiently the outlet temperature of the flue gases to induce condensation in that component. The aforementioned electrical efficiency is far better than that of commercial CHP applications producing the same range of electrical power output (between 20 kW_e and 35 kW_e). However, the exergetic analysis revealed that the exergy content of the thermal power output associated with an effectiveness of 98% is so low that the recuperated heat is not usable, removing the CHP character of the cycle. Nevertheless, the concept studied here is intended to be applied to boost the electrical efficiency. When fixing a typical wet-bulb effectiveness of 90%, the electrical efficiency drops significantly to 21.3%. Even though the thermal power output recovered in the economizer is this time usable for domestic or district heating, the limited electrical efficiency does not justify the investments in such system.

The design of the M-power unit must then allow to reach the effectiveness of 98% (of at least 97% which is associated with an electrical efficiency of 33.6%). This constitutes a rather complex technical challenge. The potential solutions of using passive and/or active methods or enlarging the heat exchange surface are associated with higher pressure drops, which might deteriorate the electrical efficiency of the cycle. The larger area goes also in hand with an increased size of the heat exchanger, associated with larger costs. Therefore, more than achieving the requested effectiveness, it is necessary to check that the associated increased pressure drops do not impact too significantly the electrical efficiency. In an economical point of view, the potential larger heat exchanger must also still allow the cycle to be profitable. Such considerations might be subject of more detailed techno-economic and thermo-economic investigations.

The best electrical performance considered here is achieved when injecting the most water possible (48 g/s with $\epsilon_{\mathrm{WB}} = 0.98$). In our model, only the thermodynamic limitations were examined : the respect of the minimal value for the hot pinch as well as the complete aspect of the combustion. But another neglected upper bound for this parameter might result from a technical issue of the compressor : the surge limit. This constitutes therefore one more technical challenge that might require modifications of the mGT used. Still linked to the design requirements associated with a considerable water injection rate, the TOT attained in the M-SAB cycle in the best performing case accounts for almost 730°C. The classical materials commonly used in mGT applications are only able to resist to a temperature lying between 620°C and 680°C. The use of more robust, and thus more expensive, materials must also be taken into account in a future economical investigation. This is also the case for the corrosion which is an intrinsic requirement in the design of humidified cycle.

Assuming that the mentioned requirements can be satisfied, the inverted nature of the M-SAB cycle offers advantages compared to the conventional configuration (able to reach an electrical efficiency of 42.1% with a 98% effectiveness M-power component [10]). Indeed, the high electrical efficiency comparable to that of mGT in the conventional BC configuration is achieved while decreasing the electrical power output of the cycle. This downsizing ability is one of the main strength of inverting a cycle and constitutes a great asset regarding the need of small-scale decentralised power units. Another technological benefit is the atmospheric combustion chamber which induces a simpler design with cheaper materials and avoids to have a fuel gas compressor. Finally, the inverted configuration is insensitive to the ambient conditions. This allows the cycle to keep the same performance all along the year while the conventional configuration might suffer from reduced performance in the summer.

In view of the above, the thermodynamic potential of the introduction of a high performing M-saturator into an inverted Brayton cycle has been proved. Yet, future investigations should focus on the design of such unit. Not only studying the feasibility of achieving the best numerical performance obtained with our model, an economical investigation should be conducted to verify if the technological requirements do not increase the investment costs to a level preventing any profitability. Another work perspective is about the modelling of the combustion chamber. A relatively simple implementation was made in our work but a more detailed model of the different emissions could be relevant to compare them with the other technologies.

Nomenclature

ϵ_{dew} Dew point effectiveness

ϵ_{WB} Wet-bulb temperature effectiveness

BC Brayton Cycle

CHP Combined Heat and Power

CIT Compressor Inlet Temperature

DEC Direct Evaporative Cooling

EGR Exhaust Gas Recirculation

HRSG Heat Recovery Steam Generator

HVAC Heating, Ventilation and Air-Conditioning

HX Heat Exchanger

IAC Inlet Air Cooling

IBC Inverted Brayton Cycle

ICE Internal Combustion Engine

IEA International Energy Agency

IEC Indirect Evaporative Cooling

M-ABC Maisotsenko Air Bottoming Cycle

M-Cycle Maisotsenko Cycle

M-SAB Maisotsenko sub-atmospheric Brayton Cycle

MBC Maisotsenko Brayton Cycle

MCTC Maisotsenko Combustion Turbine Cycle

mGT Micro Gas Turbine

mHAT micro Humid Air Turbine

TIT Turbine Inlet Temperature

TOT Turbine Outlet Temperature

UCL Université Catholique de Louvain

VUB Vrije Universiteit Brussel

Bibliography

[1] U. N. C. Change, “The paris agreement,” last accessed 01 November 2021. [Online]. Available: https://unfccc.int/process-and-meetings/the-paris-agreement/the-paris-agreement

[2] IEA, “World energy outlook 2020,” last accessed 02 November 2021. [Online]. Available: https://www.iea.org/reports/world-energy-outlook-2020

[3] L. Smoot and L. L. Baxter, “Fossil fuel power stations—coal utilization,” in *Encyclopedia of Physical Science and Technology (Third Edition)*, third edition ed., R. A. Meyers, Ed. New York: Academic Press, 2003, pp. 121–144. [Online]. Available: https://www.sciencedirect.com/science/article/pii/B012227410500257X

[4] P. Breeze, “Chapter 4 - natural gas–fired gas turbine and combined cycle power plants,” in *Power Generation Technologies (Third Edition)*, third edition ed., P. Breeze, Ed. Newnes, 2019, pp. 71–97. [Online]. Available: https://www.sciencedirect.com/science/article/pii/B9780081026311000043

[5] M. M. Carrero, “Decoupling heat and electricity production from micro gas turbines,” Ph.D. dissertation, Vrije Universiteit Brussel, 2018.

[6] IEA, “Demand response potential in the sustainable development scenario, 2018-2040,” last accessed 02 November 2021. [Online]. Available: https://www.iea.org/data-and-statistics/charts/demand-response-potential-in-the-sustainable-development-scenario-2018-2040

[7] L. Mongibello, N. Bianco, M. Caliano, and G. Graditi, “Influence of heat dumping on the operation of residential micro-chp systems,” *Applied Energy*, vol. 160, pp. 206–220, 2015. [Online]. Available: https://www.sciencedirect.com/science/article/pii/S0306261915011332

[8] *Numerical Investigation of an Inverted Brayton Cycle Micro Gas Turbine Based on Experimental Data*, ser. Turbo Expo: Power for Land, Sea, and Air, vol. Volume 3: Coal, Biomass, and Alternative Fuels; Cycle Innovations; Electric Power; Industrial and Cogeneration; Organic Rankine Cycle Power Systems, 06 2018, v003T06A013. [Online]. Available: https://doi.org/10.1115/GT2018-76377

[9] E. Agelidou, T. Monz, A. Huber, and M. Aigner, “Experimental investigation of an inverted brayton cycle micro gas turbine for chp application,” 06 2017.

[10] W. De Paepe, A. Pappa, M. Montero Carrero, L. Bricteux, and F. Contino, “Reducing waste heat to the minimum: Thermodynamic assessment of the m-power cycle concept applied to micro gas turbines,” *Applied Energy*, vol. 279, p. 115898, 2020. [Online]. Available: https://www.sciencedirect.com/science/article/pii/S0306261920313647

[11] M. Montero Carrero, W. De Paepe, S. Bram, A. Parente, and F. Contino, “Does humidification improve the micro gas turbine cycle? thermodynamic assessment based on sankey and grassmann diagrams,” *Applied Energy*, vol. 204, pp. 1163–1171, 2017. [Online]. Available: https://www.sciencedirect.com/science/article/pii/S0306261917305603

[12] IEA, “Global share of electricity generation, 2019,” last accessed 02 November 2021. [Online]. Available: https://www.iea.org/data-and-statistics/charts/global-share-of-electricity-generation-2019

[13] MTT, “Specifications enertwin,” last accessed 7 February 2022.

[14] A. Khalatov, S. Severin, P. Brodetsky, and V. Maisotsenko, “Brayton’s subatmospheric inverse cycle with regeneration of output heat by maisotsenko’s cicle,” *Reports of the National Academy of Sciences of Ukraine*, pp. 72–79, 01 2015.

[15] K. Matsui, K. Thu, and T. Miyazaki, “A hybrid power cycle using an inverted brayton cycle with an indirect evaporative device for waste-heat recovery,” *Applied Thermal Engineering*, vol. 170, p. 115029, 2020. [Online]. Available: https://www.sciencedirect.com/science/article/pii/S135943111938408X

[16] R. Boukhanouf, “15 - small combined heat and power (chp) systems for commercial buildings and institutions,” in *Small and Micro Combined Heat and Power (CHP) Systems*, ser. Woodhead Publishing Series in Energy, R. Beith, Ed. Woodhead Publishing, 2011, pp. 365–394. [Online]. Available: https://www.sciencedirect.com/science/article/pii/B9781845697952500155

[17] Capstone, “Specifications C30,” last accessed 19 May 2022. [Online]. Available: https://www.pureworldenergy.com/technology/capstone-products/c30-capstone-microturbine/

[18] Capstone, “Specifications C65,” last accessed 19 May 2022. [Online]. Available: https://www.capstonegreenenergy.com/products/energy-generation-technologies/capstone-microturbines/c65

[19] Capstone, “Specifications C200,” last accessed 19 May 2022. [Online]. Available: https://www.capstonegreenenergy.com/products/energy-generation-technologies/capstone-microturbines/c200

[20] Ansaldo Energia, “Specifications AE-T100,” last accessed 19 May 2022. [Online]. Available: https://www.ansaldoenergia.com/PublishingImages/Microturbines_Subsite/PRODUCTS/AE-T100NG.pdf

[21] T. Rosfjord, W. Tredway, A. Chen, J. Mulugeta, and T. Bhatia, “Advanced microturbine systems.” [Online]. Available: https://www.osti.gov/biblio/924484

[22] C. Soares, *Microturbines : Applications for distributed energy systems.* Elsevier, 2007.

[23] M. C. Rydstrand, M. O. Westermark, and M. A. Bartlett, “An analysis of the efficiency and economy of humidified gas turbines in district heating applications,” *Energy*, vol. 29, no. 12, pp. 1945–1961, 2004, efficiency, Costs, Optimization, Simulation and Environmental Impact of Energy Systems. [Online]. Available: https://www.sciencedirect.com/science/article/pii/S0360544204000866

[24] *Ceramic Recuperator and Turbine: The Key to Achieving a 40 Percent Efficient Microturbine*, ser. Turbo Expo: Power for Land, Sea, and Air, vol. Volume 1: Turbo Expo 2005, 06 2005. [Online]. Available: https://doi.org/10.1115/GT2005-68644

[25] W. De Paepe, M. Montero Carrero, S. Bram, A. Parente, and F. Contino, “Towards higher micro gas turbine efficiency and flexibility — humidified mgts: A review.” *Journal of Engineering for Gas Turbines and Power*, vol. 140, 11 2017.

[26] W. De Paepe, “Flexible heat production from a micro gas turbine: design and experimental analysis of humidified air cycles,” Ph.D. dissertation, Vrije Universiteit Brussel, 2014.

[27] M. Bianchi, G. Montenegro, and A. Peretto, “Inverted brayton cycle employment for low-temperature cogenerative applications,” *Journal of Engineering for Gas Turbines and Power-transactions of The Asme - J ENG GAS TURB POWER-T ASME*, vol. 124, 07 2002.

[28] *Inverted Brayton Cycle With Exhaust Gas Condensation*, ser. Turbo Expo: Power for Land, Sea, and Air, vol. Volume 8: Microturbines, Turbochargers and Small Turbomachines; Steam Turbines, 06 2017, v008T26A026. [Online]. Available: https://doi.org/10.1115/GT2017-64695

[29] M. Henke, T. Monz, and M. Aigner, “Inverted Brayton Cycle With Exhaust Gas Recirculation—A Numerical Investigation,” *Journal of Engineering for Gas Turbines and Power*, vol. 135, no. 9, 08 2013, 091203. [Online]. Available: https://doi.org/10.1115/1.4024954

[30] M. H. Mahmood, M. Sultan, T. Miyazaki, S. Koyama, and V. S. Maisotsenko, “Overview of the maisotsenko cycle – a way towards dew point evaporative cooling,” *Renewable and Sustainable Energy Reviews*, vol. 66, pp. 537–555, 2016. [Online]. Available: https://www.sciencedirect.com/science/article/pii/S1364032116304361

[31] I. Anufriev, “Review of water/steam addition in liquid-fuel combustion systems for nox reduction: Waste-to-energy trends,” *Renewable and Sustainable Energy Reviews*, vol. 138, p. 110665, 2021. [Online]. Available: https://www.sciencedirect.com/science/article/pii/S1364032120309497

[32] G. Comodi, M. Renzi, F. Caresana, and L. Pelagalli, “Enhancing micro gas turbine performance in hot climates through inlet air cooling vapour compression technique,” *Applied Energy*, vol. 147, pp. 40–48, 2015. [Online]. Available: https://www.sciencedirect.com/science/article/pii/S0306261915002615

[33] I. Reyzin, "Evaluation of the maisotsenko power cycle thermodynamic efficiency," *International Journal of Energy for a Clean Environment*, vol. 12, pp. 129–139, 01 2011.

[34] J. J. Lee, M. S. Jeon, and T. S. Kim, "The influence of water and steam injection on the performance of a recuperated cycle microturbine for combined heat and power application," *Applied Energy*, vol. 87, no. 4, pp. 1307–1316, 2010. [Online]. Available: https://www.sciencedirect.com/science/article/pii/S0306261909003018

[35] F. Delattin, S. Bram, S. Knoops, and J. De Ruyck, "Effects of steam injection on microturbine efficiency and performance," *Energy*, vol. 33, no. 2, pp. 241–247, 2008, 19th International Conference on Efficiency, Cost, Optimization, Simulation and Environmental Impactof Energy Systems. [Online]. Available: https://www.sciencedirect.com/science/article/pii/S0360544207001612

[36] M. Montero Carrero, W. De Paepe, J. Magnusson, A. Parente, S. Bram, and F. Contino, "Experimental characterisation of a micro humid air turbine: assessment of the thermodynamic performance," *Applied Thermal Engineering*, vol. 118, pp. 796–806, 2017. [Online]. Available: https://www.sciencedirect.com/science/article/pii/S1359431117315168

[37] M. Montero Carrero, W. De Paepe, A. Parente, and F. Contino, "T100 mgt converted into mhat for domestic applications: Economic analysis based on hourly demand," *Applied Energy*, vol. 164, pp. 1019–1027, 2016. [Online]. Available: https://www.sciencedirect.com/science/article/pii/S0306261915003165

[38] K. Wan, S. Zhang, J. Wang, and Y. Xiao, "Performance of humid air turbine with exhaust gas expanded to below ambient pressure based on microturbine," *Energy Conversion and Management*, vol. 51, no. 11, pp. 2127–2133, 2010. [Online]. Available: https://www.sciencedirect.com/science/article/pii/S0196890410001123

[39] M. du Toit, N. Engelbrecht, S. P. Oelofse, and D. Bessarabov, "Performance evaluation and emissions reduction of a micro gas turbine via the co-combustion of h2/ch4/co2 fuel blends," *Sustainable Energy Technologies and Assessments*, vol. 39, p. 100718, 2020. [Online]. Available: https://www.sciencedirect.com/science/article/pii/S2213138820303611

[40] *Maisotsenko Open Cycle Used for Gas Turbine Power Generation*, ser. Turbo Expo: Power for Land, Sea, and Air, vol. Volume 3: Turbo Expo 2003, 06 2003. [Online]. Available: https://doi.org/10.1115/GT2003-38080

[41] G. Zhu, T.-T. Chow, and C.-K. Lee, "Performance analysis of biogas-fueled maisotsenko combustion turbine cycle," *Applied Thermal Engineering*, vol. 195, p. 117247, 2021. [Online]. Available: https://www.sciencedirect.com/science/article/pii/S1359431121006840

[42] M. Saghafifar and M. Gadalla, "Analysis of maisotsenko open gas turbine power cycle with a detailed air saturator model," *Applied Energy*, vol. 149, pp. 338–353, 2015. [Online]. Available: https://www.sciencedirect.com/science/article/pii/S0306261915004018

[43] Mohammad Saghafifar and Mohamed Gadalla, "Analysis of maisotsenko open gas turbine bottoming cycle," *Applied Thermal Engineering*, vol. 82, pp. 351–359, 2015. [Online]. Available: https://www.sciencedirect.com/science/article/pii/S1359431115001404

[44] Saghafifar, Mohammad and Gadalla, Mohamed, "A critical assessment of thermo-economic analyses of different air bottoming cycles for waste heat recovery," *International Journal of Energy Research*, vol. 43, no. 4, pp. 1315–1341, 2019. [Online]. Available: https://onlinelibrary.wiley.com/doi/abs/10.1002/er.4243

[45] L. Chen, J. Shen, Y. Ge, Z. Wu, W. Wang, F. Zhu, and H. Feng, "Power and efficiency optimization of open maisotsenko-brayton cycle and performance comparison with traditional open regenerated brayton cycle," *Energy Conversion and Management*, vol. 217, p. 113001, 2020. [Online]. Available: https://www.sciencedirect.com/science/article/pii/S0196890420305458

[46] H. Arangi, P. Sivaram, and H. Babu, "Analysis of inlet air temperature effect on gas turbine compressor perfornance," *International Research Journal of Engineering and Technology*, vol. 2, no. 8, pp. 845–853, 2015.

[47] H. Zheng, "Chapter 6 - humidification–dehumidification solar desalination systems," in *Solar Energy Desalination Technology*, H. Zheng, Ed. Amsterdam: Elsevier, 2017, pp. 447–535. [Online]. Available: https://www.sciencedirect.com/science/article/pii/B9780128054116000063

[48] M. Papalexandris, "Lab report : Combustion inside a domestic gas burner supplied with natural gas." in *LMECA2160 : Combustion and Fuels (UCLouvain).*

[49] *Gas Turbine Engine Components.* John Wiley Sons, Ltd, 2004, ch. 5, pp. 159–291. [Online]. Available: https://onlinelibrary.wiley.com/doi/abs/10.1002/9780470774533.ch5

[50] *Micro Gas Turbine Integrated With a Supercritical CO2 Brayton Cycle Turbine: Layout Comparison and Thermodynamic Analysis*, ser. Turbo Expo: Power for Land, Sea, and Air, vol. Volume 8: Industrial and Cogeneration; Manufacturing Materials and Metallurgy; Marine; Microturbines, Turbochargers, and Small Turbomachines, 09 2020, v008T20A011. [Online]. Available: https://doi.org/10.1115/GT2020-14910

[51] *Micro Humid Air Cycle: Part A — Thermodynamic and Technical Aspects*, ser. Turbo Expo: Power for Land, Sea, and Air, vol. Volume 3: Turbo Expo 2003, 06 2003. [Online]. Available: https://doi.org/10.1115/GT2003-38326

[52] D. Johnson, J. Martin, and P. Wauters, *Thermal power plants: energetic and exergetic approaches.* Presses universitaires de Louvain, 2015.

[53] E. K. Vakkilainen, "3 - boiler processes," in *Steam Generation from Biomass*, E. K. Vakkilainen, Ed. Butterworth-Heinemann, 2017, pp. 57–86. [Online]. Available: https://www.sciencedirect.com/science/article/pii/B9780128043899000034

[54] F. Biedermann, H. Carlsen, M. Schoech, and I. Obernberger, "Operating experiences with a small-scale chp pilot plant based on a 35 kwel hermetic four cylinder stirling engine for biomass fuels," in *Proc. of the 11th International Stirling Engine Conference (ISEC)*, 2004, pp. .–.

[55] "Qalovis energy introduction and flexgen overview," last accessed 18 May 2022. [Online]. Available: https://www.biowkk.eu/wp-content/uploads/2015/02/12748858113-Qalovis-Shrieves-Flexgen.pdf

[56] J.-B. Bouvenot, B. Andlauer, P. Stabat, D. Marchio, B. Flament, B. Latour, and M. Siroux, "Gas stirling engine µchp boiler experimental data driven model for building energy simulation," *Energy and Buildings*, vol. 84, pp. 117–131, 2014. [Online]. Available: https://www.sciencedirect.com/science/article/pii/S0378778814006653

[57] "247 energy lng containerized power plant datasheet," last accessed 18 May 2022. [Online]. Available: https://247.energy/wp-content/uploads/247-LNG-CPP-XXX-datasheet-v2.pdf

[58] "Yanmar cogeneration systems overview," last accessed 18 May 2022. [Online]. Available: https://www.yanmar.com/global/energy/cogeneration_systems/

[59] "Tedom chp units," last accessed 18 May 2022. [Online]. Available: https://www.tedom.com/en/downloads/products/

[60] "Jenbacher gas engines," last accessed 18 May 2022. [Online]. Available: https://www.innio.com/en/jenbacher/gas-engines/type-2

[61] A. Onufrena, T. Koettig, J. Bremer, T. Tirolien, T. Dorau, M. Laguna, and H. ter Brake, "Design of a compact mesh-based high-effectiveness counter-flow heat exchanger and its integration in remote cooling systems," *International Journal of Heat and Mass Transfer*, vol. 183, p. 122107, 2022. [Online]. Available: https://www.sciencedirect.com/science/article/pii/S0017931021012138

[62] F. Incropera, D. DeWitt, T. Bergman, and A. Lavine, *Fundamentals of Heat and Mass Transfer*, 01 2007.

[63] M. K. Bhatnagar, M. Rai, M. Ashraf, O. Kapoor, T. Mamatha, and M. Vishnoi, "Efficiency enhancement of heat exchanger using inserts and nano-fluid - a review," *Materials Today: Proceedings*, vol. 44, pp. 4399–4403, 2021, international Conference on Advances

in Materials Processing Manufacturing Applications. [Online]. Available: https://www.sciencedirect.com/science/article/pii/S2214785320381980

[64] G. O. Musgrove, S. Sullivan, D. Shiferaw, P. M. Fourspring, and L. Chordia, “8 – heat exchangers,” 2017.

Appendix

Chapter 4 - Inverted Brayton Cycle

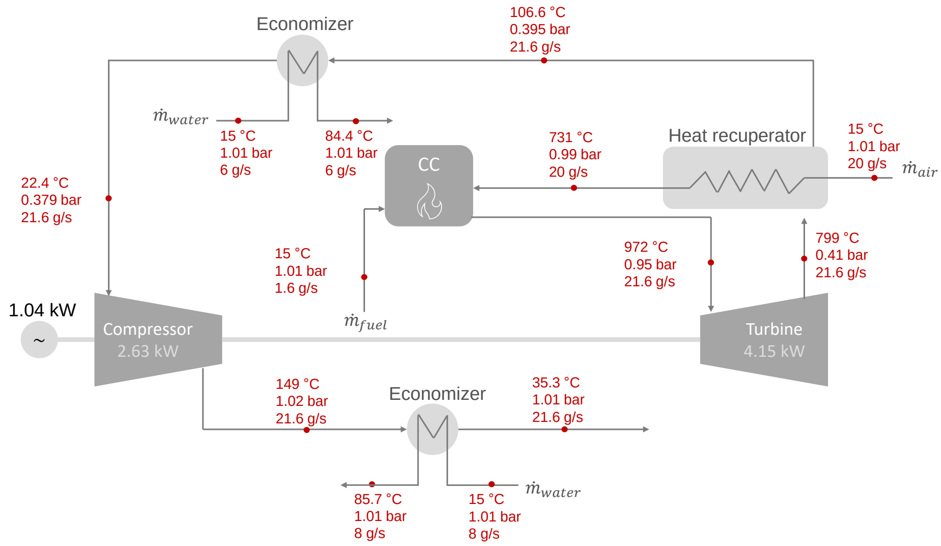

Figure 10.1: Temperatures, pressures and mass flows at all points of the IBC and compressor, turbine and generator work.

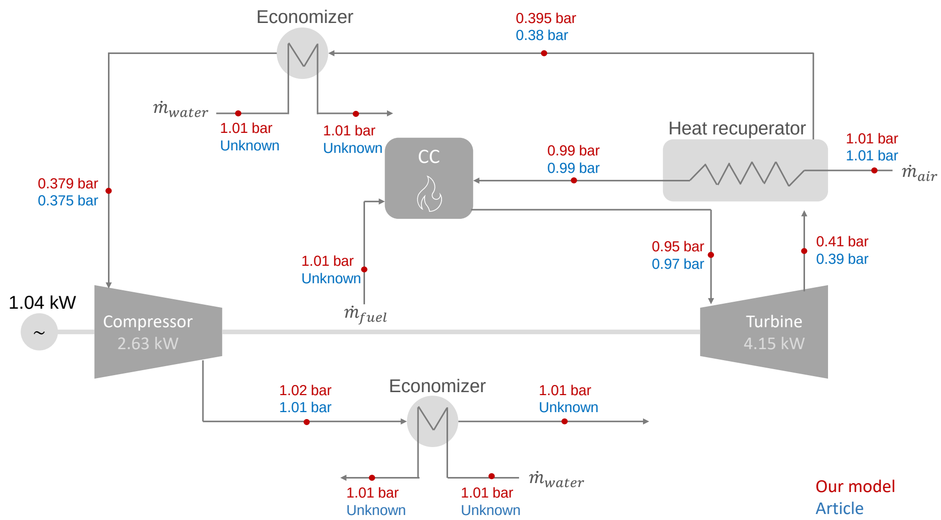

Figure 10.2: Comparison of the pressure evolution from our model with [8].

Chapter 5 - Maisotsenko Cycle

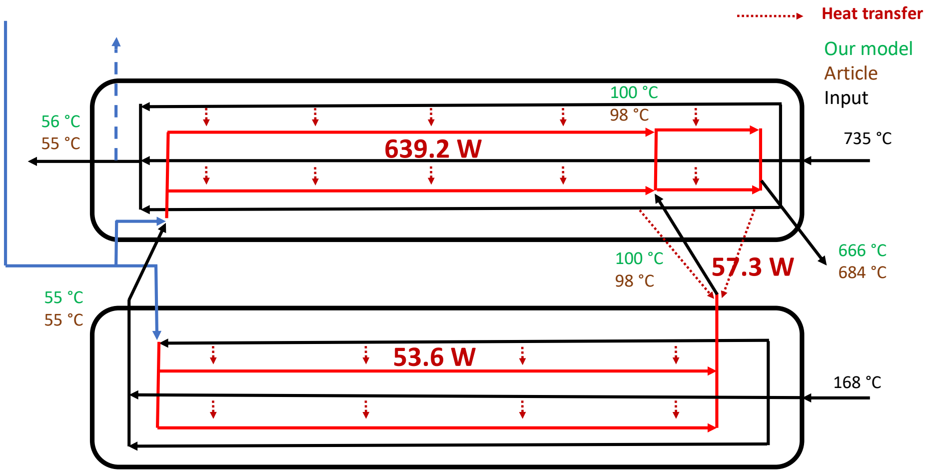

Figure 10.3: An additional heat transfer from the upper part towards the lower part is needed to evaporate all the injected water in the lower part (case with $\Delta T = 50$°C).

Chapter 6 - M-SAB cycle

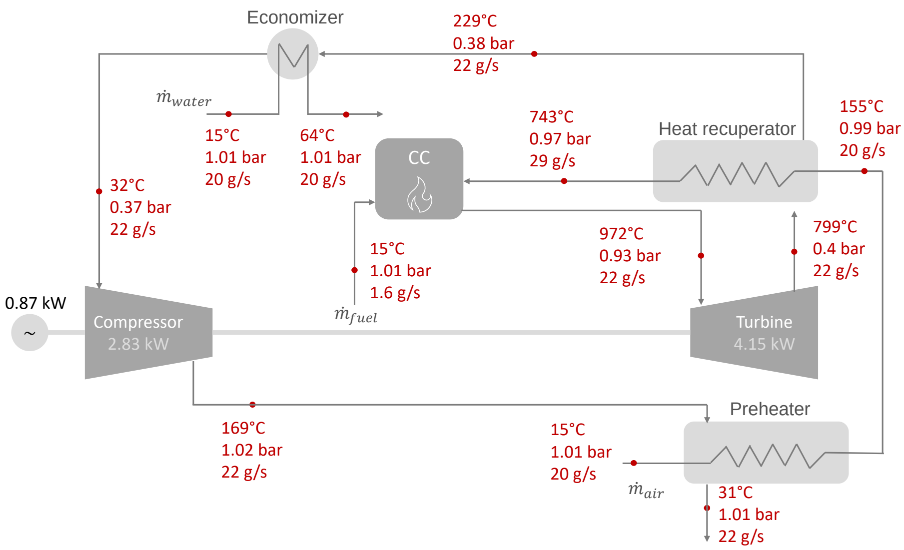

Figure 10.4: The introduction of the preheater in the IBC with the MTT mGT allows to increase the inlet temperature of the heat exchanger to 155°C.

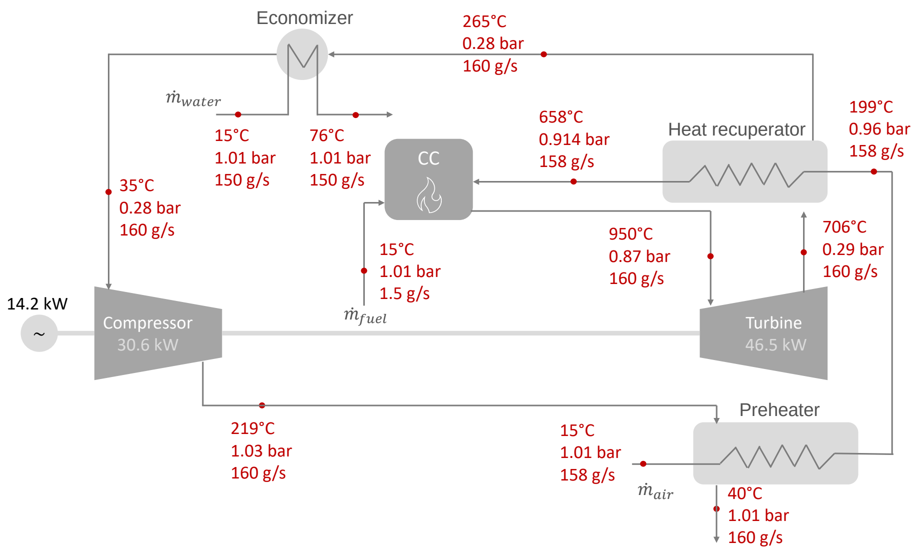

Figure 10.5: Temperatures, pressures and mass flows at all points of the IBC with the T100 mGT and compressor, turbine and generator work.

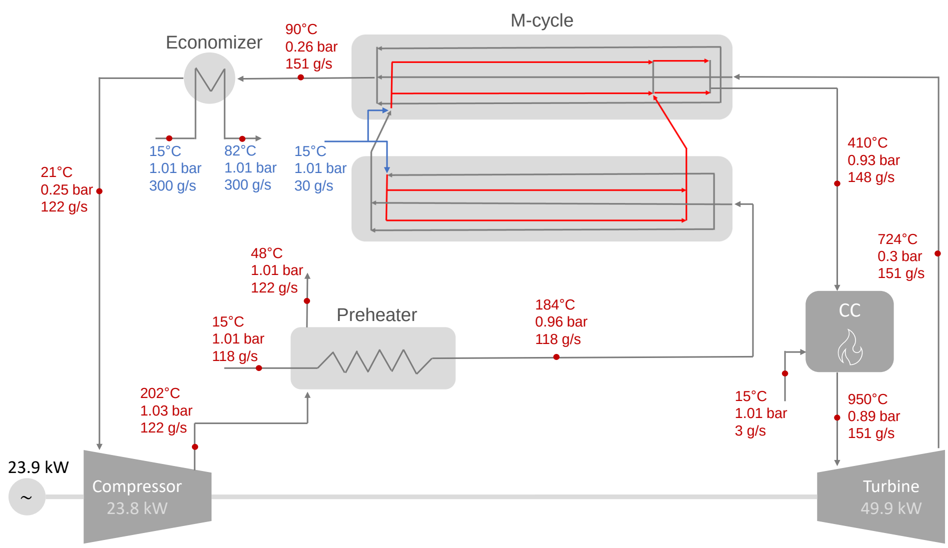

Figure 10.6: Temperatures, pressures and mass flows at all points of the M-SAB cycle and compressor, turbine and generator work. Results obtained with $\epsilon_{\mathrm{WB}} = 0.9$ and $\dot{m}_{\mathrm{H2O}} = 30$ g/s.

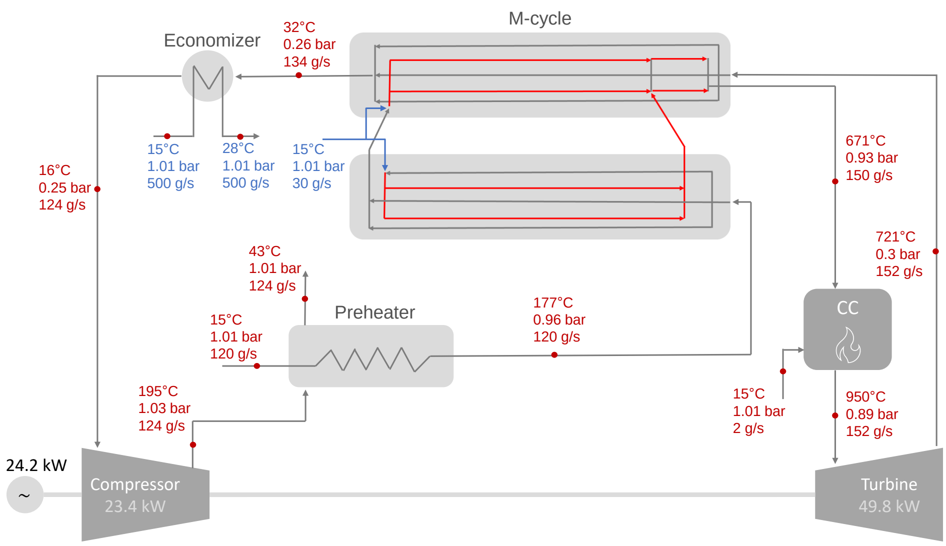

Figure 10.7: Temperatures, pressures and mass flows at all points of the M-SAB cycle and compressor, turbine and generator work. Results obtained with $\Delta T = 50°\mathrm{C}$ and $\dot{m}_{\mathrm{H2O}} = 30$ g/s.

UNIVERSITÉ CATHOLIQUE DE LOUVAIN
École polytechnique de Louvain
Rue Archimède, 1 bte L6.11.01, 1348 Louvain-la-Neuve, Belgique | **www.uclouvain.be/epl**